A Study of Conflict Detection and Resolution in Free Flight

by Jianghai Hu

Research Project

Submitted to the Department of Electrical Engineering and Computer Sciences, University of California at Berkeley, in partial satisfaction of the requirements for the degree of **Master of Science, Plan II**.

Approval for the Report and Comprehensive Examination:

Committee:

Professor S. Shankar Sastry, Research Advisor

Date

* * * * * *

Professor Laurent El Ghaoui, Second Reader

Date

A Study of Conflict Detection and Resolution in Free Flight

Abstract

A Study of Conflict Detection and Resolution in Free Flight

by

Jianghai Hu

Master of Science in Electrical Engineering and Computer Sciences

University of California at Berkeley

Professor Shankar Sastry, Chair

Some aspects of conflict detection and resolution problem in the free flight situation are studied in this paper. In the first part approximated probabilities of conflict (PC) for typical encounters of aircraft pair are proposed by modeling the perturbation in aircraft motion as Brownian motion (BM), both within finite horizon and within infinite horizon. Theoretical bounds on the errors of the approximations are also obtained. In the second part, homotopy types of resolution maneuvers of multiple aircraft are classified according to their images in the space-time coordinates, which can be shown to bear a one-to-one correspondence with the well-known braid group $\mathbf{B}_n$. For maneuver within each class, we propose the energy as the cost function and solve both analytically and algorithmically the optimal resolution maneuver for two aircraft case. Various properties of optimal maneuver for multiple aircraft resolution are studied and its two-legged approximation is calculated by convex optimization technique. Finally, based on the conflict probability obtained in the first part, a decentralized multi-aircraft resolution algorithm under the presence of noise is proposed. Simulations results for some typical encounters are presented and compared with the optimal maneuvers. This algorithm can either be implemented by itself at the strategic level or be used as a random "type chooser" for the convex optimization process, leading to a randomized solution to the combinatorial optimization problem.

To my family

Contents

List of Figures

Acknowledgements

First of all, the author would like to thank Professor Shankar Sastry, whose valuable advice and constant encouragement made this academic expedition much more fun for the author than he originally thought. It is a warm and pleasant experience to be able to work with him.

The author wants also to thank Professor Laurent El Ghaoui for his willingness to be the second reader for this thesis and the excellent course he taught on convex optimization in Fall, 1999 at Berkeley. The author is also grateful for the help from his co-worker, John and Maria, for their painful effort to make this paper more legible, and for the fruitful discussions between us.

Finally, special thanks goes to Professor Jim Pitman, whose course introduces the author to the wonderland of randomness and whose advice and pointers to the vast literature of probability theory proves to be invaluable.

Chapter 1

Overview

The dramatically increasing demand for air travel in recent years has been the source of great challenges for Air Traffic Management System (ATMS). Despite technological advances such as the availability of relatively inexpensive on-board computers and global positioning systems (GPS), the current ATMS remains largely intact as it was developed in the 70's and 80's and has increasingly become the bottleneck for a system with less ground holds and airborne delays. It is believed that by improving the efficiency of currently semi-automated ATMS, the increased demand in air traffic can be handled in a more reliable way, without resorting to such costly (and often political) options as building larger airports or adding more runways. The notion of free flight has been proposed ([3]) to shift the totally centralized decision making in the current ATMS to individual aircraft, in a hope to alleviate the burden of central (human) controller and decrease travel times, unplanned delays and fuel consumption. For a detailed account of the current ATMS practice, see [18]. [16] highlights the hierarchical and hybrid control issues associated with free flight.

The most important goal of the new ATMS is to improve the safety of air travel. Safety is typically characterized in terms of the number of conflicts (collisions and near misses). For the current system, a *conflict* is defined as a situation where two aircraft come within 5 nautical miles (nmi) of one another horizontally and within 1000 or 2000 feet (ft) vertically, depending on whether the flight level is below or above 29,000 ft respectively (see [13]). Conflict avoidance is typically decomposed into two separate procedures: conflict detection and conflict resolution. For a survey of various conflict detection and resolution modeling methods, see [8]. In this paper, we will focus on the probabilistic scheme. In the conflict detection stage, the motions of aircraft with the potential for conflict are predicted based on their positions, headings and flight plans and the probability of a future conflict is estimated. This information is then used in the resolution stage to re-plan the trajectories for the aircraft involved in the conflict.

This paper consists of two parts. In the first part, we study the conflict detection by deriving the probability of conflict (PC) for aircraft pair, both within finite horizon or within infinite horizon, under some suitable probabilistic setting. One of the difficulty is to model the wind effect, which is a major contributor to the uncertainty in the aircraft motion, and which does not admit a consistent physical model so far. However, since the prediction error can be modeled as the sum of a large number of independent random perturbations in disjoint time intervals, it is expected to be Gaussian. This hypothesis was indeed verified by empirical data in [13]. It is also suggested in [13] that the uncertainty can be decomposed into two components, an along track component whose standard deviation grows with time, and a cross track component whose standard deviation

remains roughly constant. Based on this probabilistic model, a number of methods have been proposed for predicting the probability of conflict (PC) for pairs of aircraft, over horizons of the order of 20 minutes. In [13] the notion of an *uncertainty ellipse* is used to obtain a closed form over-approximation for PC. In spite of its simplicity, which makes it very attractive for on-line computation, the exact interpretation of the results of [13] remains to be clarified. In [15], a *randomized estimation* algorithm is proposed for computing PC. Finally, [20] uses *Monte Carlo simulation* to determine PC for typical encounters.

In this paper we give an alternative treatment from a sample path viewpoint by modeling the perturbation as white noise. The motion of the aircraft is then the sum of a deterministic one plus a (scaled) Brownian motion (BM) perturbation. We will focus on the two dimensional case, assuming that both aircraft fly at the same altitude. Intuitively, the probability of conflict is the proportion of paths leading to a collision among all possible paths. BM gives us a measure of the probability of each path, where paths of large and steady deviation are less likely than paths of small and fluctuating deviation. One major advantage of our approach is that it provides closed form formulae (though approximations), which not only makes its implementation computationally inexpensive, but also enables us to easily derive a resolution algorithm. Theoretical bounds for the approximated PC are given in Chapter 5.

Starting from Chapter 6, we study the various aspect of multiple aircraft conflict resolution. It is found in Chapter 6 that the commonly used notion of "cross pattern" is insufficient to characterize fully the different types of planar resolution maneuvers when the number of aircraft is more than two. In fact, there is a one to one correspondence between types of multiple aircraft resolutions and the mathematically well-studied group of braids. In Chapter 7, we let ourself carried further by this geometric interpretation. The notion of *energy* of maneuvers is proposed and the optimal maneuver within each resolution type with minimal energy is studied. The machinery we employed here is similar to that of the classical variation of calculus technique, except that we have the minimal separation constraint on the resolution paths. The braid representation of maneuvers comes into play naturally and will serve as the primal source of inspiration for various transformations of resolution maneuvers which leave their minimal separation invariant. As the number of aircraft gets larger, it is difficult if not impossible to get the analytical expression of optimal resolutions. Instead, convex optimization will be used to get good approximations of it.

In spite of all the research, the problem remains largely unsolved because of its combinatorial nature. When the number of aircraft involved in the conflict is large, as is the case for airspace over any major airport, the number of resolution types becomes extremely large, rendering the exhausting search method completely impractical. By combining the PC obtained in this paper and potential field methods, we are able to come up with a *decentralized* multiple aircraft resolution algorithm. This autonomous algorithm is found to be successful in tracking the optimal resolution maneuver despite the presence of noise and performs reasonably well. Moreover, it can be used as the random "type chooser" for the optimization procedure if such a central optimization scheme is allowed in the future ATMS. Generally speaking, different resolution schemes can be classified according to the trust each aircraft put on the other. At one end of the spectrum, we have the game theoretical method ([17]), which assume the worst case, or in other words, zero trust. On the other far end, we have the central controller scheme, whether it is based on human operators or some optimization procedure, in which each aircraft trust wholeheartedly on the central controller and hence the other aircraft as well. In this respect, our scheme can be viewed as somewhere in the middle in that each aircraft assumes that other aicraft will try to behave rationally while at the same time this effort is undermined by the various uncertainties inherent in the environment.

Part I

Conflict Detection

Chapter 2

Motivation

Consider the following first order stochastic differential equation in $\mathbf{R}^1$:

$$\frac{dx}{dt} = f(t) + w(t) \tag{2.1}$$

where f is a piecewise continuous function defined on $[0, \infty)$ and $w(t)$ is white noise with power spectral density σ^2, *i.e.* $E[w(t)w(t+s)] = \sigma^2\,\delta(s)$ for all $s, t \geq 0$. Integrating equation (2.1), we have

$$x(t) = \int_0^t f(s)\,ds + b_t$$

where $b_t = \int_0^t w(s)\,ds$ is a Gaussian process with stationary, independent increment. Furthermore $E[b_t] = \int_0^t E[w(s)]\,ds = 0$ and

$$\mathrm{Var}[b_t] = \int_0^t\!\!\int_0^t E[w(s_1)w(s_2)]\,ds_1\,ds_2 = \sigma^2 t \tag{2.2}$$

These properties together with the assumption that b_t is continuous in t imply that, after scaling by $1/\sigma$, b_t is a standard Brownian Motion (BM). Although the continuous path assumption is not a logical consequence of the previous hypotheses, (2.2) and the Kolmogorov continuity theorem implies that b_t has a continuous version B_t, i.e. $P(\{\omega : b_t(\omega) = B_t(\omega)\}) = 1$ for all $t \geq 0$ and $\{B_t(\omega), t \geq 0\}$ is continuous in t with probability 1 (see [12]). The continuity assumption is further justified when equation (2.1) is used to model the motion of physical objects, since in this case $x(t)$ cannot make instantaneous jumps.

Application of equation (2.1) can be, for example, the motion of a cruising aircraft, where $\int_0^t f(s)\,ds$ is the trajectory prescribed by the central controller, and $w(t)$ is the effect of wind on the velocity of aircraft. Since aircraft can only control directly its air velocity, its ground velocity is obtained by combining nominal velocity $f(t)$ and wind effect $w(t)$.

Another example is the Automated Highway System (AHS [19]) in which a car in the platoon needs to predict the motions of adjacent cars on the highway to determine a safe distance. Such a prediction is based upon the assumption (belief) that adjacent cars will try to maintian their current speeds while these effort are deviated by various factors such as road condition, wind, mechanical malfunction and so on. For application of equation (2.1) in this respect, the interested reader is referred to [5].

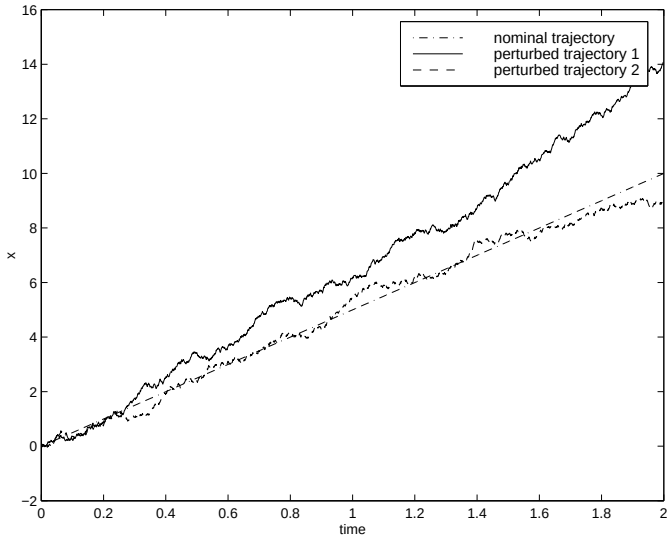

Figure 2.1: samples of perturbed motions of constant velocity $v = 5$

The use of BM as the disturbance in motion can also be justified by the fact that BM can be thought of as the accumulation of a large number of independent small disturbances. More precisely, subdividing time into intervals of length Δt, assuming the disturbance in different time intervals are independent and identically distributed (IID), and integrating, we get a random walk which, after appropriate scaling, converges in distribution to a standard BM as $\Delta t \to 0$ (see [2]). In [13] it is verified by empirical data that the prediction error for a cruising aircraft is indeed Gaussian with a growing variance.

Samples of perturbed trajectory are shown in Figure 2.1. It should be noted that BM possesses many unusual local properties; for example, at any fixed time its sample path is not differentiable with probability 1. However, here we are mainly concerned with its collective properties, *i.e.* the probability that the perturbed trajectory experiences a large deviation from the nominal one, or more precisely, the state x evolves outside some subset of the state space called the *safe set*. In case of such a event, we say a *conflict* occurs. Safe sets vary from model to model. In the aircraft case, a state is safe if any aircraft pair has horizontal and vertical seperations above some prescribed thresolds depending on their flight level as specified in Chapter 1. Intuitively the probability of conflict is the 'ratio' of number of sample paths leading to conflicts to the total number of sample paths, and BM serves to give us a measure of the possibility of each sample path. Here we use the word ratio in the extended sense since both numbers are infinite.

By subtracting the nominal motion $\int_0^t f(s)\,ds$ and properly scaling, we can adopt the alternative view point that the perturbed motion consists only of a standard BM and the safe set is time-varying. In this new coordinate system, the problem reduces to calculating the escaping probability of the standard BM with respect to a time-varying region. This change of viewpoint will be employed frequently in the later developments. In general, it is very hard, if not impossible, to get an analytical expression of this escaping probability, all one can hope for is an approximation of it, and probably lower and upper bound on the approximation error. There is, however, one case which is simple enough to allow for such an exact expression. Namely,

Lemma 1 (Bachelier-Levy [2]) *Let B_t be a standard one dimensional BM starting from the*

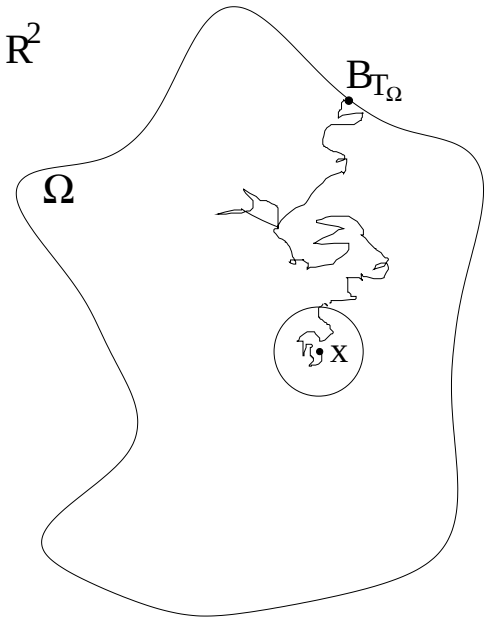

Figure 2.2: Exit distribution of BM from a region $\Omega \subset \mathbf{R}^2$

origin. Then $B_t^\mu = B_t + \mu t$ *is the BM with drift* μ *for some* $\mu \in \mathbf{R}^1$. *Define* $T_a^\mu = \inf\{t \geq 0 : B_t^\mu = a\}$ *to be the first time* B_t^μ *hits* a. *Then* T_a^μ *has probability density function:*

$$p(t) = \frac{a}{\sqrt{2\pi t^3}} \exp[-\frac{(a-\mu t)^2}{2t}], \quad t \geq 0$$

This lemma will prove to be of utmost importance for deriving the approximated probability of conflict in the later development.

Remark 1 In the case of a time-invariant safe set, a deep connection exists between the exit distribution of a standard BM and the classical potential theory, which can be used to calculate the exit distribution of the BM with respect to certain regions. For example, let $\Omega \subset \mathbf{R}^2$ be an open region with boundary $\partial\Omega$ smooth enough such that for a two dimensional BM B_t starting from any point $x \in \Omega$, the first exit position B_{T_Ω} is measurable. Here T_Ω denotes the first exit time of B_t from Ω (see Figure 2.2). Now if $g : \partial\Omega \to \mathbf{R}$ is a measurable function defined on $\partial\Omega$, then

$$f(x) \triangleq E_x[B_{T_\Omega}], \quad \forall x \in \Omega$$

defines a measurable function f on $\bar{\Omega}$ which coincides with g on $\partial\Omega$. In fact, it can be proved (see [14]) that f thus defined is harmonic, *i.e.*

$$\begin{cases} \Delta f \equiv 0, & \forall x \in \Omega \\ f = g \text{ on } \partial\Omega \end{cases} \tag{2.3}$$

where $\Delta = \partial^2/\partial x^2 + \partial^2/\partial y^2$. In other words, we can run a BM to solve the Dirichlet problem (2.3) with boundary condition. For some Ω, say, the sphere, equation (2.3) can be solved analytically, hence yielding the expression for the probability density function p of $\mathbf{B}_{T_\Omega}$ since $f = \int_{x \in \partial\Omega} g(x)p(x)\,dx$. However, this machinery is not applicable here since we are considering the exit *time* distribution of BM from a *time-varying* safe set.

Chapter 3

Model

Consider two aircraft, labeled 1 and 2, flying on the same horizontal plane. Assume without loss of generality that at time $t = 0$, aircraft 1 is at the origin of a global coordinate frame, flying from left to right with a velocity $u_1 \in \mathbf{R}^2$, while aircraft 2 is at position $z_0 \in \mathbf{R}^2$, flying with a velocity $u_2 \in \mathbf{R}^2$ which makes an angle θ with u_1 (Figure 3.1). We refer to aircraft 2 as the *intruder*. A conflict occurs if the intruder enters the protected zone of aircraft 1 or vice versa. For flight with altitude below 29,000 ft, the protected zone is simply a disc of radius $R = 5$ nmi.

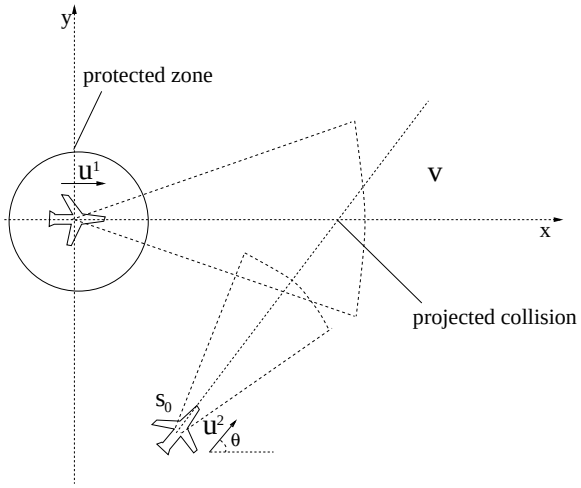

Figure 3.1: Typical encounter situation.

For the positions $z_1(t)$ and $z_2(t)$ of the two aircraft, we propose a kinematic model of the following form:

$$z_1(t) = u_1 t + \Sigma B_1(t) \tag{3.1}$$

$$z_2(t) = z_0 + u_2 t + T(\theta)\Sigma B_2(t) \tag{3.2}$$

Here $\Sigma = \mathrm{diag}(\sigma_a, \sigma_c)$. σ_a, σ_c model the variance growth rate in the along track and cross track component respectively ($\sigma_a > \sigma_c$ typically). $T(\theta)$ is the matrix corresponding to a rotation by θ

counterclockwise:

$$T(\theta) = \begin{pmatrix} \cos\theta & -\sin\theta \\ \sin\theta & \cos\theta \end{pmatrix}$$

$B_1(t)$ and $B_2(t)$ are independent standard 2-D BM's.

Subtracting equation (3.1) from equation (3.2) leads to

$$\Delta z(t) = z_0 + \Delta u \cdot t - w(t), \tag{3.3}$$

where $\Delta z(t) = z_2(t) - z_1(t)$, $\Delta u = u_2 - u_1$, and $w(t) = \Sigma B_1(t) - T(\theta)\Sigma B_2(t)$. Equation (3.3) suggests that one can think of the motion of aircraft 1 as consisting only of the perturbation $w(t)$, and the motion of aircraft 2 as deterministic with constant velocity Δu starting from z_0. Furthermore, $w(t)$ can be transformed to a standard 2-D BM by the following proposition.

Proposition 1 *There exists a nonsingular matrix P, such that $P^{-1}w(t)$ is a standard 2-D BM.*

Proof: Using the fact that for standard 2-D BM $B_i(t)$, $i = 1, 2$, $E[B_i(t)B_i(t+s)^T] = tI$ for all $s, t \geq 0$, we calculate the autocorrelation of process $w(t)$ as:

$$E[w(t)w^T(t+s)] = t[\Sigma^2 + T(\theta)\Sigma^2 T(\theta)^T]$$

where I is the 2 by 2 identity matrix. It can be checked that $\Sigma^2 + T(\theta)\Sigma^2 T(\theta)^T = PP^T$ holds for $P = \sqrt{2}\,T(\frac{\theta}{2})\Lambda$, and $\Lambda = \mathrm{diag}(\lambda_1, \lambda_2)$ with:

$$\begin{cases} \lambda_1 = \sqrt{\sigma_a^2 \cos^2(\frac{\theta}{2}) + \sigma_c^2 \sin^2(\frac{\theta}{2})} \\ \lambda_2 = \sqrt{\sigma_a^2 \sin^2(\frac{\theta}{2}) + \sigma_c^2 \cos^2(\frac{\theta}{2})} \end{cases} \tag{3.4}$$

Therefore by defining $n(t) = P^{-1}w(t)$, we have $E[n(t)n^T(t+s)] = tI$ for all $s, t \geq 0$. Since $\{n(t), t \geq 0\}$ is a Gaussian process, for which uncorrelatedness implies independence, $n(t)$ is a standard 2-D BM, which proves the conclusion. ∎

Therefore, by performing the transformation P^{-1}, we can assume that the motion of aircraft 1 is a standard 2-D BM starting from the origin, while the motion of aircraft 2 is of constant velocity $v = (v_x, v_y)^T$ starting from $s = (s_x, s_y)^T$, where

$$s = P^{-1}z_0, \qquad v = P^{-1}\Delta u. \tag{3.5}$$

The new coordinate system is plotted in Figure 3.2. Define x_d as the distance from the origin to the line h along which aircraft 2 is flying, and a as the distance from aircraft 2 at $t = 0$ to the projection H of the origin on h. Then, in the new coordinate system:

$$x_d = \frac{|s^T T_{\frac{\pi}{2}} v|}{\|v\|} \qquad a = -\frac{s^T v}{\|v\|}. \tag{3.6}$$

Ignore the noise temporarily. Then in the new coordinate system, a positive a indicates that the two aircraft are approaching each other and the minimal separation during the encounter is x_d. On the other hand, a negative a indicates that they are flying away from each other and the minimal

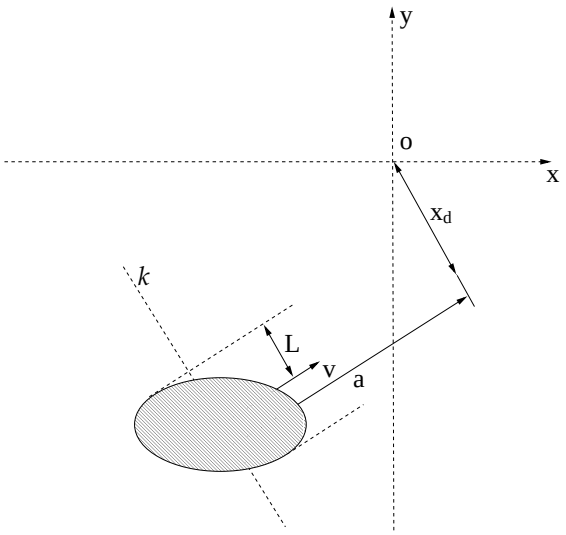

Figure 3.2: Transformed protection zone.

separation occurs at time $t = 0$. Moreover, the circular protection zone of radius $R = 5$ nmi around aircraft 2 is transformed into an ellipse centered initially at s and with boundary described by:

$$\lambda_1^2(x - s_x)^2 + \lambda_2^2(y - s_y)^2 = R^2/2, \tag{3.7}$$

and moves along with aircraft 2. A conflict occurs if and only if the 2-D BM (*i.e.*, the motion of aircraft 1 in the new coordinate system) ever wanders into this moving ellipse.

The model proposed here assumes that the initial positions of the aircraft are known precisely, i.e., it ignores errors in the radar and GPS measurements. This can be justified by the fact that uncertainty in the initial position will become rapidly dominated by the perturbation to the aircraft motion as time goes on (see [20]). Another assumption we make is that the perturbations to the motions of different aircraft are independent. This assumption, though inaccurate, is commonly made in the literature (see [13, 15]). We will address this issure in the future work.

Remark: In the model of [13], the cross track variance saturates once it reaches a fixed value (typically 0.5-1 nmi^2) and the along track variance grows quadratically in time. By comparison, in our model both the cross and along track variances grow linearly with time. The justification is that we intend to apply our model to the free flight situation, in which each aircraft will receive advisory rather than mandatory trajectory specification from the central controller. In this case, saturation, which in [13] is attributed to pilot feedback to maintain the aircraft on a *specific* trajectory, may become less meaningful. Moreover, for free flight, early conflict detection and resolution is done by individual aircraft which only have partial information about the intentions of their neighbors. This may include no more than the current positions and heading of surrounding aircraft. In this situation, there is no reason to assume that the intruder will make an effort to maintain its current heading precisely. Finally, the quadratically increasing along track variance in [13] might be largely due to "global" wind effects which, although unknown, remain constant and affect the motion of both aircraft in a similar way over the relatively short conflict horizon. Therefore, they tend to cancel out in the relative position. The perturbations in (3.1) and (3.2) model mainly local wind effects such as air turbulence as well as deviations due to mechanical and human factors for each aircraft.

Chapter 4

Approximated Probability of Conflict

Following [16], we distinguish three different kinds of conflict, and derive the probability of conflict (PC) for each particular case.

1. *Overtake*: Two aircraft fly along the same path with the faster one trailing the slower one.
2. *Collision*: Two aircraft fly along crossing paths and exact collision is predicted.
3. *Near miss*: Similar to collision, except that "exact collision" is replaced by "approach within 5 nmi".

4.1 PC for Overtake

Suppose that aircraft 1 and 2 are both flying from left to right along the x axis, with an initial distance Δx and aircraft 1 following aircraft 2 at a higher speed $u_1 > u_2$. In this setting, equation (3.3) simplifies to:

$$\begin{cases} \Delta x(t) &= \Delta x + \Delta u\, t + \sigma_1\, B_t^x \\ \Delta y(t) &= \sigma_2\, B_t^y \end{cases}$$

where $(\Delta x(t), \Delta y(t))$ is the relative position of aircraft 2 with respect to aircraft 1 at time t, $\Delta u \triangleq u_2 - u_1$, B_t^x, B_t^y are independent standard 1-D BM's, and $\sigma_1 = \sqrt{2}\sigma_a$, $\sigma_2 = \sqrt{2}\sigma_c$ are the combined variances of the perturbations of both aircraft (assuming they are independent).

By Proposition 1, a coordinate transformation $P = \mathrm{diag}(\sigma_1, \sigma_2)$ allows us to adopt the viewpoint that the motion of aircraft 1 is a standard 2-D BM $B_t = (B_t^1, B_t^2)$ starting from the origin, while aircraft 2 is moving at constant speed $v = |\Delta u|/\sigma_1$ to the left, with an initial distance $a = \Delta x/\sigma_1$ from aircraft 1. In the new coordinate system, the protected zone of aircraft 2 is transformed into an ellipse with long axis $L = R/\sigma_2$ and short axis $S = R/\sigma_1$ moving along with aircraft 2 (See Figure 4.1).

A conflict occurs if and only if B_t ever wanders into the moving ellipse. Denote this event as F. The probability $P(F)$ does not admit a closed form formula. However we can approximate it by a "decoupled" event. Let l be the vertical line which passes through the center of the ellipse and moves together with it. Denote by τ the first time B_t hits l and define $A \triangleq \{\omega : |B_\tau^2(\omega)| \leq L\}$, *i.e.* A is the event that the first time B_t hits line l, it is within a distance of L from the center

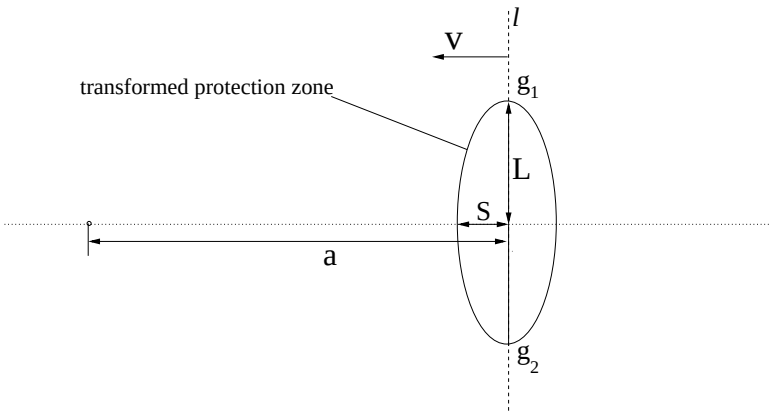

Figure 4.1: Transformed protection zone.

of the ellipse. Since $A \subseteq F$, $P(A) \leq P(F)$. However since usually $|\Delta u|$ is much larger than the variance growth rate of the BM, and because of the shape of the ellipse, it can be expected that $P(F) \simeq P(A)$. We will discuss the error of this approximation more formally in the next chapter.

Evidently τ has the same distribution as T_a^v, the first time the BM B_t^v starting from the origin with drift v reaches value a. So by Lemma 1, τ has probability density:

$$p_\tau(t) = \frac{a}{\sqrt{2\pi t^3}} \exp(-\frac{(a - v\,t)^2}{2t}).$$

and the approximate probability of conflict for overtake case can be written as:

$$P(A) = \int_0^\infty p_\tau(t) \int_{|y|<L} \frac{1}{\sqrt{2\pi t}} \exp(-\frac{y^2}{2t})\, dt = 1 - 2\int_0^\infty p_\tau(t) Q(\frac{L}{\sqrt{t}})\, dt, \tag{4.1}$$

where $Q(x) \triangleq \int_x^\infty \frac{1}{\sqrt{2\pi}} \exp(-t^2/2)\, dt$. Notice that by Formula 5 in Appendix A, $E[\tau] = a/v$. In case v is larger than 1 or equivalently $|\Delta u| > \sigma_1$, $p_\tau(t)$ concentrates near $t_0 \triangleq a/v = \Delta x/|\Delta u|$. Since function $q(t) \triangleq Q(L/\sqrt{t})$ is relatively flat near t_0, we can expand $q(t)$ about t_0 to get:

$$q(t) \simeq q(t_0) + q'(t_0)(t - t_0) + \frac{1}{2} q''(t_0)(t - t_0)^2. \tag{4.2}$$

where $q'(t_0), q''(t_0)$ are the first and second order derivatives of $q(t)$ at t_0 and can be calculated as

$$\begin{aligned} q'(t_0) &= \frac{1}{\sqrt{2\pi}} \exp(-\frac{L^2}{2t_0}) \frac{L}{2\sqrt{t_0^3}}; \\ q''(t_0) &= \frac{1}{\sqrt{2\pi}} \exp(-\frac{L^2}{2t_0}) [\frac{L^3}{4\sqrt{t_0^7}} - \frac{3L}{4\sqrt{t_0^5}}] \end{aligned} \tag{4.3}$$

Substituting equation (4.2) into equation (4.1), we have after some calculation:

Assertion 1 *PC for overtake can be approximated by:*

$$P_{ot}^3 \triangleq 1 - 2 \cdot Q(\frac{L}{\sqrt{t_0}}) - \frac{K}{4v^2\sqrt{2\pi}} \exp(-\frac{L^2}{2t_0}), \tag{4.4}$$

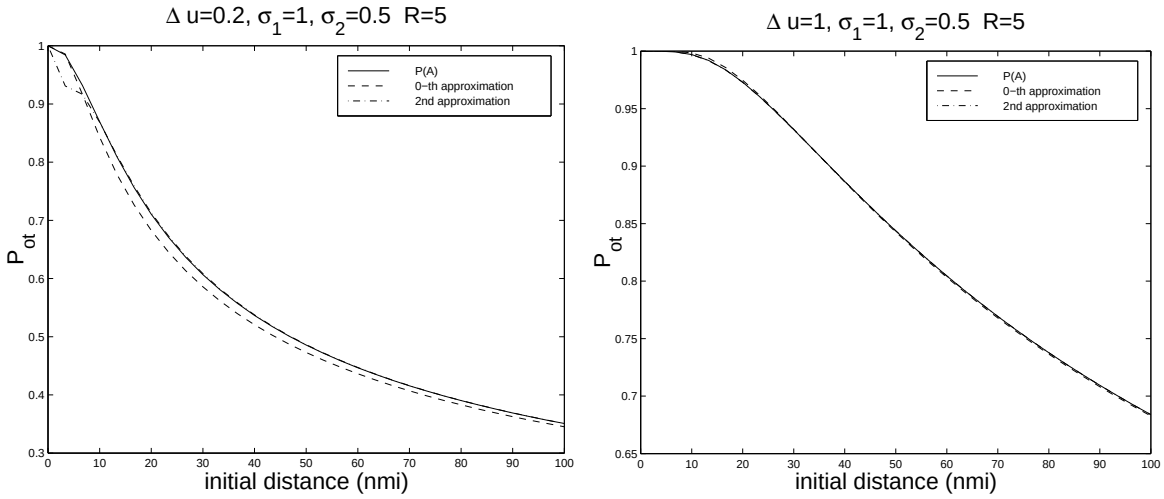

Figure 4.2: Comparison of $P(A)$, P_{ot}^0 and P_{ot}^3 (Left: $\Delta u = 0.2$ nmi/min, Right: $\Delta u = 1$ nmi/min).

where $t_0 = \Delta x/|\Delta u|$ *and* $K = L^3/\sqrt{t_0^5} - 3L/\sqrt{t_0^3}$. *If only the first term in equation (4.2) is used in the expansion, then we get the simpler 0-th order approximation:*

$$P_{ot}^0 \triangleq 1 - 2 \cdot Q(L/\sqrt{t_0}). \tag{4.5}$$

In Figure 4.2, $P(A)$ computed by numerical integration and its 0-th and 3-rd order approximation are plotted as functions of Δx, for the two cases $\Delta u = 0.2$ nmi/min and $\Delta u = 1$ nmi/min. Here $\sigma_1 = 1, \sigma_2 = 0.5$ (whose squares are in nmi^2/min, which is omitted from now on for simplicity), and $R = 5$ nmi. From these plots, it can be seen that Assertion 1 gives us a remarkably sharp estimate of $P(A)$ (and hence $P(F)$) even in the case when v is much smaller than 1 (the approximation error when $v > 1$ is barely visible).

Sometimes it is more reasonable to limit the prediction to a finite horizon, since a situation where PC is nearly 1 but with a projected collision time $\bar{t}$ of 30 minutes may not be as dangerous as a situation with a smaller PC but $\bar{t} = 15$ min. Instead of simply weighting PC and $\bar{t}$, we can alternatively compute PC for the overtake case within a fixed horizon t_f as:

$$P(A \cap \{\tau \le t_f\})) = \int_0^{t_f} p_\tau(t) \int_{|y|<L} \frac{1}{2\pi t} \exp(-\frac{y^2}{2t})\, dt = \int_0^{t_f} p_\tau(t)\big[1 - 2Q(\frac{L}{\sqrt{t}})\big]\, dt. \tag{4.6}$$

Following a procedure similar to that used for the infinite horizon case, except that Formula 4 is used instead of Formula 5, we get the approximation of equation (4.6) as:

Assertion 2 *PC within time* t_f *for overtake can be approximated by:*

$$P_{ot}^{t_f} \triangleq Q(\frac{a - v\,t_f}{\sqrt{t_f}})G_1 + e^{2av}Q(\frac{a + v\,t_f}{\sqrt{t_f}})G_2 + 2q''(t_0)\frac{a\sqrt{t_f}}{v^2\sqrt{2\pi}} \exp\big[-\frac{(a - v\,t_f)^2}{2t_f}\big], \tag{4.7}$$

where G_1, G_2 *are constants defined by*

$$G_1 \triangleq 1 - 2q(t_0) - q''(t_0)a/v^3,$$
$$G_2 \triangleq 1 - 2q(t_0) + 4q'(t_0)t_0 - q''(t_0)(4t_0^2 - a/v^3).$$

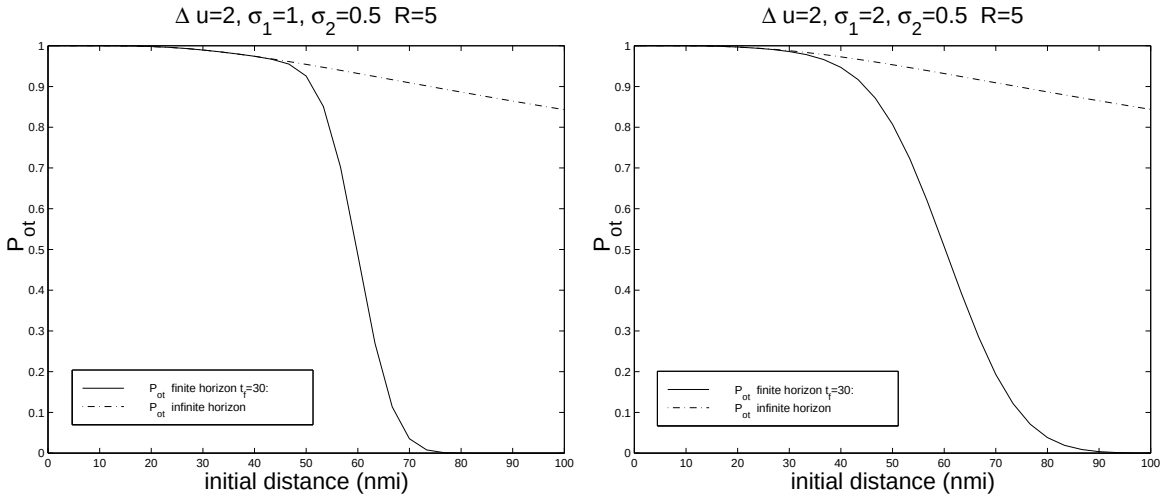

Figure 4.3: Comparison of P_{ot}^3 and $P_{ot}^{t_f}$ with $t_f = 30$ min, $\Delta u = 2$ nmi/min. Left: $\sigma_1 = 1$, Right: $\sigma_1 = 2$.

Figure 4.3 shows the comparison between P_{ot}^3 and $P_{ot}^{t_f}$ ($t_f = 30$ min) as functions of Δx for two different values of σ_1 ($\sigma_1 = 1$ and $\sigma_1 = 2$), with $\sigma_2 = 0.5$ and $R = 5$ nmi. Notice that $P_{ot}^{t_f}$ coincides with P_{ot} for small Δx, but drops to zero at around $\Delta u\, t_f$. The larger the σ_1, the slower the drop.

Remark 2 : Although we have pointed out that $P(A)$ is a valid approximation of $P(F)$ if $\Delta u > 1$, it is interesting to know what this approximation becomes when Δu is nearly zero, i.e. two aircraft have almost the same speed and heading. A well known result in probability theory (see [1]) is that the hitting distribution on a line l for a 2-D BM B_t starting from $z \notin l$ is Cauchy, which implies that the probability a fixed segment of l is hit by B_t first than any other part of l depends only on the angle that the segment makes to z. So the contour of $P(A)$ when $v = 0$ consists of the family of all arcs passing through points g_1 and g_2 in Figure 4.1, which is acceptable.

4.2 PC for Collision and Near Miss

We now deal with the case when the paths of the two aircraft cross at an arbitrary angle θ. In the following discussion we use the concepts introduced in Chapter 3. In particular, the circular protected zone of radius R is transformed into an ellipse centered around aircraft 2, with initial boundary determined by equation (3.7) and moves at velocity $v = (v_x, v_y)^T$ along with aircraft 2.

A conflict occurs if and only if the 2-D BM B_t starting from the origin wanders into this moving ellipse. In the spirit of the previous section, we calculate the projected width $2L$ of the ellipse along the direction of v as (see Figure 3.2):

$$L = \frac{R}{\lambda_1 \lambda_2} \sqrt{\frac{v_x^2 \lambda_1^2 + v_y^2 \lambda_2^2}{2(v_x^2 + v_y^2)}}. \tag{4.8}$$

where λ_1 and λ_2 are determined by equation (3.4).

Now we estimate PC by approximating the event of conflict as the event that the first time B_t hits line k, it is within a distance L from the center of the ellipse. Line k is assumed to pass though the

center of the ellipse at an angle orthogonal to v and move along with it at velocity v. Although the ellipse may be far from symmetrical with respect to the line h, the error introduced in our approximation is partly reduced due to the shape of the ellipse on different sides of h. We will give more detailed treatment in the next chapter.

By some rotation, we can assume that v is aligned with the positive x axis. An important property of BM is that it is invariant with respect to rotations, which implies that the motion of aircraft 1 is still a standard BM. Therefore the time τ for aircraft 1 to reach the line k has probability density:

$$p_\tau(t) = \frac{a}{\sqrt{2\pi t^3}} \exp\big[-\frac{(a-\mu t)^2}{2t}\big], \quad t \geq 0$$

where $\mu = \pm\|v\|$, the plus or minus sign chosen according to whether the two aircraft are approaching of flying away from each other. a is given by equation (3.6). Assume $a > 0$. Following the last paragraph, we propose the following approximation of PC for collision and near miss cases:

$$\int_0^\infty p_\tau(t) \int_{|y-x_d|<L} \frac{1}{2\pi t} \exp(-\frac{y^2}{2t})\, dt = \int_0^\infty p_\tau(t) \big[Q(\frac{x_d - L}{\sqrt{t}}) - Q(\frac{x_d + L}{\sqrt{t}})\big]\, dt. \tag{4.9}$$

A procedure similar to the one used in the overtake case provides closed form approximations for equation (4.9). For example, if the 0-th order term is used, we get:

Assertion 3 *PC for collision and near miss can be approximated by:*

$$P_{nm} \triangleq Q(\frac{x_d - L}{\sqrt{t_0}}) - Q(\frac{x_d + L}{\sqrt{t_0}}). \tag{4.10}$$

where $t_0 = a/\mu$. L is given by equation (4.8), a and x_d are given by equation (3.6).

Higher order approximation and finite horizontal version can also be obtained. For example, the probability of conflict before time t_f can be approximated by:

$$\int_0^{t_f} p_\tau(t) \big[Q(\frac{x_d - L}{\sqrt{t}}) - Q(\frac{x_d + L}{\sqrt{t}})\big]\, dt.$$

By employing the same expansion technique and using Formula 4 from Appendix A, we have

Assertion 4 *The approximated PC within time t_f for collision and near miss case is:*

$$\begin{aligned} P_{nm}(t_f) = {} & Q(\frac{a-\mu t, t_f}{\sqrt{t_f}})\big[q_1(t_0) - q_2(t_0) + \frac{a}{2\mu^3}(q_1''(t_0) - q_2''(t_0))\big] \\ & + e^{2a\mu} Q(\frac{a+\mu\, t_f}{\sqrt{t_f}})\big[q_1(t_0) - q_2(t_0) - 2(q_1'(t_0) - q_2'(t_0))t_0 \\ & \quad + 2(q_1''(t_0) - q_2''(t_0))t_0^2 - \frac{a}{2\mu^3}(q_1''(t_0) - q_2''(t_0))\big] \\ & - \frac{a}{\mu^2}\sqrt{\frac{t_f}{2\pi}} \exp\big[-\frac{(a-\mu\, t_f)^2}{2t_f}\big][q_1''(t_0) - q_2''(t_0)] \end{aligned} \tag{4.11}$$

where $q_1'(t_0), q_1''(t_0), q_2'(t_0), q_2''(t_0)$ are derivatives at $t_0 = a/\mu$ of the following functions:

$$q_1(t) \triangleq Q(\frac{x_d - L}{\sqrt{t}}) \qquad q_2(t) \triangleq Q(\frac{x_d + L}{\sqrt{t}})$$

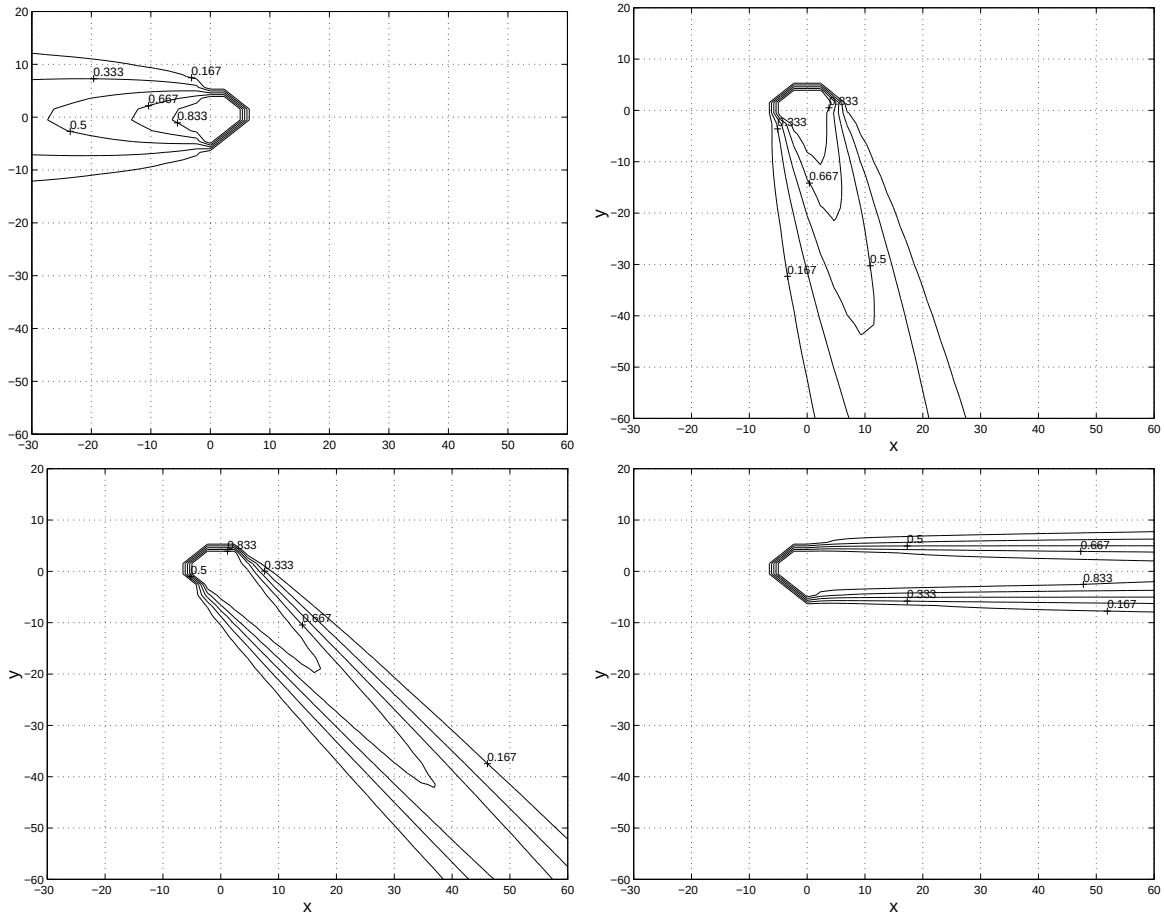

Figure 4.4: P_{nm} for path angles $\theta = 0°$ (upper left); $\theta = 45°$ (upper right); $\theta = 90°$ (lower left); $\theta = 180°$ (lower right) with $\|u_1\| = 7$ nmi/min, $\|u_2\| = 8$ nmi/min, $\sigma_a = 2$, σ_c=1, $R = 5$ nmi

Figure 4.4 shows some level curves of P_{nm} as a function of the initial position z_0 of aircraft 2 for the path angles $\theta = 0°, 45°, 90°, 180°$. In each plot, aircraft 1 is moving from left to right at velocity $\|u_1\| = 7$ nmi/min starting from the origin and aircraft 2 is moving at velocity $\|u_2\| = 8$ nmi/min. To see the results more compactly, we used relatively large σ_a and σ_c ($\sigma_a = 2$, $\sigma_c = 1$) and $R = 5$ nmi. It can be seen that as the path angle θ gets larger and larger, the region delimited by the same P_{nm} equi-probability line gets more and more extended, which means that for a fixed distance of the two aircraft, the situation of headon conflict is the most dangerous, while overtake is the least dangerous. This important property of P_{nm} will be used to construct potential functions to generate trajectories with less abrupt turn for aircraft in the later chapter.

Figure 4.5 shows the level curves of $P_{nm}^{t_f}$ with $\theta = 90°$, and $t_f = 10, 15$ min respectively. It is observed that $P_{nm}^{t_f}$ looks like a truncation of the corresponding infinite horizon version P_{nm}. As σ_a and σ_c increase, the truncation becomes smoother, as can be anticipated.

Remark 3 In [7], 0-th order approximation (4.10) is obtained under a different probabilistic model, which, the author believe, is naive and the probabilistic analysis therein is flawed. To get results which make sense mathematically and which can be easily extended to the general case, say, the finite horizontal case, one has to approach the problem from the process point of view.

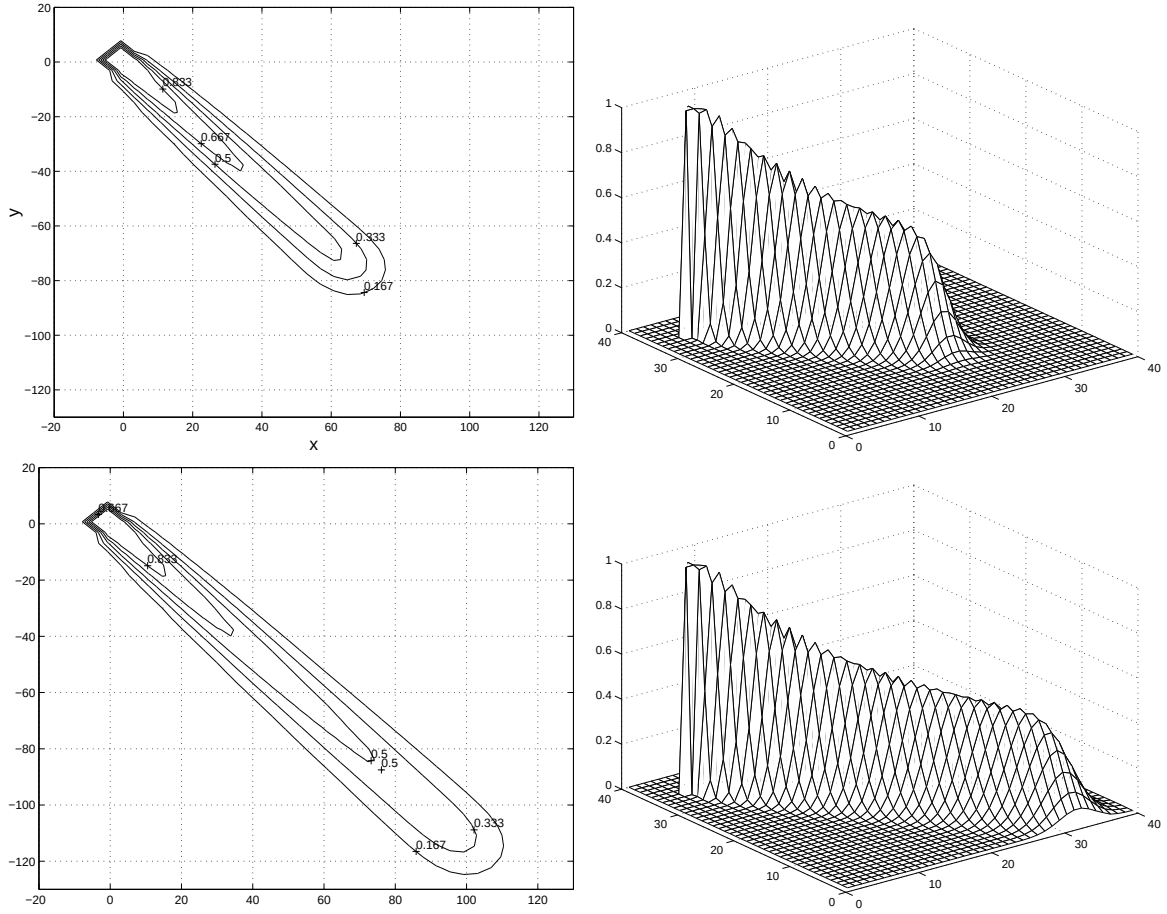

Figure 4.5: $P_{nm}^{t_f}$ for $t_f = 10$ min (top); $t_f = 15$ min (bottom) with $\theta = 90°$, $\|u_1\| = 7$ nmi/min, $\|u_2\| = 8$ nmi/min, $\sigma_a = 2$, $\sigma_c = 1$, $R = 5$ nmi.

4.3 Alternative View of the Method of Uncertainty Ellipse

There are various other quantities which can be used to characterize the degree of danger of a particular situation. In this section we analyze the notion of uncertainty ellipse used in [13] to calculate an index also called PC in [13]. The idea is to model the position of an aircraft at each time instance as a Gaussian random variable whose mean is determined by the deterministic motion and whose variance grows with time. The probability of collision at each future instant is then the probability that this Gaussian random variable lies inside the protection zone of the other aircraft, and the overall PC is defined as the maximal value of such probability over the period of potential collision. Despite its simplicity, which makes it very attractive for on-line implementation, a meaningful interpretation is not so obvious. However, it can be shown to have a close relationship with the expected occupation time in *unsafe set* by the following argument.

Let $\Delta x(t)$ be the relative position of two aircraft. $S = D(0, R)$ is the protection zone. Then the total time two aircraft stay inside the protection zone is:

$$T = \int_0^\infty 1_{\Delta x(t) \in S} \, dt$$

T is a random variable whose expectation can be calculated via Fubini theorem as:

$$\begin{aligned} E[T] &= E[\int_0^\infty 1_{\Delta x(t)\in S}\, dt] = \int_0^\infty E[1_{\Delta x(t)\in S}]\, dt \\ &= \int_0^\infty P(\Delta x(t) \in S)\, dt \\ &= \int_0^\infty PC(t)\, dt \end{aligned}$$

where $PC(t) \triangleq P(\Delta x(t) \in S)$ is defined as in [13]. Therefore from this relation, the average value of $PC(t)$ during the encounter gives the expected time that the two aircraft stayed in conflict status if the current travel plans are followed.

Other indices can be easily derived in a similar way. For example, if only collision within a certain horizon t_f is of interest and taking into consideration of the fact that collision at a later time pose less threat, then

$$\int_0^{t_f} PC(t)e^{-\lambda t}\, dt$$

can be also be used as another index (and possibly a more meaningful one than the maximum or average of $PC(t)$). Here λ is the discount factor.

It should be noted that although some of these indices lie in the range $[0, 1]$, they don't admit a probability interpretation, i.e. they are not the probability of an event in some measure space. Value thus obtained is only of relative meaning, and therefore is different from the probability of collision calculated in this paper. The major advantage of working with these quantities is that they are relatively easier to calculate, even in the case when the deterministic trajectories of both aircraft are not constant speed motions, for example, they are piecewise linear motions specified by a set of waypoints. There are various technique to calculate $PC(t)$. For an application of randomize algorithm to such calculation, refer to [15], which also contains bounds on the estimation error in the probabilistic sense.

Chapter 5

Bounds on Approximation Error

In this chapter some preliminary efforts are made to derive theoretical bounds on the error of approximation obtained in the previous chapter.

Consider the following situation: $B_t = (B_t^1, B_t^2)^T$ is a standard 2-D BM starting from the origin. Then $(a,b)^T + B_t$ is the 2-D BM starting from $(a,b)^T$ for some $(a,b)^T \in \mathbf{R}^2$. Denote with $S = \{(x,y)|x \geq 0, y \leq 0\}$ the closed quarter plane. Then $S_t \triangleq S + t \cdot (v,0)^T$ is the quarter plane moving at speed v to the right and with initial position S. Define

$$H^v(a,b) = \{\omega : (a + B_t^1(\omega), b + B_t^2(\omega)) \in S_t \quad \text{for some } t \geq 0\}$$

i.e. H is the event that the 2-D BM starting from (a,b) ever hits the moving quarter plane S_t. Write its probability as:

$$G^v(a,b) \triangleq P(H^v(a,b))$$

We will study the properties of $G^v(a,b)$ as a function of a,b and v. First of all, $G^v(a,b) = 1$ for $(a,b) \in S$ and it is easy to establish the following lemma:

Lemma 2 *For each fixed a, $G^v(a,b)$ is a decreasing function of b, and for each fixed b, $G^v(a,b)$ is an increasing function of a.*

Proof: (Sample path point of view) For each sample path $(B_t^1(\omega), B_t^2(\omega))$ of B_t that hits S_t after a translation of (a_1, b_1), it will also hits S_t after a translation of (a_2, b_2) with $a_2 \geq a_1, b_2 \leq b_1$. In other words, $H^v(a_1,b_1) \subseteq H^v(a_2,b_2)$. ■

We quote the following important property of BM from [2]:

Lemma 3 (Scaling invariant of BM) *If B_t is a 2-D BM with $B_0 = 0$, then for any $\lambda > 0$,*

$$\{\frac{1}{\lambda} B_{\lambda^2 t}, t \geq 0\} \stackrel{d}{=} \{B_t, t \geq 0\}$$

where $\stackrel{d}{=}$ means that the two processes have the same finite dimensional distributions.

In other word, $\frac{1}{\lambda} B_{\lambda^2 t}$ is also a BM (although not independent with B_t). It is remarked here that Lemma 3 is true for BM in $\mathbf{R}^n$ for arbitrary n. Using Lemma 3, a less obvious result about $G^v(a,b)$ can be obtained as:

Proposition 2 *$G^{\lambda v}(\frac{a}{\lambda}, \frac{b}{\lambda}) = G^v(a,b)$ for any $\lambda > 0$.*

Proof: By the definition of $G^v(a,b)$,

$$G^v(a,b) = P(H^v(a,b)) = P(B_t^1 \geq -a + vt \text{ and } B_t^2 \leq -b \quad \text{for some } t \geq 0) \tag{5.1}$$

On the other hand, define $\hat{B}_t^1 \triangleq \frac{1}{\lambda} B_{\lambda^2 t}^1$, $\hat{B}_t^2 \triangleq \frac{1}{\lambda} B_{\lambda^2 t}^2$ and let $t = \lambda^2 s$, we have,

$$\begin{aligned}
& P(B_t^1 \geq -a + vt \text{ and } B_t^2 \leq -b \quad \text{for some } t \geq 0) \\
= \; & P(B_{\lambda^2 s}^1 \geq -a + \lambda^2 vs \text{ and } B_{\lambda^2 s}^2 \leq -b \quad \text{for some } s \geq 0) \\
= \; & P(\hat{B}_s^1 \geq -a/\lambda + \lambda vs \text{ and } \hat{B}_s^2 \leq -b/\lambda \quad \text{for some } s \geq 0) \\
= \; & P(B_s^1 \geq -a/\lambda + \lambda vs \text{ and } B_s^2 \leq -b/\lambda \quad \text{for some } s \geq 0)
\end{aligned}$$

where the last equality follows since $(\hat{B}_t^1, \hat{B}_t^2)$ has the same distribution as (B_t^1, B_t^2) by Lemma 3. By comparison with equation (5.1), the last expression is exactly $G^{\lambda v}(\frac{a}{\lambda}, \frac{b}{\lambda})$. ∎

Let $\lambda = 1/v$ in Proposition 2, we have

$$G^v(a,b) = G^1(av, bv) \triangleq G(av, bv) \tag{5.2}$$

So we need only to investigate $G(a,b)$ instead of $G^v(a,b)$ for every v. Assume $v = 1$ from now on. For (a,b) on the left half plane, *i.e.* $a \leq 0$, a simple bound on $G(a,b)$ can be obtained as follows:

Proposition 3 *$G(a,b) < e^{2a}$ for $a \leq 0$.*

Proof: Denote with $\tau = \inf\{t \geq 0 : a + B_t^1 = t\}$ the first time $(a + B_t^1, b + B_t^2)$ hits the moving half-plane U_t with initial position $U_0 = \{(x,y) : x \geq 0\}$ and velocity $v = 1$ to the right. Then $\{\tau < \infty\} = \{(a + B_t^1, b + B_t^2) \in U_t \text{ for some } t \geq 0\} \triangleq H_U^1(a,b)$. By Lemma 1, τ has probability density function of the form:

$$p_\tau(t) = \frac{|a|}{\sqrt{2\pi t^3}} \exp(-\frac{(|a| + t)^2}{2t})$$

Integrating from 0 to ∞ and using Formula 6 with $x = |a|$ and $v = 1$, we have

$$P(\tau < \infty) = \int_0^\infty p_\tau(t)\, dt = e^{-2|a|} = e^{2a}$$

Notice that $S_t \subseteq U_t$ for all $t \geq 0$ implies $H^1(a,b) \subseteq H_U^1(a,b)$. Hence the conclusion. ∎

The same idea can be applied to get a bound for the case when $b \geq 0$. Suppose (a,b) has polar coordinates (r, θ) with $0 \leq \theta \leq \pi$.

Proposition 4 *$G(a,b) \leq e^{-r(1-\cos\theta)}$.*

Proof: Draw a line l through the origin and at an angle α with the postive x-axis ($0 \leq \alpha \leq \theta$). Suppose u_1 is the projection of u along the direction orthogonal to l (see Figure 5.1). Define $l_t \triangleq l + u_1 \cdot t$. Then event $H^1(a,b) = \{\omega : (a + B_t^1(\omega), b + B_t^2(\omega)) \in S_t \text{ for some } t \geq 0\}$ is contained in the event $\{\omega : (a + B_t^1(\omega), b + B_t^2(\omega)) \in l_t \text{ for some } t \geq 0\}$ which has a probability e^{-2dv_1}. Here $d = r\sin(\theta - \alpha)$ is the distance of (a,b) to l, $v_1 = |u_1| = \sin\alpha$. So

$$G(a,b) \leq \exp[-2r\sin(\theta - \alpha)\sin\alpha] = \exp[-r(\cos(\theta - 2\alpha) - \cos\theta)] \quad \forall\, 0 \leq \alpha \leq \theta \tag{5.3}$$

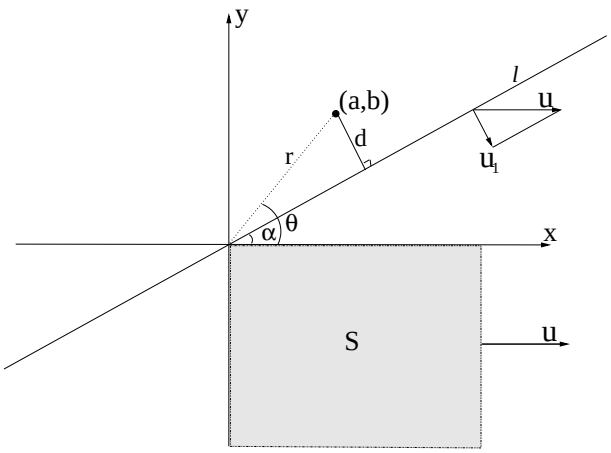

Figure 5.1: Bound for $G(a,b)$ with $b \geq 0$

The conclusion follows by noticing that the RHS of equation (5.3) is minimized at $\alpha = \theta/2$. ■

Basically, Proposition 4 tells us that $G(a,b)$ decreases exponentially fast as (a,b) get farther away from the origin along a certain direction, and the decay rates depend on that particular direction. Due to the simplicity of the idea, it is expected that the bound given in Proposition 4 is a loose one, especially when $a \geq 0, b \geq 0$. Starting from this point, we will focus on the case $a \geq 0, b \geq 0$ and try to get sharper bounds by looking deeper into the event $H^1(a,b)$.

Proposition 5 *For $a \geq 0, b \geq 0$, $G(a,b)$ is bounded by*

$$G(a,b) \leq 2 \int_0^\infty g_a(s) Q(\frac{b}{\sqrt{s}})\, ds \tag{5.4}$$

where $g_a(s)$ is defined as

$$g_a(s) = \frac{1}{\sqrt{2\pi s}} \exp\big[-\frac{(a-s)^2}{2s}\big], \quad \forall s \geq 0 \tag{5.5}$$

Proof: Denote with η the first time $(a + B_1(t), b + B_2(t))$ hits the x axis. Then η has the same distribution as T_b^0, the first time a standard BM starting from the origin hits b, which by Lemma 1, has probability density function:

$$p_\eta(t) = \frac{b}{\sqrt{2\pi t^3}} \exp(-\frac{b^2}{2t}) \qquad t \geq 0$$

Notice that $P(\eta < \infty) = 1$ but $E[\eta] = \infty$. For brevity denote $H = H^1(a,b)$. Then

$$\begin{aligned}
1 - G(a,b) = P(H^c) &= \int_0^\infty p_\eta(t)\, P(H^c|\eta = t)\, dt \\
&= \int_0^\infty p_\eta(t) \int_{-\infty}^t \frac{1}{\sqrt{2\pi t}} \exp\big[-\frac{(x-a)^2}{2t}\big]\, P(H^c|\eta = t, a + B_1(t) = x)\, dx\, dt \\
&= \int_0^\infty p_\eta(t) \int_{-\infty}^t \frac{1}{\sqrt{2\pi t}} \exp\big[-\frac{(x-a)^2}{2t}\big]\, [1 - G(x-t, 0)]\, dx\, dt \qquad (5.6) \\
&\geq \int_0^\infty p_\eta(t) \int_{-\infty}^t \frac{1}{\sqrt{2\pi t}} \exp\big[-\frac{(x-a)^2}{2t}\big][1 - e^{-2(t-x)}]\, dx\, dt \quad \text{(By Proposition 3)} \\
&= \int_0^\infty p_\eta(t) \big[Q(\frac{a-t}{\sqrt{t}}) - Q(\frac{a+t}{\sqrt{t}})e^{2a}\big]\, dt
\end{aligned}$$

Notice that by Formula 4,

$$Q(\frac{a-t}{\sqrt{t}}) - Q(\frac{a+t}{\sqrt{t}})e^{2a} = \int_0^t g_a(s)\, ds$$

So the above inequality can be rewriten as:

$$G(a,b) \leq 1 - \int_0^\infty p_\eta(t) \int_0^t g_a(s)\, ds\, dt = 1 - \int_0^\infty g_a(s) \int_s^\infty p_\eta(t)\, dt\, ds = 2\int_0^\infty g_a(s) Q(\frac{b}{\sqrt{s}})\, ds \qquad (5.7)$$

In the last step we use the fact that $\int_0^s p_\eta(t)\, dt = 2Q(b/\sqrt{s})$ and $\int_0^\infty g_a(s)\, ds = 1$ which follow from Formula 4 and Formula 5 in Appendix A respectively. ■

The reason why we prefer bound given by equation (5.4) than that given by the last equation of (5.6) is becasue $E[\eta] = \infty$, hence $p_\eta(t)$ tends to have a large tail, making numerical integration more difficult. While in equation (5.4), $g_a(s)$ is the probability density function of some random variable T_a with $E[T_a] = a + 1$ and $\mathrm{Var}[T_a] = a + 2$ (see Formula 5). Since much of the density of $g_a(s)$ concentrates around $E[T_a]$, it is expected that

$$2\int_0^\infty g_a(s) Q(\frac{b}{\sqrt{s}})\, ds \simeq 2Q(\frac{b}{\sqrt{a+1}}) \qquad (5.8)$$

Level curves for both sides of equation (5.8) are shown in Figure 5.2. It can be seen that the dicrepency between them is barely observable except when both a and b are very small. We conjecture that the right hand side of equation (5.8) is still a valid bound for $G(a,b)$.

Using Proposition 2 and the above approximation, we know that $G^v(a,b) = G(av, bv)$ is bounded approximately by $Q(bv/\sqrt{av+1})$ which by the following lemma decreases to 0 at the same speed as $\frac{1}{\sqrt{v}} e^{-v/2}$ as $v \to \infty$ for any fixed a and b, even faster than exponentially.

Lemma 4 ([2]) *$Q(x) = \int_x^\infty \frac{1}{\sqrt{2\pi}} \exp(-t^2/2)\, dt$ satisfies:*

$$(\frac{1}{x} - \frac{1}{x^3})e^{-x^2/2} \leq \sqrt{2\pi} Q(x) \leq \frac{1}{x} e^{-x^2/2} \qquad \forall x > 0$$

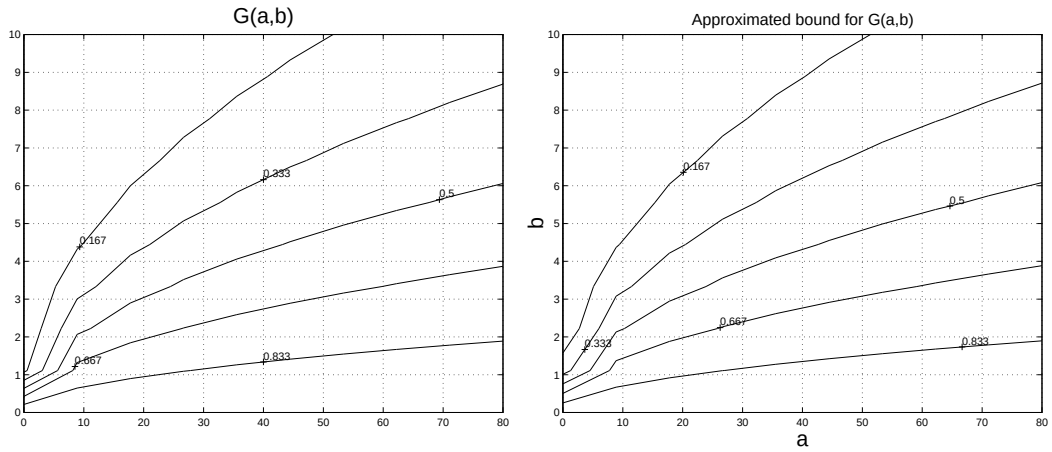

Figure 5.2: Level curves: Left: $2\int_0^\infty g_a(s)Q(\frac{b}{\sqrt{s}})\,ds$ Right: $2Q(\frac{b}{\sqrt{a+1}})$

To get bounds which are easier to compute than the one given in equation (5.4), we can use the observation that $g_a(s)$ concentrates near $a+1$ and $Q(b/\sqrt{s})$ is an increasing function of s. We omit the detail here.

In the case $a = 0$, Proposition 5 takes an especially simple form.

Corollary 1 *$G(0,b) \le \frac{2}{\pi}\int_0^{\frac{\pi}{2}} e^{-\frac{b}{\sin\beta}}\,d\beta$ for all $b \ge 0$.*

Proof: Using Proposition 5 and the transform $z = \tan\theta$, we have

$$\begin{aligned} G(0,b) &\le 2\int_0^\infty \frac{1}{\sqrt{2\pi s}}\exp(-\frac{s}{2})Q(\frac{b}{\sqrt{s}})\,ds \\ &= 2\int_0^\infty \frac{1}{\sqrt{2\pi s}}\exp(-\frac{s}{2})\int_{b/s}^\infty \frac{\sqrt{s}}{\sqrt{2\pi}}\exp(-\frac{z^2 s}{2})\,dz\,ds \\ &= 2\int_0^\infty \int_{b/z}^\infty \frac{1}{2\pi}\exp(-\frac{(1+z^2)s}{2})\,ds\,dz \\ &= 2\int_0^\infty \frac{1}{\pi(1+z^2)}\exp(-\frac{(1+z^2)b}{2z})\,dz \\ &= 2\int_0^{\frac{\pi}{2}} \frac{1}{\pi}\exp(-\frac{b}{\sin(2\theta)})\,d\theta \end{aligned} \tag{5.9}$$

Conclusion follows if we let $\beta = 2\theta$ and note the symmetry about $\frac{\pi}{2}$ of the resulting integrand. ■

Remark 4 It will be helpful at this point to make a comparison between the new bound we have just derived in Corollary 1 with that given by Proposition 4, which reduces to e^{-b} in the case $a = 0$ and $b \ge 0$. As is easily verified, the bound given in Corollary 1 is strictly less than e^{-b} for all b and is actually a higher order infinitesmal than e^{-b} as $b \to \infty$. So our extra work is rewarded with a sharper bound on $G(a,b)$.

Now we can analyze the general situation we encountered in the overtake case of Chapter 4. Consider the following situation: In Figure 5.3, a rectangular box is moving at speed v to the right

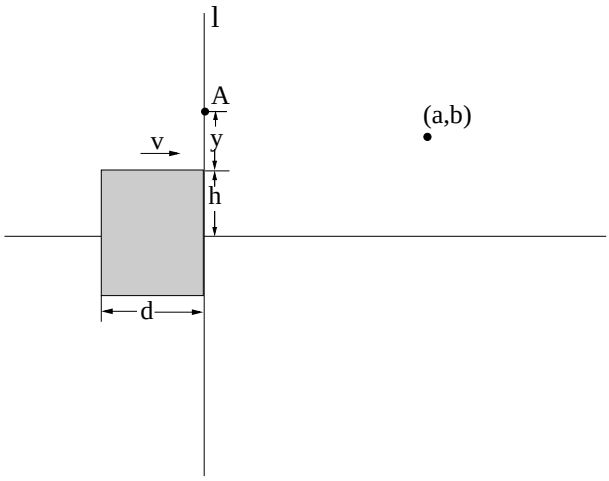

Figure 5.3: moving box

with initial position $\{(x,y) : |x + d/2| \le d/2, |y| \le h\}$. Define $F^v(a,b)$ to be the probability that 2-D BM starting from $(a,b)^T$ will ever hit the moving box. For example let the BM start from point $A = (0,z)^T$ on the line l where $z = h + y$ for some $y > 0$. Then by Proposition 5,

$$F^v(0,z) \le G^v(d,y) \le 2\int_0^\infty g_{dv}(s)Q(\frac{yv}{\sqrt{s}})\,ds \tag{5.10}$$

Notice that $F^v(0,z)$ is symmetric in z and $F^v(0,z) = 1$ for $|z| \le h$, so if we define

$$K(z) = \begin{cases} 2\int_0^\infty g_{dv}(s)Q(\frac{(|z|-h)v}{\sqrt{s}})\,ds, & \text{if } |z| > h \\ 1, & \text{if } |z| \le h. \end{cases} \tag{5.11}$$

Then we have

$$1_{(|z|\le h)} \le F^v(0,z) \le K(z), \quad \forall z \in \mathbf{R}^1. \tag{5.12}$$

For general $(a,b)^T \in \mathbf{R}^2$ satisfying $a \ge 0$, we can condition on the time τ that the BM starting from $(a,b)^T$ first hits the moving line l to get:

$$F^v(a,b) = \int_0^\infty p_\tau(t)\int \frac{1}{\sqrt{2\pi t}}\exp\big[-\frac{(x-b)^2}{2t}\big]F^v(0,x)\,dx\,dt \tag{5.13}$$

where $p_\tau(t)$ is the probability density function of τ:

$$p_\tau(t) = \frac{a}{\sqrt{2\pi t}}\exp\big[-\frac{(a-vt)^2}{2t}\big], \quad \forall t \ge 0$$

Combining equation (5.11), (5.12) and (5.13), we have

Proposition 6 *$F^v(a,b)$ can be bounded by*

$$\begin{aligned} F^v(a,b) &\ge \int_0^\infty p_\tau(t)\big[Q(\frac{x-h-b}{\sqrt{t}}) - Q(\frac{x+h-b}{\sqrt{t}})\big]\,dx\,dt \\ F^v(a,b) &\le 2\int_0^\infty p_\tau(t)\int \frac{1}{\sqrt{2\pi t}}\exp\big[-\frac{(x-b)^2}{2t}\big]K(x)\,dx\,dt \end{aligned} \tag{5.14}$$

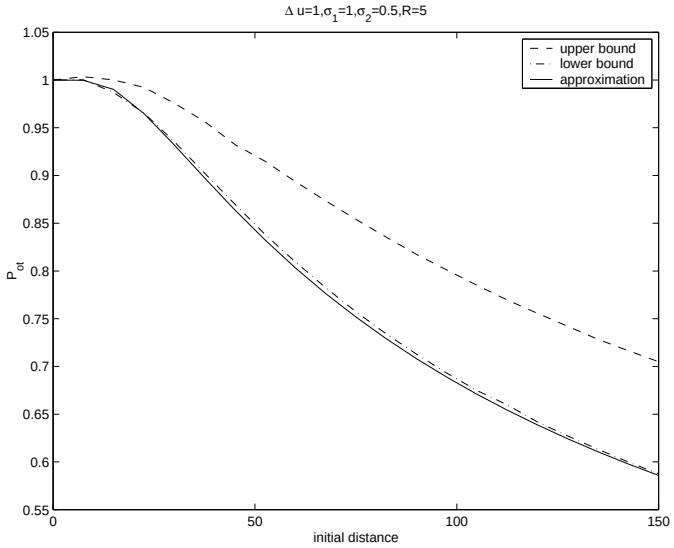

Figure 5.4: Lower and upper bounds on P_{ot}

To get a feeling of its implication, take as an example the aircraft overtake case, where $\Delta u = 1$ nmi/min, $R = 5$ nmi, $\sigma_1 = 1$, $\sigma_2 = 0.5$. Then $d = 2R/\sigma_1 = 10$, $h = L = R/\sigma_2 = 10$, $v = \Delta u/\sigma_1 = 1$. We have encounter this situation before in Chapter 4 (see Figure 4.2). The simulation result of the above proposition is shown in Figure 5.4. We use numerical integration to evaluate equation (5.14). Since $K(x)$ can be calculated by equation (5.11) beforehand and once for all, this will leads to a double integration for which *dblquad* function in MATLAB is used for evaluation. Solid line shows the approximated PC calculated by equation (4.5). It can be observed that even when Δu is small, the upper bound and lower bound are reasonably close to each other. As Δu gets bigger and bigger, the gap between them will become more and more narrow until closing up completely when $\Delta u = \infty$. Furthermore, in this case we are actually dealing with an eclipse encapulated within the box, so the upper and lower bound should be even closer to each other if we redefine $F^v(a, b)$ as the hitting probability of BM starting from $(a, b)^T$ hitting this moving ellispe.

Remark 5 For the general collision and near miss cases, similar procedures as above can be carried out to obtain bounds for the approximated PC. In addition, there are some obvious ways to refine the bounds obtained in this chapter, which we will not pursue here due to the existence of bounds on the time and energy that can be spend.

Part II

Conflict Resolution

Chapter 6

Classification of Resolution Maneuvers

In this chapter, we will try to classify qualitatively different resolution maneuvers involving multiple aircraft. Although this notion has been explicitly or inexplicitly taken into consideration by most researchers on multi-aircraft resolution, often under different names, for example, "cross pattern" in [4], a formal treatment has never appeared before. The main point of this chapter is that the structure of this problem is more subtle than merely combinatorial, though not subtle enough to elude a mathematical description. In fact, is is found that the types of resolution maneuvers involving n aircraft have a one-to-one correspondence with the elements of the *braid group* $\mathbf{B}_n$.

In the following, we will start from the simplest two aircraft case and clarify what we mean by "qualitatively different". It is found the the angle one aircraft turns with respect to the other during the maneuver plays a central role in classifying the type of maneuver. Similar technique can be extended to the multiple aircraft case to get all the "fundamental" types. However, although this leads to a complete classification of two aircraft case, it is generally not the case for multiple aircraft case. For this purpose, the notion of braid will be introduced.

6.1 Two Aircraft Case

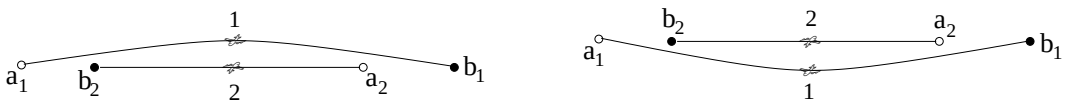

Figure 6.1: Head-on conflict resolution. Left: Maneuver 1, Right: Maneuver 2

Consider two aircraft, starting from a_1 and a_2 (marked with hollow circles in Figure 6.1) at time t_0 and trying to arrive at destinations b_1 and b_2 (marked with solid circles) at time t_f respectively. If both of them fly strictly according to their pre-arranged flight plans which are the constant velocity motions along the lines joining their starting points and destinations respectively, then a conflict, which is defined as the event that the distance of two aircraft falls below some safe distance, (say, R), is projected to happen somewhere between t_0 and t_f.

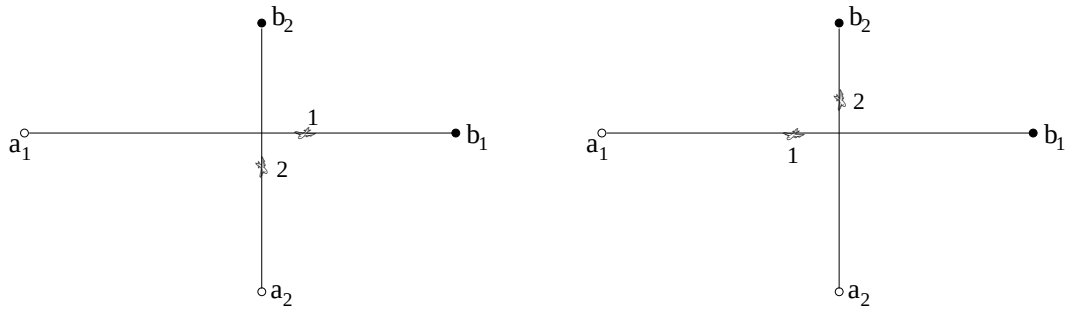

Figure 6.2: Resolution for conflict at an angle 90°. Left: Maneuver 1, Right: Maneuver 2

As shown in Figure 6.1, two resolution maneuvers can be proposed to resolve the head-on conflict arising in this situation. Intuitively, these two maneuvers are qualitatively distinctive in the sense that switching from one to the other can not be done smoothly without incurring situations of higher danger of conflict. Therefore, if one maneuver is chosen, it is preferable to stick to it during the time interval $[t_0, t_f]$. Qualitatively different maneuvers for another conflict configuration are shown in Figure 6.2 in which the original unresolved motions of two aircraft are at a right angle to each other. The above ideas will be made precise in this section.

Define $\mathbf{P}_1$ as the space of all continuous paths joining a_1 to b_1:

$$\mathbf{P}_1 \triangleq \{\alpha \in C(T_h, \mathbf{R}^2) : \alpha(t_0) = a_1, \alpha(t_f) = b_1\}$$

where $T_h = [t_0, t_f]$, and $C(T_h, \mathbf{R}^2)$ consists of all the continuous maps from T_h to $\mathbf{R}^2$. Similarly

$$\mathbf{P}_2 \triangleq \{\beta \in C(T_h, \mathbf{R}^2) : \beta(t_0) = a_2, \beta(t_f) = b_2\}$$

$\mathbf{P}_1$ and $\mathbf{P}_2$ inherit the uniform convergence metric D_1 and D_2 from $C(T_h, \mathbf{R}^2)$ respectively, *e.g.*

$$D_1(\alpha_1, \alpha_2) = \sup_{t \in T_h} ||\alpha_1(t) - \alpha_2(t)|| \quad \text{for } \alpha_1, \alpha_2 \in \mathbf{P}_1,$$

Denote $\mathbf{P} = \mathbf{P}_1 \times \mathbf{P}_2$. We will call each element of $\mathbf{P}$ a (joint) *maneuver* of two aircraft. *Minimum Separation over Encounter (MSE)* for each maneuver $(\alpha, \beta) \in \mathbf{P}$ is defined as:

$$\Delta(\alpha, \beta) = \inf_{t \in T_h} ||\alpha(t) - \beta(t)|| \tag{6.1}$$

It is easily seen that $\Delta : \mathbf{P} \to \mathbf{R}$ is continuous since

$$||\Delta(\alpha_1, \beta_1) - \Delta(\alpha_2, \beta_2)|| \leq D_1(\alpha_1, \alpha_2) + D_2(\beta_1, \beta_2) \quad \forall \alpha_1, \alpha_2 \in \mathbf{P}_1, \forall \beta_1, \beta_2 \in \mathbf{P}_2$$

We are interested in those maneuvers with a MSE at least R for some prescribed safe distance R (usually taken to be 5 nautical miles in the current ATMS). Therefore define

$$\mathbf{P}(R) \triangleq \mathbf{P} \setminus \Delta^{-1}([0, R]) = \{(\alpha, \beta) \in \mathbf{P} : \Delta(\alpha, \beta) > R\}$$

We distinguish different maneuvers according to the following equivalence relation ($I = [0, 1]$):

Definition 1 *An R-homotopy between two maneuvers (α_1, β_1) and (α_2, β_2) in $\mathbf{P}(R)$ is a continuous map $H : I \times T_h \to \mathbf{R}^4$ (or $H = (H_1, H_2)$ where H_1, H_2 are continuous maps from $I \times T_h$ to $\mathbf{R}^2$) satisfying:*

1. $H(0,\cdot) = (H_1(0,\cdot), H_2(0,\cdot)) = (\alpha_1, \beta_1)$;
2. $H(1,\cdot) = (H_1(1,\cdot), H_2(1,\cdot)) = (\alpha_2, \beta_2)$;
3. *For any $s \in I$, $H_1(s,\cdot) \in \mathbf{P}_1$, $H_2(s,\cdot) \in \mathbf{P}_2$ and $\Delta(H_1(s,\cdot), H_2(s,\cdot)) > R$.*

Alternatively, an R-homotopy can be viewed as a continuous path in $\mathbf{P}(R)$ joining (α_1, β_1) to (α_2, β_2). Two maneuvers (α_1, β_1) and (α_2, β_2) in $\mathbf{P}(R)$ are called *R-homotopic* (denoted as $(\alpha_1, \beta_1) \overset{R}{\sim} (\alpha_2, \beta_2)$) if and only if there exists an R-homotopy between them, or alternatively, if and only if they are in the same connected component of $\mathbf{P}(R)$.

We will try to determine structure of connected components of $\mathbf{P}(R)$. Compared with the classical fundamental group problem in algebraic topology, the problem discussed here is harder since it not only deals with trajectories, but also with their parameterizations. For example, it is not immediately obvious that the two maneuvers shown in Figure 6.1 are not R-homotopic. However, it turns out that the two problems are intimately related as can be illustrated by the following simple transformation.

For the sake of brevity, we focus on the case $R = 0$. The discussion for this case applied without much modification to the case for any $R > 0$. Then $\mathbf{P}(0)$ consists of all those maneuvers such that a strict collision does not happen during T_h (two aircraft are viewed as points in $\mathbf{R}^2$). Fixed a global coordinate system in $\mathbf{R}^2$, and denote with $\mathbf{S}^1$ the unit circle equipped with the usual topology. Then each $(\alpha, \beta) \in \mathbf{P}(0)$ define a path $\Psi(\alpha, \beta)$ in $\mathbf{S}^1$ in the following way: for each $t \in T_h$, since $\alpha(t) \neq \beta(t)$, together they determine a direction in $\mathbf{R}^2$ (measured from $\alpha(t)$ to $\beta(t)$), or equivalently, a point $\Psi(\alpha, \beta)(t)$ in $\mathbf{S}^1$. More formally, define equivalence relation $\propto$ on $\mathbf{R}^2 \setminus \{0\}$ as:

$$x \propto y \text{ if and only if } x = \lambda y \quad \text{for some } \lambda > 0 \quad \forall x, y \in \mathbf{R}^2 \setminus \{0\}$$

Then the quotient space $\mathbf{R}^2 \setminus \{0\} / \propto$ can be identified with $\mathbf{S}^1$. Denote with $[x]$ the $\propto$-equivalence class x belongs to. Then $\Psi(\alpha, \beta) : T_h \to \mathbf{S}^1$ is defined by:

$$\Psi(\alpha, \beta)(t) = [\beta(t) - \alpha(t)] \quad \forall t \in T_h \tag{6.2}$$

which is easily seen to be continuous in t.

Summing up the procedure described above, we have actually defined a map $\Psi : \mathbf{P}(0) \to \mathbf{P}_S$ where

$$\mathbf{P}_S \triangleq \{\gamma \mid \gamma : T_h \to \mathbf{S}^1 \text{ is continuous, } \gamma(t_0) = [a_2 - a_1],\ \gamma(t_f) = [b_2 - b_1]\}$$

Let $\mathbf{P}_S$ be equipped with the uniformly convergence metric. By the compactness of T_h we have

Lemma 5 *$\Psi : \mathbf{P}(0) \to \mathbf{P}_S$ is continuous.*

Similar to Definition 1, two elements $\gamma_1, \gamma_2 \in \mathbf{P}_S$ is homotopic if there exists a homotopy between them, *i.e.* a continuous map $H' : I \times T_h \to \mathbf{S}^1$ such that

1. $H'(0,\cdot) = \gamma_1(\cdot)$, $H'(1,\cdot) = \gamma_2(\cdot)$.

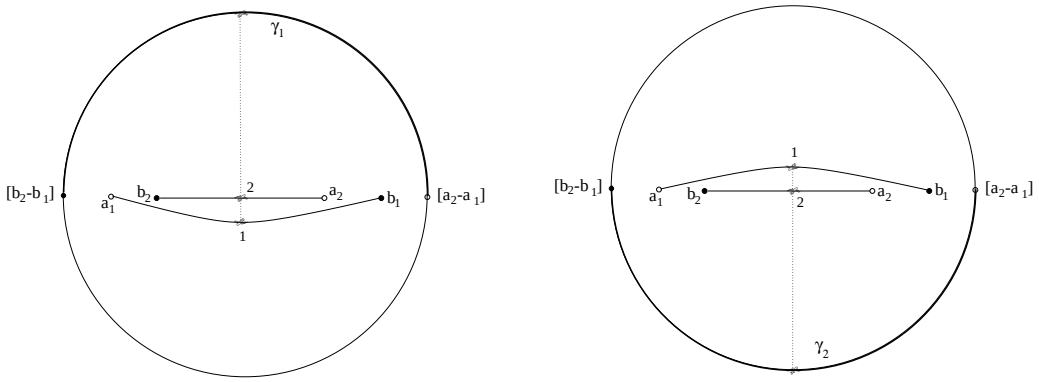

Figure 6.3: Induced paths in $\mathbf{S}^1$

2. $H'(s,t_0) = [a_2 - a_1]$, $H'(s,t_f) = [b_2 - b_1]$ for all $s \in I$.

Lemma 6 *For any two maneuvers* $(\alpha_1,\beta_1),(\alpha_2,\beta_2) \in \mathbf{P}(0)$, *if* $(\alpha_1,\beta_1) \overset{0}{\sim} (\alpha_2,\beta_2)$, *then* $\Psi(\alpha_1,\beta_1)$ *and* $\Psi(\alpha_2,\beta_2)$ *are homotopic in* $\mathbf{P}_S$.

Proof: Let $H : I \times T_h \to \mathbf{R}^4$ be the 0-homotopy between (α_1,β_1) and (α_2,β_2). Then $H(s,\cdot) = (H_1(s,\cdot), H_2(s,\cdot))$ can be viewed as a continuous map from I to $\mathbf{P}(0)$ joining (α_1,β_1) to (α_2,β_2) and $H' = \Psi \circ (H_1,H_2)$ gives the desired homotopy in $\mathbf{P}_S$ between $\Psi(\alpha_1,\beta_1)$ and $\Psi(\alpha_2,\beta_2)$. ■

Shown in Figure 6.3 are the Ψ transformations for the two maneuvers in Figure 6.1. Since the fundamental group of $\mathbf{S}^1$ is $\pi_0(\mathbf{S}^1) = \mathbf{Z}$, we have actually proved that the two maneuvers are not 0-homotopic. In other word, there is no way of continuously deforming one to the other without incurring collision somewhere in the middle. However, for a thorough classification of maneuvers, we need the following more technical lemma:

Lemma 7 *For any two maneuvers* $(\alpha_1,\beta_1),(\alpha_2,\beta_2) \in \mathbf{P}(0)$, *if* $\Psi(\alpha_1,\beta_1)$ *and* $\Psi(\alpha_2,\beta_2)$ *are homotopic in* $\mathbf{P}_S$, *then* $(\alpha_1,\beta_1) \overset{0}{\sim} (\alpha_2,\beta_2)$.

Proof: Let $H' : I \times T_h \to \mathbf{S}^1$ be the homotopy in $\mathbf{S}^1$ between $\Psi(\alpha_1,\beta_1)$ and $\Psi(\alpha_2,\beta_2)$. We need only to construct a homotopy H_1 in $\mathbf{P}_1$ between α_1 and α_2 and a homotopy H_2 in $\mathbf{P}_2$ between β_1 and β_2 such that for each $s \in I$, $\Delta(H_1(s,\cdot), H_2(s,\cdot)) > 0$. To this end, H_1 can be chosen to be:

$$H_1(s,t) = (1-s)\cdot\alpha_1(t) + s\cdot\alpha_2(t), \quad \forall s \in I, t \in T_h$$

Define $R : I \times T_h \to \mathbf{R}$ as:

$$R(s,t) = (1-s)||\alpha_1(t) - \beta_1(t)|| + s||\alpha_2(t) - \beta_2(t)||, \quad \forall s \in I, t \in T_h$$

Since $(\alpha_1,\beta_1),(\alpha_1,\beta_1) \in \mathbf{P}(0)$ and I is compact, we have

$$\inf_{s\in I, t\in T_h} R(s,t) > 0$$

Identifying each element of $\mathbf{S}^1$ with an angle and denoting with $(r,\theta)_{polar} = (r\cos\theta, r\sin\theta)$ the point in $\mathbf{R}^2$ with radius r and phase angle θ, we can define $H_2 : I \times T_h \to \mathbf{P}_2$ as

$$H_2(s,t) = H_1(s,t) + (R(s,t), H'(s,t))_{polar}$$

It is easily verified that (H_1, H_2) is the desired homotopy in $\mathbf{P}(0)$ between (α_1, β_1) and (α_2, β_2). ■

Assembling the results obtained so far, we get

Theorem 1 *Two maneuvers $(\alpha_1, \beta_1), (\alpha_2, \beta_2) \in \mathbf{P}(0)$ are 0-homotopic if and only if $\Psi(\alpha_1, \beta_1)$ and $\Psi(\alpha_2, \beta_2)$ are homotopic in $\mathbf{S}^1$.*

Remark 6 Several remarks are evident at this point.

- The conclusion of Theorem 1 remains valid if we change "0-homotopic" and "$\mathbf{P}(0)$" to "R-homotopic" and "$\mathbf{P}(R)$" respectively for any $R > 0$.
- It might be more illuminating in the above deduction if instead of the map Ψ, we use the map $(\alpha, \beta) \mapsto \beta - \alpha$, and transform the problem into determining the homotopy types of all paths in $\mathbf{R}^2 \setminus B(0, R)$ starting from $b_1 - a_1$ and ending at $b_2 - a_2$. However, we adopt Ψ since it captures the key notion in classifying different maneuvers, *i.e.* it is the number and direction of turns one aircraft makes with respect to the other during the maneuver that determine its qualitative type.

Corollary 2 *Fix the starting points and ending points of the two aircraft, say, as show in Figure 6.1, then each resolution maneuver (α, β) is homotopic to exactly one of the following:*

1. *Maneuver 1 in Figure 6.1;*
2. *Maneuver 2 in Figure 6.1;*
3. *Maneuver 1 followed by the motion that aircraft 2 stays at b_2, aircraft 1 starts from b_1, circles around aircraft 2 n time clockwise for some $n \geq 1$ and returns to b_1.*
4. *Maneuver 2 followed by the motion that aircraft 2 stays at b_2, aircraft 1 starts from b_1, circles around aircraft 2 n time counterclockwise for some $n \geq 1$ and returns to b_1.*

In reality, unless in airspace with high air traffic density such as those near airport, it is usually implausible that one aircraft turns more than 360° during one maneuver. Define the *fundamental* maneuver as those for which one aircraft turns less than 360° in whichever direction with respect to the other. Then the above corollary says that there is exactly two fundamental types of maneuvers for two aircraft resolution.

6.2 Multiple Aircraft Case

Now consider the general scenario in which there are n aircraft with starting position $a_1, \cdots, a_n$ and destination position $b_1, \cdots, b_n$ respectively. Similar to Section 6.1, we define

$$\mathbf{P}_i \triangleq \{\alpha \in C(T_h, \mathbf{R}^2) : \alpha(t_0) = a_i, \alpha(t_f) = b_i\}, \quad i = 1, \cdots, n$$

Each element $(\alpha_1, \cdots, \alpha_n)$ of $\mathbf{P} \triangleq \prod_{i=1}^{n} \mathbf{P}_i$ is called a (joint) maneuver and its minimal separation over encounter (MSE) is defined as:

$$\Delta(\alpha_1, \cdots, \alpha_n) = \min_{1 \leq i < j \leq n} \Delta_{ij}(\alpha_i, \alpha_j) \quad \forall \alpha_k \in \mathbf{P}_k,\ k = 1, \cdots, n$$

where $\Delta_{ij}(\alpha_i, \alpha_j)$ is the MSE between α_i and α_j defined in (6.1) of Section 6.1 with $\mathbf{P}_i$ and $\mathbf{P}_j$ in the place of $\mathbf{P}_1$ and $\mathbf{P}_2$ respectively. Let $\mathbf{P}(R) \triangleq \mathbf{P} \setminus \Delta^{-1}([0, R])$ be the set of all maneuvers with a MSE greater than R. Two maneuvers $(\alpha_1, \cdots, \alpha_n)$ and $(\beta_1, \cdots, \beta_n)$ in $P(R)$ are *R-homotopic* if there exists an *R-homotopy* H between them, *i.e.* a map $H = (H_1, \cdots, H_n) : I \times T_h \to \mathbf{R}^{2n}$ satisfying:

1. $H(0, \cdot) = (H_1(0, \cdot), \cdots, H_n(0, \cdot)) = (\alpha_1(\cdot), \cdots, \alpha_n(\cdot))$;
2. $H(1, \cdot) = (H_1(1, \cdot), \cdots, H_n(1, \cdot)) = (\beta_1(\cdot), \cdots, \beta_n(\cdot))$;
3. $H(s, \cdot) = (H_1(s, \cdot), \cdots, H_n(s, \cdot)) \in \mathbf{P}(R)$ for all $s \in I$.

This equivalence relation partitions $\mathbf{P}(R)$ into disjoint components and it is the task of this section to determine the structure of these components.

Similar to Section 6.1, for each aircraft pair i and j, we can define a map $\Psi_{ij} : (\mathbf{P}_i \times \mathbf{P}_j) \setminus \Delta_{ij}^{-1}([0, R]) \to \mathbf{P}_{ij}^S$ as in (6.2) with $\mathbf{P}_i$ and $\mathbf{P}_j$ in the place of $\mathbf{P}_1$ and $\mathbf{P}_2$ respectively. Here $\mathbf{P}_{ij}^S$ is the set of all paths in $\mathbf{S}^1$ starting from $[a_j - a_i]$ and ending at $[b_j - b_i]$. Therefore $\Psi = \prod_{1 \le i < j \le n} \Psi_{ij}$ defines a continuous map from $\mathbf{P}$ to $\mathbf{P}^S \triangleq \prod_{1 \le i < j \le n} \mathbf{P}_{ij}^S$ which maps $(\alpha_1, \cdots, \alpha_n)$ to $(\Psi_{ij}(\alpha_i, \alpha_j))_{1 \le i < j \le n}$. Homotopy in $\mathbf{P}^S$ is defined in an obvious way. The proof of the following proposition is similar to that of Lemma 6.

Proposition 7 *If two maneuvers $(\alpha_1, \cdots, \alpha_n)$ and $(\beta_1, \cdots, \beta_n)$ in $\mathbf{P}(R)$ are R-homotopic, then $\Psi(\alpha_1, \cdots, \alpha_n)$ and $\Psi(\beta_1, \cdots, \beta_n)$ are homotopic in $\mathbf{P}^S$.*

Since homotopy in product space induces homotopy in each coordinate space naturally, we have

Corollary 3 *If two maneuvers $(\alpha_1, \cdots, \alpha_n)$ and $(\beta_1, \cdots, \beta_n)$ in $\mathbf{P}(R)$ are R-homotopic, then for each pair $1 \le i < j \le n$, (α_i, α_j) and (β_i, β_j) are R-homotopic in $(\mathbf{P}_i \times \mathbf{P}_j) \setminus \Delta_{ij}^{-1}([0, R])$.*

In other word, if the 2-joint maneuver for any pair of aircraft is not R-homotopic, then the n-joint maneuvers are not R-homotopic. Therefore there are at least $2^{n(n-1)/2}$ different types of maneuver for n-aircraft resolution. Shown in Figure 6.4 are the plots of 8 qualitatively distinctive maneuvers for 3 aircraft case. We assume as in reality no backward motion for any aircraft and place the aircraft symbol in such a way that there is no confusion for each aircraft pair as for which one passes the cross point first.

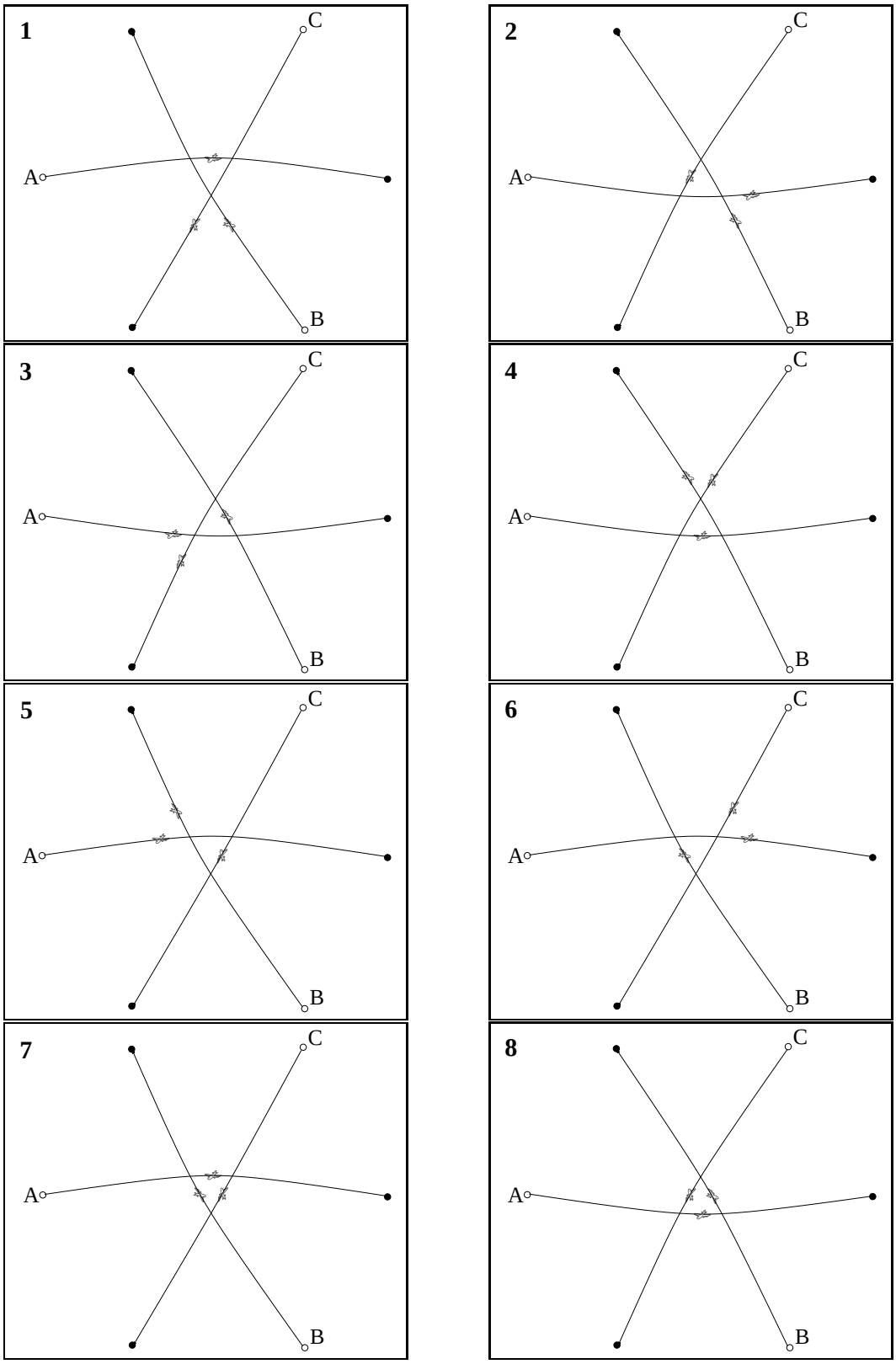

Figure 6.4: Fundamental types of resolution for conflict involving 3 aircraft

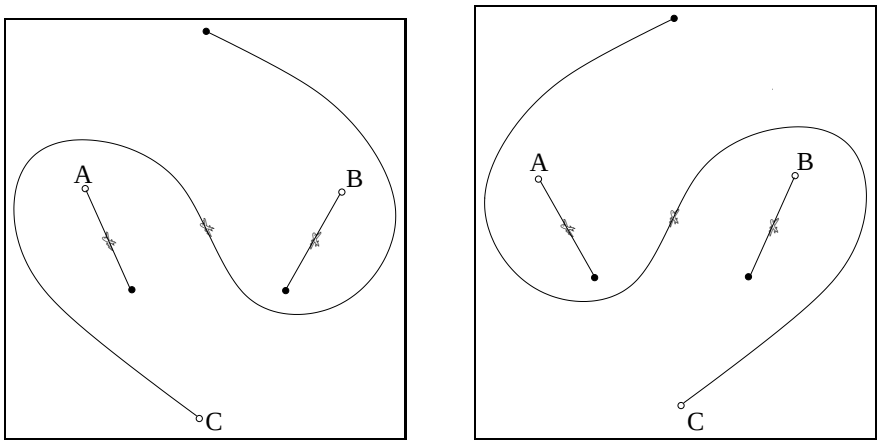

Figure 6.5: two different maneuvers with the same Ψ images

Unfortunately, unlike the 2 aircraft case, the converse of Proposition 7 is not true when $n > 2$. Figure 6.5 show two maneuvers with the same Ψ images but are not R-homotopic.

For a thorough classification of resolution maneuvers, we need the following concepts: (For the same reason as in the previous subsection we assume $R = 0$, thus $\mathbf{P}(0)$ contains all maneuvers without strict collision). Each maneuver $\alpha = (\alpha_1, \cdots, \alpha_n) \in \mathbf{P}(0)$ can be extended to a map $\hat{\alpha} : T_h \to \mathbf{R}^2 \times T_h$ by attaching the time as the last coordinate, *i.e.*

$$\hat{\alpha}(t) = (\alpha_1(t), \cdots, \alpha_n(t), t), \quad \forall t \in T_h$$

which has a natural representation as a pure n-braid. An *n-braid* joining $\mathbf{a} = (a_1, \cdots, a_n) \in \mathbf{R}^{2n}$ to $\mathbf{b} = (b_1, \cdots, b_n) \in \mathbf{R}^{2n}$ is a set of n curves $\{\gamma_1, \cdots, \gamma_n\}$ in $\mathbf{R}^2 \times T_h \subset \mathbf{R}^3$ satisfying

- Each point (a_i, t_0) is joined by exactly one curve in $\{\gamma_1, \cdots, \gamma_n\}$ to one of the point (b_j, t_f) for some $1 \leq j \leq n$ (i and j are not necessarily identical);
- The plane $z = t$ intersects each curve at exactly one point if $t_0 \leq t \leq t_f$ and none otherwise;
- $\gamma_i \cap \gamma_j = \emptyset$ whenever $i \neq j$.

To avoid technicality in the topology of $\mathbf{R}^3$, the following assumption is further assumed, which, considering the nature of the problem we are dealing with, is purely pedagogical.

- Each curve is (or can be deformed continuously without intersecting other curves into) a finite polygonal curve which consists of finite number of straight line segments piecing together.

We denote the set of all such braids as $\mathbf{B}(\mathbf{a}, \mathbf{b})$. If in the first assumption (a_i, t_0) is required to be joined to (b_i, t_f) for the same i, then the braid is called *pure*. The set of all pure braids is denoted as $\mathbf{PB}(\mathbf{a}, \mathbf{b})$. Evidently $\alpha \mapsto \hat{\alpha}$ is a one-to-one correspondence between maneuver in $\mathbf{P}(0)$ and pure braid in $\mathbf{PB}(\mathbf{a}, \mathbf{b})$. One example is shown in Figure 6.6. Broken line segments are used to indicate which curve is in the front.

Two braids $\hat{\alpha}, \hat{\beta}$ in $\mathbf{B}(\mathbf{a}, \mathbf{b})$ are said to be *string isotopic* (denoted as $\hat{\alpha} \sim \hat{\beta}$) if there exists a continuous deformation of one to the other satisfying all four assumptions above throughout the

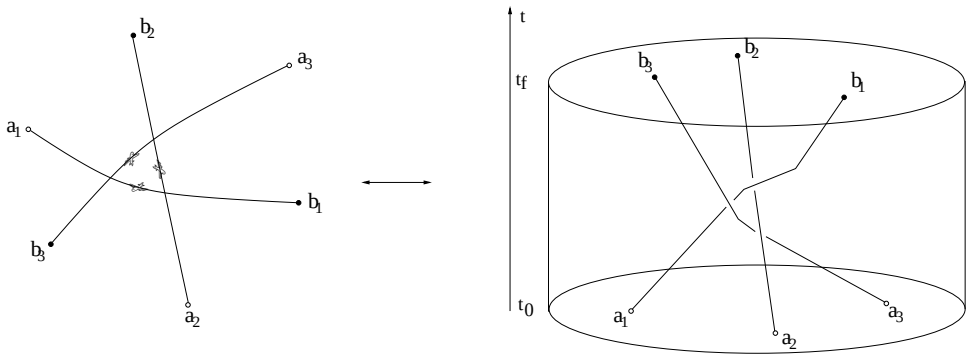

Figure 6.6: Maneuver and its braid representation

deformation. String isotopy is obviously an equivalence relation on $\mathbf{B}(\mathbf{a},\mathbf{b})$ and the equivalence class $\hat{\alpha}$ belongs to is denoted $\langle\hat{\alpha}\rangle$. It is clear from the definition of map $\alpha \mapsto \hat{\alpha}$ that

Proposition 8 *Any two maneuvers α,β in $\mathbf{P}(0)$ are 0-homotopic if and only if $\hat{\alpha}$ and $\hat{\beta}$ are string isotopic.*

There is a canonical way of defining product operation on braids. Given braid $\hat{\alpha} \in \mathbf{B}(\mathbf{a},\mathbf{b})$ and $\hat{\beta} \in \mathbf{B}(\mathbf{b},\mathbf{c})$, their product $\hat{\gamma} = \hat{\beta}\cdot\hat{\alpha} \in \mathbf{B}(\mathbf{a},\mathbf{c})$ is defined to be the knot joining $\mathbf{a}$ to $\mathbf{c}$ obtained by concatenating the n curves of $\hat{\beta}$ with those of $\hat{\alpha}$ and then re-normalizing the t axis back to T_h, *i.e.* $\hat{\gamma}(t) = (\gamma_1(t),\cdots,\gamma_n(t),t)$ for $t \in T_h$ with

$$\gamma_i(t) = \begin{cases} \alpha_i(2t-t_0) & t_0 \le t \le \frac{t_0+t_f}{2}; \\ \beta_i(2t-t_f) & \frac{t_0+t_f}{2} \le t \le t_f \end{cases} \qquad i = 1,\cdots,n$$

This product operation respects string isotopy in the sense that

Lemma 8 *If $\hat{\alpha} \sim \hat{\alpha}' \in \mathbf{B}(\mathbf{a},\mathbf{b})$ and $\hat{\beta} \sim \hat{\beta}' \in \mathbf{B}(\mathbf{b},\mathbf{c})$, then $\hat{\beta}\cdot\hat{\alpha} \sim \hat{\beta}'\cdot\hat{\alpha}' \in \mathbf{B}(\mathbf{a},\mathbf{c})$.*

The proof of this lemma is straightforward and hence omitted. Therefore there induces a product operation on the isotopy classes of braids denoted as $\langle\hat{\alpha}\rangle\cdot\langle\hat{\beta}\rangle$ and the associative law $(\langle\hat{\alpha}\rangle\cdot\langle\hat{\beta}\rangle)\cdot\langle\hat{\gamma}\rangle = \langle\hat{\alpha}\rangle\cdot(\langle\hat{\beta}\rangle\cdot\langle\hat{\gamma}\rangle)$ holds whenever the products are well defined.

For each $\hat{\alpha} \in \mathbf{B}(\mathbf{a},\mathbf{b})$, we define its inverse $\hat{\alpha}^{-1} \in \mathbf{B}(\mathbf{b},\mathbf{a})$ as $\hat{\alpha}^{-1}(t) = (\alpha_1^{-1}(t),\cdots,\alpha_n^{-1}(t),t)$ where

$$\alpha_i^{-1}(t) = \alpha_i(t_0+t_f-t), \quad \forall t \in T_h,\ i = 1,\cdots,n$$

In other word, $\hat{\alpha}^{-1}$ is the mirror image of $\hat{\alpha}$ upside down. It is easily checked that it is indeed the inverse of $\hat{\alpha}$ in the sense that

$$\langle\hat{\alpha}^{-1}\rangle\cdot\langle\hat{\alpha}\rangle = \langle\hat{e}_a\rangle, \quad \langle\hat{\alpha}\rangle\cdot\langle\hat{\alpha}^{-1}\rangle = \langle\hat{e}_b\rangle$$

where $\hat{e}_a$ is the identity pure braid in $\mathbf{B}(\mathbf{a},\mathbf{a})$ consisting of n vertical strings joining each (a_i,t_0) to (a_i,t_f) respectively. Similarly for $\hat{e}_b$. For example, the string isotopy H between $\hat{\alpha}^{-1}\cdot\hat{\alpha}$ and $\hat{e}_a$ can be chosen to be

$$H(s,t) = \begin{cases} (\alpha_1(2t-t_0),\cdots,\alpha_n(2t-t_0),t) & 0 \le t \le \frac{t_0+t_f}{2} + \frac{t_0-t_f}{2}s \\ (\alpha_1(\frac{t_0+t_f}{2}+\frac{t_0-t_f}{2}s),\cdots,\alpha_n(\frac{t_0+t_f}{2}+\frac{t_0-t_f}{2}s),t) & \frac{t_0+t_f}{2}+\frac{t_0-t_f}{2}s \le t \le \frac{t_0+t_f}{2}+\frac{t_f-t_0}{2}s \\ (\alpha_1^{-1}(2t-t_f),\cdot,\alpha_n^{-1}(2t-t_f),t) & \frac{t_0+t_f}{2}+\frac{t_f-t_0}{2}s \le t \le t_f \end{cases}$$

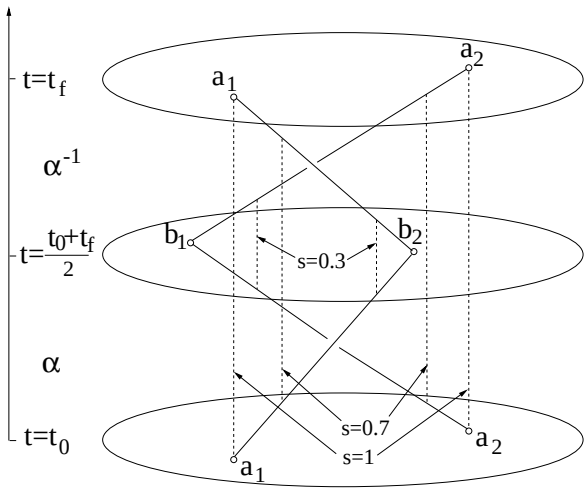

Figure 6.7: String isotopy between $\hat{\alpha}^{-1} \cdot \hat{\alpha}$ and $\hat{e}_a$

which is shown visually in Figure 6.7. The inverse operation also respects string isotopy and therefore $\langle \hat{\alpha} \rangle^{-1} \triangleq \langle \hat{\alpha}^{-1} \rangle$ makes sense. Now we can redefine 0-homotopy as

Proposition 9 *Two maneuvers $\alpha, \beta \in \mathbf{P}(0)$ are 0-homotopic if and only if $\langle \hat{\beta} \rangle^{-1} \cdot \langle \hat{\alpha} \rangle = \langle \hat{e}_a \rangle$.*

Proof: By Proposition 8, α and β are 0-homotopic if and only if $\hat{\alpha} \sim \hat{\beta}$ in $\mathbf{B}(\mathbf{a}, \mathbf{b})$. It follows easily from Lemma 8 that $\hat{\alpha} \sim \hat{\beta}$ implies $\hat{\beta}^{-1} \cdot \hat{\alpha} \sim \hat{\alpha}^{-1} \cdot \hat{\alpha} \sim \hat{e}_a$, *i.e.* $\langle \hat{\beta} \rangle^{-1} \cdot \langle \hat{\alpha} \rangle = \langle \hat{e}_a \rangle$. Conversely, if $\hat{\beta}^{-1} \cdot \hat{\alpha} \sim \hat{e}_a$, then another application of Lemma 8 and associativity of the product yields

$$\hat{\alpha} \sim (\hat{\beta} \cdot \hat{\beta}^{-1}) \cdot \hat{\alpha} \sim \hat{\beta} \cdot (\hat{\beta}^{-1} \cdot \hat{\alpha}) \sim \hat{\beta} \cdot \hat{e}_a \sim \hat{\beta}$$

which complete the proof of the other direction. ■

Therefore if we fix an arbitrary maneuver $\gamma \in \mathbf{P}(0)$, then for any other maneuver α in $\mathbf{P}(0)$, $\alpha \mapsto \langle \hat{\alpha} \rangle^{-1} \cdot \langle \hat{\gamma} \rangle$ establishes a one-to-one correspondence between the connected components of $\mathbf{P}(0)$ and the isotopic classes of pure n-braids $\mathbf{PB}(\mathbf{a}, \mathbf{a})$, and the problem translates itself into the the classification of isotopic type of (pure) braids. There are excellent account of this problem in the references. We give the main results below and refer the interested reader to [10].

Actually, the previous analysis suggests that the isotopy classes of $\mathbf{B}(\mathbf{a}, \mathbf{a})$ form a group under the product operation. Denoted it by $\mathbf{B}_n$. Then its identity is $\langle \hat{e}_a \rangle$ and the inverse of an arbitrary element $\langle \hat{\alpha} \rangle$ is $\langle \hat{\alpha} \rangle^{-1}$. Isotopy classes of pour braids form a subgroup of $\mathbf{B}_n$ and is denoted as $\mathbf{PB}_n$. Moreover, it is an normal subgroup since $\beta^{-1} \cdot \alpha \cdot \beta$ is pure for any $\beta \in \mathbf{B}(\mathbf{a}, \mathbf{a})$ provided α is pure.

Without loss of generality we assume that the x coordinates of $a_1, \cdots, a_n$ are strictly increasing. We pay special attention to a set of elements of $\mathbf{B}_n$. One such element $\langle \hat{\sigma}_i \rangle$ together with its inverse is shown in Figure 6.8 in which there is a "twist" between the curves joining a_i and a_{i+1} and all the other curves are vertical. $\langle \hat{\sigma}_1 \rangle, \cdots, \langle \hat{\sigma}_{n-1} \rangle$ generate the group $\mathbf{B}_n$, or equivalently, every element of $\mathbf{B}_n$ is a finite product of such elements and possibly their inverses. These generators are not "free" since they satisfy two sets of relations:

1. $\langle \hat{\sigma}_i \rangle \cdot \langle \hat{\sigma}_j \rangle = \langle \hat{\sigma}_j \rangle \cdot \langle \hat{\sigma}_i \rangle$ for $1 \leq i, j \leq n-1$ and $|i - j| \geq 2$;

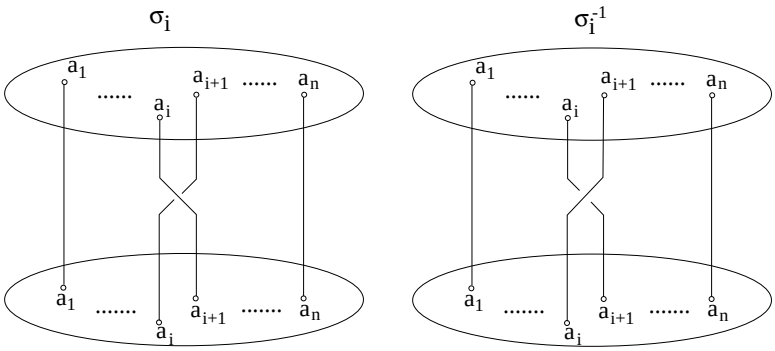

Figure 6.8: Braid $\hat{\sigma}_i$ and its inverse

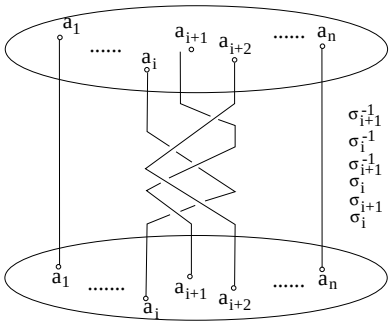

Figure 6.9: Relation $\langle\hat{\sigma}_i\rangle \cdot \langle\hat{\sigma}_{i+1}\rangle \cdot \langle\hat{\sigma}_i\rangle = \langle\hat{\sigma}_{i+1}\rangle \cdot \langle\hat{\sigma}_i\rangle \cdot \langle\hat{\sigma}_{i+1}\rangle$

2. $\langle\hat{\sigma}_i\rangle \cdot \langle\hat{\sigma}_{i+1}\rangle \cdot \langle\hat{\sigma}_i\rangle = \langle\hat{\sigma}_{i+1}\rangle \cdot \langle\hat{\sigma}_i\rangle \cdot \langle\hat{\sigma}_{i+1}\rangle$ for $1 \leq i \leq n-2$.

The first relation is easy to see. To verify the second relation, one needs to draw explicitly the composition $\hat{\sigma}_{i+1}^{-1} \cdot \hat{\sigma}_i^{-1} \cdot \hat{\sigma}_{i+1}^{-1} \cdot \hat{\sigma}_{i+1} \cdot \hat{\sigma}_i \cdot \hat{\sigma}_{i+1}\cdot$ and conclude that it is string isotopic to the identity braid, as can be easily seen from Figure 6.9.

A profound result in braid theory states that these two sets of relations are enough to describe $\mathbf{B}_n$. More precisely

Theorem 2 *Group $\mathbf{B}_n$ is isomorphic to the free product of $\langle\hat{\sigma}_1\rangle, \cdots, \langle\hat{\sigma}_{n-1}\rangle$ together with the two sets of relations defined above.*

The pure braid group is a normal subgroup of $\mathbf{B}_n$ and admits the following presentation

Theorem 3 *Pure n-braid group $\mathbf{PB}_n$ is generated by*

$$A_{j,k} = \sigma_{k-1}\sigma_{k-2}\cdots\sigma_{j+1}\sigma_j^2\sigma_{j+1}^{-1}\cdots\sigma_{k-2}^{-1}\sigma_{k-1}^{-1}, \quad \textit{for } 1 \leq j < k \leq n$$

together with the relations

1. $A_{r,s}$ *and* $A_{i,j}$ *commutes if* $1 \leq r < s < i < j \leq n$ *or if* $1 \leq r < i < j < s \leq n$;
2. $A_{r,s}A_{r,j}A_{r,s}^{-1} = A_{s,j}^{-1}A_{r,j}A_{s,j}$ *if* $1 \leq r < s < j \leq n$;
3. $A_{r,s}A_{s,j}A_{r,s}^{-1} = A_{s,j}^{-1}A_{r,j}^{-1}A_{s,j}A_{r,j}A_{s,j}$ *if* $1 \leq r < s < j \leq n$;

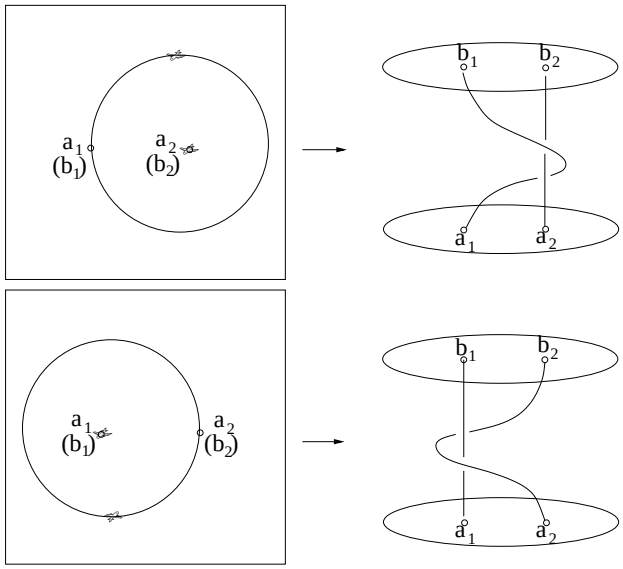

Figure 6.10: Two homotopic maneuvers

4. $A_{i,j}^{-1} A_{s,j} A_{i,j}$ *and* $A_{r,i}$ *commute if* $1 \leq r < s < i < j \leq n$.

For a proof of the above theorems, see [11]. Therefore Theorem 3 together with Proposition 9 and the comments thereafter implies that we have characterized the structure of 0-homotopy types of resolution maneuvers in $\mathbf{P}(0)$ completely.

Remark 7 We have the following remarks about the new perspective:

- The finite presentation of groups are notorious unsatisfactory in characterizing groups. However, they offer the only complete descriptions of $\mathbf{B}_n$ and $\mathbf{PB}_n$. In some special cases, they can be simplified, though still finite presentation, with less generators and simpler relations defined on them. For example, $\mathbf{B}_3 = \langle \hat{\sigma}_1, \hat{\sigma}_2 \,; \hat{\sigma}_1\hat{\sigma}_2\hat{\sigma}_1 = \hat{\sigma}_2\hat{\sigma}_1\hat{\sigma}_2 \rangle$ can be shown to be isomorphic to $\langle a, b \,; a^3 = b^2 \rangle$ with $a = \hat{\sigma}_1\hat{\sigma}_2$ and $b = \hat{\sigma}_1\hat{\sigma}_2\hat{\sigma}_1$ ([11]).

- In the light of the new perspective, the results obtained in the previous section about the classification of two aircraft resolution maneuvers becomes a special case since $\mathbf{B}_2$ is the free cyclic group generated by $\langle \hat{\sigma}_1 \rangle$, hence the conclusion of Corollary 2. Two fundamental maneuvers correspond to the generator $\langle \hat{\sigma}_1 \rangle$ and its inverse respectively. It will be instructive to draw the maneuvers and corresponding braids explicitly.

- The braid perspective often provides us with clearer view than that if simply the planar image of each maneuver is drawn. The two maneuvers in Figure 6.10 give us such an example. In each of them, one of the aircraft remains at fixed position while the other one circles around it and returns to the original position. It is much clearer that they are string isotopic in the braid representations.

- Although many of the examples in this chapter seems unrealistic at the first sight, one can easily constructed similar situations with more practical settings. This is especially the case for airspace near airport, where aircraft might need to hover and make multiple turns before it gets the permission to land.

Chapter 7

Optimal Resolution

7.1 Cost Function

In Chapter 6, we discuss the qualitative classification of resolution maneuvers. Two resolution maneuvers are of the same type if and only if there exists a continuous conflict-free deformation from one to the other. However, they are not the same in practical terms such as travel distance, fuel consumption, *etc.* A natural question we will ask ourselves then is: among all the representatives of a given type of maneuvers, which one is the best?

The answer of this question depends on the optimality criteria we choose. A natural candidate is the travel distance which, under the same notation of previous chapter, can be written as:

$$L(\alpha) = \int_{t_0}^{t_f} ||v(t)|| \, dt$$

where $v(t) = \dot{\alpha}(t)$ is the velocity of the aircraft at time t. Here we assume that the maneuver α is piecewise differentiable. The problem with L is that although favoring resolution path of shorter length, it is only a function of the image of α, a reparameterization yields the same L, more precisely, suppose $u : T_h \to T_h$ is a diffeomorphism, then $\alpha \circ u$ and α have the same length.

Alternatively, the "energy" defined below will be adopted:

$$J(\alpha) = \int_{t_0}^{t_f} ||v(t)||^2 \, dt \tag{7.1}$$

An application of Cauchy-Schwartz inequality yields

$$(t_f - t_0)J(\alpha) \geq [L(\alpha)]^2$$

where equality holds if and only if $||v(t)||$ is constant, *i.e.* if and only if the motion is of constant speed $L(\alpha)/(t_f - t_0)$. This serves perfectly for our purpose since the J-minimal maneuver joining a to b is the constant motion along the line segment between them. If the maneuvers is required to lie on some curve other than the line segment, then of all the different parameterizations, the one with the least energy J is the one with the constant speed. This has practical interpretation in aircraft context since safety and capability limit and passenger comfort prohibit the aircraft from making abrupt turns. For application of energy defined in (7.1) to the study of geodesics on Riemmanian manifolds, the reader can refer to [9].

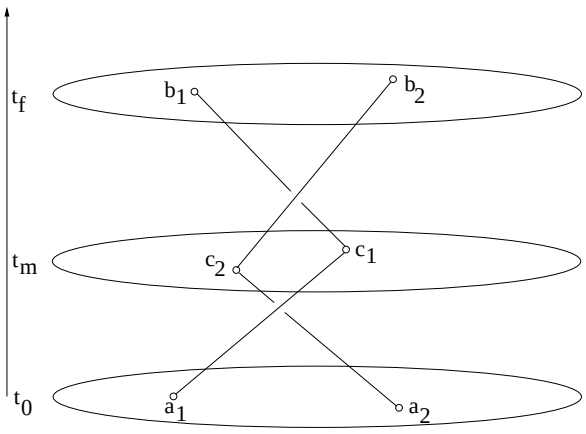

Figure 7.1: Braid corresponding to one-legged maneuver

7.2 Two Aircraft Case: Two Legged Solution

Consider the two aircraft resolution scenario first. As before, the two aircraft have starting positions a_1, a_2 (at time t_0) and destinations b_1, b_2 (at time t_f) respectively. However, we redefine $\mathbf{P}_1$ to be the set of all continuous motions $\alpha_1 : T_h \to \mathbf{R}^2$ which starts from a_1 at time t_0 and ends at b_1 at time t_f *and* which is piecewise differentiable, in other word, there exist a finite partition $t_0 < t_1 < \cdots < t_{n-1} < t_n = t_f$ of $[t_0, t_f]$ such that α_1 is differentiable on each subinterval $[t_i, t_{i+1}]$ for $i = 0, 1, \cdots, n-1$ (*i.e.* α_1 can be extended to a differentiable map on an open neighborhood $(t_i - \varepsilon, t_{i+1} + \varepsilon)$ of $[t_i, t_{i+1}]$ for some ε small enough). $\mathbf{P}_2$ is defined similarly. The minimal separation over encounter $\Delta(\alpha_1, \alpha_2)$ for each maneuver $(\alpha_1, \alpha_2) \in \mathbf{P} = \mathbf{P}_1 \times \mathbf{P}_2$ is defined as before and $\mathbf{P}(R)$ is the set of all such maneuvers with a MSE of *at least* R. Notice that this new definition of $\mathbf{P}(R)$ is different from the one given in Chapter 6. We choose "at least" to make $\mathbf{P}(R)$ a close set such that the solution to the following problem exists:

$$\text{Minimize } J(\alpha_1) + J(\alpha_2) \quad \text{for } (\alpha_1, \alpha_2) \in \mathbf{P}(R). \tag{7.2}$$

By assigning different weights to terms $J(\alpha_1)$ and $J(\alpha_2)$, we can have a priority of the two aircraft. However, the subsequent analysis remains largely intact.

As a first step, we will focus on a special class of resolution maneuvers in this section and postpone the discussion of general case to later sections. A *two-legged* motion α_1 for aircraft 1 is characterized by a single waypoint c_1 and an epoch $t_m \in (t_0, t_f)$ and the motion consists of two stages, each of which is in straight line and of constant speed: First from a_1 at time t_0 to c_1 at time t_m, then from c_1 at time t_m to b_1 at time t_f. Denote the set of all such motions as $\mathbf{P}_1^2$. Similarly for aircraft 2 we have $\mathbf{P}_2^2$, each element of which is characterized by the waypoint c_2 and the *same* epoch t_m. $\mathbf{P}^2 \triangleq \mathbf{P}_1^2 \times \mathbf{P}_2^2$ is the set of all (joint) two-legged maneuvers for both aircraft and its subset consisting of all those with a MSE of at least R is denoted $\mathbf{P}^2(R)$. Each maneuver $\alpha = (\alpha_1, \alpha_2)$ in $\mathbf{P}^2(R)$ corresponds to a braid $\hat{\alpha} \in \mathbf{B}(a, b)$ consisting of two line segments piecing together in the state-time coordinate (see Figure 7.1). We now have a restricted version of problem (7.2) as:

$$\text{Minimize } J(\alpha_1) + J(\alpha_2) \quad \text{for } (\alpha_1, \alpha_2) \in \mathbf{P}^2(R). \tag{7.3}$$

Solution to problem (7.3) will give a suboptimal solution to problem (7.2).

Before proceeding, we need the following lemma whose proof can be easily checked.

Lemma 9 *For $x, a_1, a_2 \in \mathbf{R}^n$ and $\lambda_1, \lambda_2 > 0$, the following identity holds*

$$\lambda_1\|x-a_1\|^2 + \lambda_2\|x-a_2\|^2 = (\lambda_1+\lambda_2)\left\|x - \frac{\lambda_1 a_1 + \lambda_2 a_2}{\lambda_1+\lambda_2}\right\|^2 + \frac{\lambda_1\lambda_2}{\lambda_1+\lambda_2}\|a_1-a_2\|^2$$

In particular, if $\lambda_1 = \lambda_2 = 1$, then the above identity simplified to

$$\|x-a_1\|^2 + \|x-a_2\|^2 = 2\left\|x - \frac{a_1+a_2}{2}\right\|^2 + \frac{\|a_1-a_2\|^2}{2}$$

Since each $\alpha \in \mathbf{P}^2(R)$ is completely characterized by c_1 and c_2, the cost function can be rewritten by Lemma 9 as

$$\begin{aligned} J(\alpha_1)+J(\alpha_2) &= \sum_{i=1}^{2}\left[(\frac{\|c_i-a_i\|}{t_m-t_0})^2(t_m-t_0) + (\frac{\|b_i-c_i\|}{t_f-t_m})^2(t_f-t_m)\right] \\ &= \sum_{i=1}^{2}[\frac{\|c_i-a_i\|^2}{t_m-t_0} + \frac{\|b_i-c_i\|^2}{t_f-t_m}] \\ &= \sum_{i=1}^{2}\frac{t_f-t_0}{(t_f-t_m)(t_m-t_0)}\left[\left\|c_i - \frac{(t_f-t_m)a_i + (t_m-t_0)b_i}{t_f-t_0}\right\|^2 + \frac{\|a_i-b_i\|^2}{t_f-t_0}\right] \end{aligned}$$

Ignoring the constant terms, we get an equivalent version of problem (7.3) as

$$\text{Minimize } \|c_1-c_1^u\|^2 + \|c_2-c_2^u\|^2 \quad \text{for } (\alpha_1,\alpha_2) \in \mathbf{P}^2(R). \tag{7.4}$$

where c_1^u, c_2^u is the unconstrained optimal value of c_1 and c_2 minimizing $J(\alpha_1)+J(\alpha_2)$:

$$c_i^u = \frac{(t_f-t_m)a_i + (t_m-t_0)b_i}{t_f-t_0}, \quad i=1,2 \tag{7.5}$$

In the case when t_m is chosen to be the midpoint between t_0 and t_f, (7.5) simplified to

$$c_i^u = \frac{a_i+b_i}{2}, \quad i=1,2$$

The constraint can be simplified as well. Let us calculate the MSE of a maneuver $\alpha = (\alpha_1,\alpha_2) \in \mathbf{P}^2$ with way points c_1 and c_2 first. In the first stage, the motions of two aircraft are:

$$\alpha_1(t) = a_1 + (c_1-a_1)\frac{t-t_0}{t_m-t_0}, \quad \alpha_2(t) = a_2 + (c_2-a_2)\frac{t-t_0}{t_m-t_0}, \quad t_0 \le t \le t_m \tag{7.6}$$

Simple calculation show that

Lemma 10 *The minimal distance of two aircraft during time interval $[t_0, t_m]$ is*

$$d^* = \begin{cases} \|a_1-a_2\|, & \text{if } \lambda > 0; \\ \|c_1-c_2\|, & \text{if } \lambda < -\|c_1-c_2-a_1+a_2\|^2; \\ \sqrt{\|a_1-a_2\|^2 - \lambda^2/\|c_1-c_2-a_1+a_2\|^2}, & \text{if } -\|c_1-c_2-a_1+a_2\|^2 \le \lambda \le 0 \end{cases}$$

where $\lambda = (a_1-a_2)^T(c_1-c_2-a_1+a_2)$.

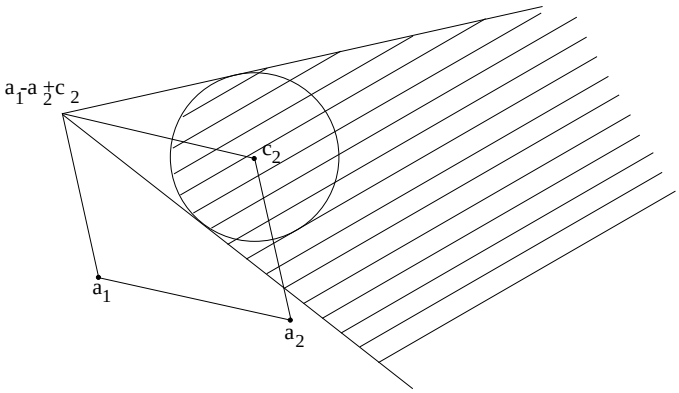

Figure 7.2: Plot of $\{c_1 : d^*(a_1 - a_2, c_1 - c_2) \geq R\}$

A careful inspection of the above formulae shows that d^* is a function of relative positions $a_1 - a_2$ and $c_1 - c_2$ only and is independent of the time t_m. Hence we shall use $d^*(a_1 - a_2, c_1 - c_2)$ to denote it explicitly whenever necessary. For the latter half of the maneuver, the motions can be written in a similar way as

$$\alpha_1(t) = c_1 + (b_1 - c_1)\frac{t - t_m}{t_f - t_m}, \quad \alpha_2(t) = c_2 + (b_2 - c_2)\frac{t - t_m}{t_f - t_m}, \quad t_m \leq t \leq t_f \tag{7.7}$$

The minimal distance between two aircraft during time interval $[t_m, t_f]$ is $d^*(c_1 - c_2, b_1 - b_2)$ and the overall MSE is $\min\{d^*(a_1 - a_2, c_1 - c_2), d^*(c_1 - c_2, b_1 - b_2)\}$.

To make sure that the maneuver defined by (7.6) and (7.7) belongs to $\mathbf{P}^2(R)$, both $d^*(a_1 - a_2, c_1 - c_2)$ and $d^*(c_1 - c_2, b_1 - b_2)$ have to be greater than or equal to R. Fix c_2, and suppose we have the freedom of choosing c_1 arbitrarily. Figure 7.2 shows the set $\{c_1 : d^*(a_1 - a_2, c_1 - c_2) \geq R\}$ by shaded region, which is obtained by drawing a circle of radius R around c_2 and two lines starting from point $a_1 - a_2 + c_2$ tangent to that circle. This is always possible since by the assumption $\|a_1 - a_2\| > R$, $a_1 - a_2 + c_2$ is outside of the circle. Set $\{c_1 : d^*(c_1 - c_2, b_1 - b_2) \geq R\}$ can be obtained in a similar way. The final feasible set of c_1 is the intersection of two such sets and, depending on the relative position of $a_1 - a_2$ and $b_1 - b_2$, has four possible configurations shown in Figure 7.3. We will denote this set as $A(c_2)$, highlighting its dependence on c_2.

The problem can be considerably simplified if we observe that in all but the first configuration, the unconstrained optimal c_1^u, c_2^u is feasible. To see this, notice that by equation (7.5),

$$c_1^u = \frac{t_f - t_m}{t_f - t_0}(a_1 - a_2 + c_2^u) + \frac{t_m - t_0}{t_f - t_0}(b_1 - b_2 + c_2^u) \tag{7.8}$$

So if we choose $c_2 = c_2^u$ in Figure 7.3, then c_1^u lies on the line segment between $a_1 - a_2 + c_2$ and $b_1 - b_2 + c_2$, and is feasible in the last three configurations.

Therefore we will assume the first configuration from now on. Then for any given c_2, $A(c_2)$ is the union of two disjoint convex sets corresponding to the two fundamental types of maneuver. Moreover, for different c_2, $A(c_2)$ can be obtained simply by a translation (*i.e.* $A(c_2) = c_2 + A(0)$). Fixed c_2. Let

$$q = \frac{t_f - t_m}{t_f - t_0}(a_1 - a_2 + c_2) + \frac{t_m - t_0}{t_f - t_0}(b_1 - b_2 + c_2) \tag{7.9}$$

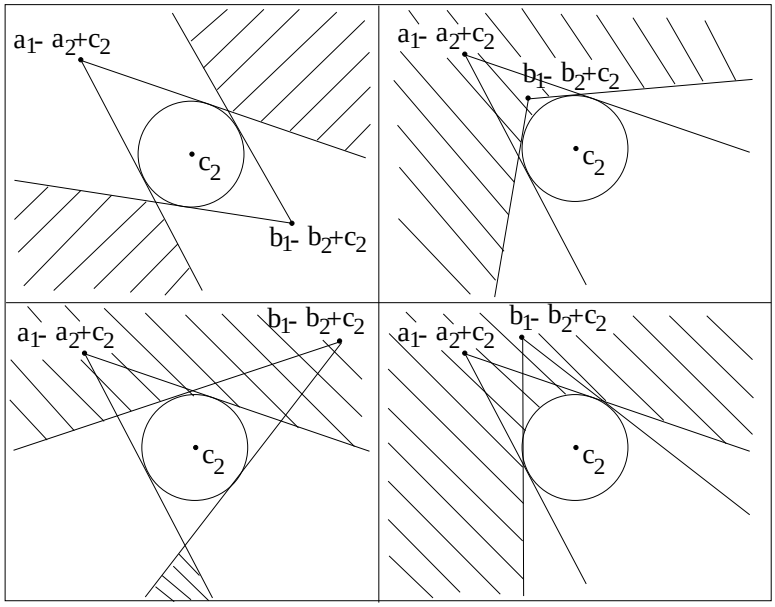

Figure 7.3: Feasible set of c_1 for fixed c_2.

and let p be the point in $A(c_2)$ nearest to q (See Figure 7.4). If p is not unique, we can choose any of them. This is the case if and only if there is an exact collision in the unresoluted maneuver. Notice that $p - q$ is independent of the choice of c_2. Let

$$o_1 = \frac{p+q}{2}, \quad o_2 = c_2 + \frac{p-q}{2}$$

Then problem (7.4) is minimized if we choose $c_2 = c_2^*$ such that o_1 and o_2 coincide with c_1^u and c_2^u respectively. And in this case the optimal c_1^* is p. More precisely,

Proposition 10 *For the first configuration, the optimal solution to problem (7.4) has waypoints*

$$c_1^* = c_1^u + \frac{p-q}{2}, \quad c_2^* = c_2^u - \frac{p-q}{2}$$

where p, q are defined in the above paragraph. Moreover, if in addition one of the two fundamental types of resolution is required, then the optimal c_1^* and c_2^* are unique.

Proof: By equation (7.8) and (7.9),

$$c_1^u - c_2^u = q - c_2 = \frac{t_f - t_m}{t_f - t_0}(a_1 - a_2) + \frac{t_m - t_0}{t_f - t_0}(b_1 - b_2) \tag{7.10}$$

is independent of the choice of c_2. Since we have used c_2 so far for an arbitrary but *fixed* point, in

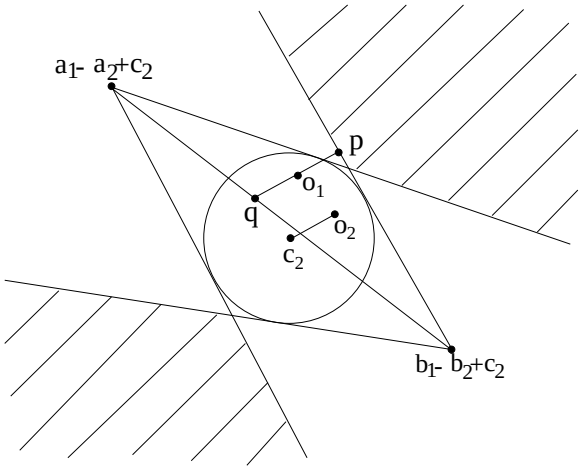

Figure 7.4: Optimal c_1 and c_2 for the first configuration.

the following we will use $\hat{c}_1$ and $\hat{c}_2$ to denote the optimization variable. Hence

$$\begin{aligned}
&\min\{\|\hat{c}_1 - c_1^u\|^2 + \|\hat{c}_2 - c_2^u\|^2 : \text{for all way points } (\hat{c}_1, \hat{c}_2) \text{ such that } (\alpha_1, \alpha_2) \in \mathbf{P}^2(R)\} \\
&= \min_{\hat{c}_2} \min_{\hat{c}_1 \in A(\hat{c}_2)} \left[\|\hat{c}_1 - c_1^u\|^2 + \|\hat{c}_2 - c_2^u\|^2\right] \\
&= \min_{\hat{c}_2} \min_{\hat{c}_1 - \hat{c}_2 \in A(0)} \left[\|\hat{c}_1 - c_1^u\|^2 + \|\hat{c}_2 - c_2^u\|^2\right] \qquad \text{(translation invariant of } A(\hat{c}_2)) \\
&= \min_{\Delta\hat{c} \in A(0)} \min_{\hat{c}_2} [\|\hat{c}_2 + \Delta\hat{c} - c_1^u\|^2 + \|\hat{c}_2 - c_2^u\|^2] \qquad \text{(define } \Delta\hat{c} = \hat{c}_1 - \hat{c}_2) \\
&= \min_{\Delta\hat{c} \in A(0)} \|q - c_2 - \Delta\hat{c}\|^2/2 \qquad \text{(by Lemma 9)} \\
&= \min_{\hat{c} \in A(c_2)} \|q - \hat{c}\|^2 \qquad \text{(define } \hat{c} = c_2 + \Delta\hat{c}) \\
&= \|q - p\|^2
\end{aligned}$$

The last step follows from the definition of p. For the equality to hold, we must have $\hat{c} = p$, *i.e.* $\Delta\hat{c} = p - c_2$ and $\hat{c}_2 = (c_1^u + c_2^u - \Delta\hat{c})/2$ by Lemma 9, which, together with (7.10), leads to

$$\hat{c}_2 = \frac{c_1^u + c_2^u - p + c_2}{2} = c_2^u - \frac{p - q}{2} \quad \text{and} \quad \hat{c}_1 = \hat{c}_2 + \Delta\hat{c} = c_1^u + \frac{p - q}{2}$$

The uniqueness of c_1^* and c_2^* follows from the above deduction and the fact that p is unique since the one connected component chosen from $A(c_2)$ is convex. ■

Denote the solution in Proposition 10 as $c_1^*(\mathbf{a}, \mathbf{b}, t_0, t_m, t_f)$ and $c_2^*(\mathbf{a}, \mathbf{b}, t_0, t_m, t_f)$ where $\mathbf{a} = (a_1, a_2)$ and $\mathbf{b} = (b_1, b_2)$. For any configuration other than the first one, c_1^*, c_2^* can be simply defined as the unconstrained optimal c_1^u and c_2^u. Therefore the previous analysis shows that c_1^*, c_2^* thus defined is the waypoints for the optimal solution of problem (7.3). Furthermore, they satisfy the following property which is evident from the above deduction and will be used later.

Proposition 11 *For any $a_1, a_2, b_1, b_2 \in \mathbf{R}^2$ and any $t_0 < t_m < t_f$, we have*

$$\frac{c_1^*(\mathbf{a}, \mathbf{b}, t_0, t_m, t_f) + c_2^*(\mathbf{a}, \mathbf{b}, t_0, t_m, t_f)}{2} = \frac{c_1^u + c_2^u}{2} = \frac{(t_f - t_m)(a_1 + a_2) + (t_m - t_0)(b_1 + b_2)}{2(t_f - t_0)}$$

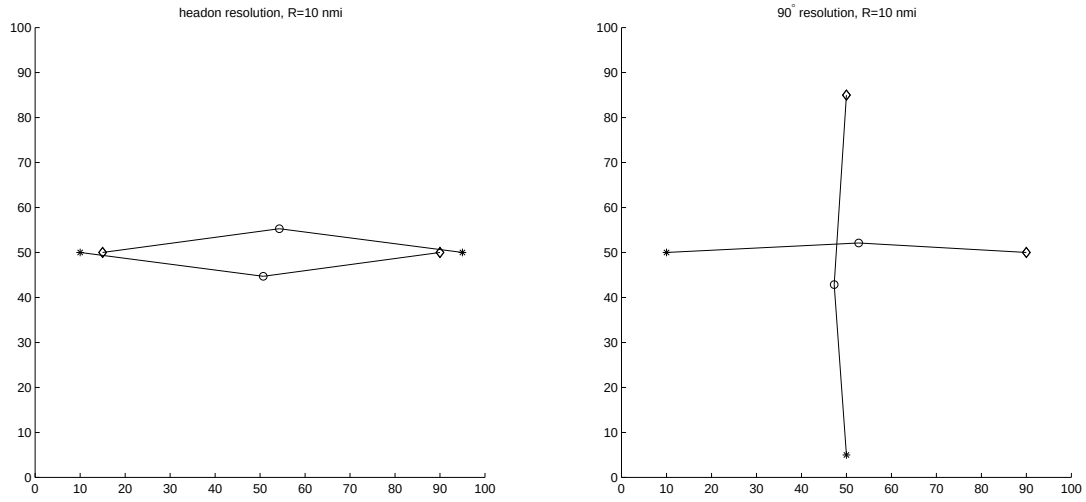

Figure 7.5: Two-legged optimal resolution maneuvers

Figure 7.5 shows the optimal two-legged resolution maneuvers for two typical situations of conflict. In each plot, the starting points are marked with stars and the ending points with diamonds. The circles are the way points computed by Proposition 10. If it is required that a specific type of resolution is adopted, then a similar procedure can be used to locate the optimal waypoints. One need only to restrict p in one particular connect component of $A(c_2)$.

7.3 Two Aircraft Case: Multi-legged Solution

The result in the last section can be generalized to multi-legged case, in which we have a set of waypoints instead of only one. More specificly, fixed a set of epochs $t_0 < t_1 < \cdots < t_{n-1} < t_n = t_f$, an n-legged motion for aircraft 1 is the piecewise linear motion with waypoints $(c_{1,0} = a_1, t_0), (c_{1,1}, t_1), \cdots, (c_{1,n} = b_1, t_n)$. $\mathbf{P}_1^n$ is the set of all such motions. Similarly for $\mathbf{P}_2^n$ with waypoints $c_{2,0} = a_2, c_{2,1}, \cdots, c_{2,n} = b_2$ and the same epochs. $\mathbf{P}^n = \mathbf{P}_1^n \times \mathbf{P}_2^n$ and its subset consisting of all joint n-legged maneuvers with a MSE of at least R is denoted $\mathbf{P}^n(R)$. The problem in this section is:

$$\text{Minimize } J(\alpha_1) + J(\alpha_2) \quad \text{for } (\alpha_1, \alpha_2) \in \mathbf{P}^n(R). \tag{7.11}$$

Or in term of waypoints

$$\text{Minimize } \sum_{i=1}^{2} \sum_{j=1}^{n} \frac{\|c_{i,j} - c_{i,j-1}\|^2}{t_j - t_{j-1}} \quad \text{for } (\alpha_1, \alpha_2) \in \mathbf{P}^n(R). \tag{7.12}$$

Evidently a necessary condition for the optimal solution to problem (7.12) is:

$$\begin{cases} c_{1,j} = c_1^*((c_{1,j-1}, c_{2,j-1}), (c_{1,j+1}, c_{2,j+1}), t_{j-1}, t_j, t_{j+1}) \\ c_{2,j} = c_2^*((c_{1,j-1}, c_{2,j-1}), (c_{1,j+1}, c_{2,j+1}), t_{j-1}, t_j, t_{j+1}) \end{cases} \tag{7.13}$$

for $j = 1, \cdots, n-1$. c_1^* and c_2^* are functions defined in the last subsection. Define

$$o_j = \frac{c_{1,j} + c_{2,j}}{2}, \quad j = 0, 1, \cdots, n$$

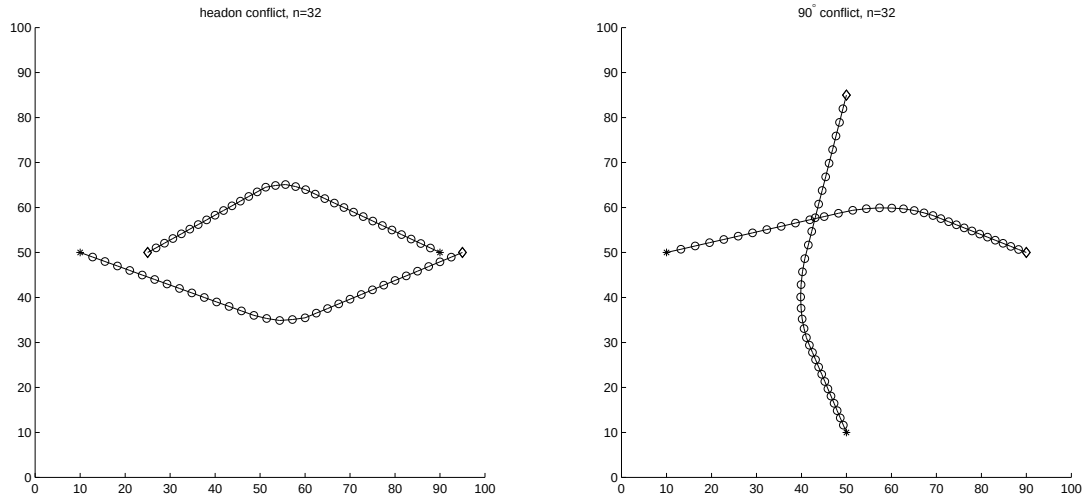

Figure 7.6: Multi-legged resolution maneuvers

Then by Proposition 11, condition (7.13) implies

$$o_j = \frac{(t_{j+1} - t_j)o_{j-1} + (t_j - t_{j-1})o_{j+1}}{t_{j+1} - t_{j-1}} \quad j = 1, 2, \cdots, n-1$$

This is possible if and only if in the space-time coordinate, $(o_0, t_0), (o_1, t_1), \cdots, (o_n, t_f)$ are on a straight line, in other word

$$o_j = \frac{(t_f - t_j)o_0 + (t_j - t_0)o_n}{t_f - t_0} = \frac{(t_f - t_j)(a_1 + a_2) + (t_j - t_0)(b_1 + b_2)}{2(t_f - t_0)} \tag{7.14}$$

Instead of deriving the analytic expression for the optimal solution α^* of problem (7.11), we contend ourselves by providing the following algorithm.

Algorithm 1 1. Pick any feasible waypoints $c_{i,j}^{(0)}$, $i = 1, 2$, $j = 0, 1, \cdots, n$ such that $c_{1,0}^{(0)} = a_1, c_{2,0}^{(0)} = a_2, c_{1,n}^{(0)} = b_1, c_{2,n}^{(0)} = b_2$ and $d^*(c_{1,j}^{(0)} - c_{2,j}^{(0)}, c_{1,j+1}^{(0)} - c_{2,j+1}^{(0)}) \geq R$, $j = 0, 1, \cdots, n-1$.

2. for $k = 0, 1, \cdots$, define

$$\begin{cases} c_{1,j}^{(k+1)} = c_1^*((c_{1,j-1}^{(k)}, c_{2,j-1}^{(k)}), (c_{1,j+1}^{(k)}, c_{2,j+1}^{(k)}), t_{j-1}, t_j, t_{j+1}) \\ c_{2,j}^{(k+1)} = c_2^*((c_{1,j-1}^{(k)}, c_{2,j-1}^{(k)}), (c_{1,j+1}^{(k)}, c_{2,j+1}^{(k)}), t_{j-1}, t_j, t_{j+1}) \end{cases} \quad j = 1, 2, \cdots, n-1$$

3. Repeat procedure 2 until some condition, say, the decrease in energy is below some threshold ε, is met.

It is easily seen that the energy is a nonincreasing function in the number of iterations and is strictly decreasing whenever the maneuver does not satisfy condition (7.13). Therefore the iteration will converge to a maneuver satisfying condition (7.13). It is conjectured that for a fixed fundamental resolution type, the optimal α^* is the only maneuver satisfying condition (7.13). We will postpone its discussion to the next section. Figure 7.6 gives the simulation results for two typical conflict situations. We choose a large $R = 30$ nmi to make the 32-legged solution more obvious. Also the

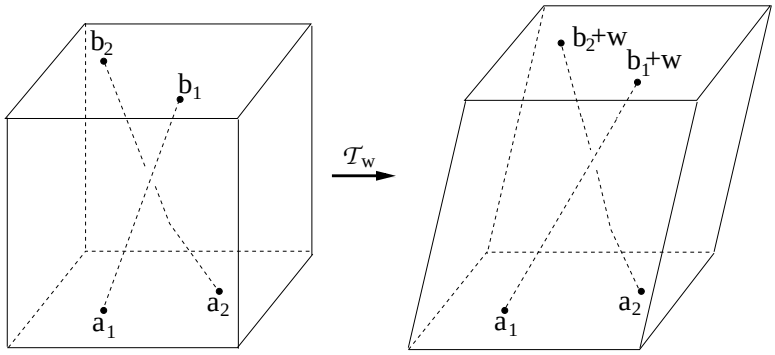

Figure 7.7: Operation $\mathcal{T}_w$

epochs t_j, $j = 0, 1, \cdots, 32$ evenly divides $[t_0, t_f]$ and the corresponding waypoints are marked with small circles. Therefore the denser the circle, the slower the motion is. Notice in addition that the solution in neither case is of constant speed and the speed variation in the second case is larger than in the first one. These phenomena will be explained in a more general setting in the next section.

7.4 Two Aircraft Case: Infinite-legged Solution

In this section we will deal with the general case. The most important difference from the previous two sections in methodology is that from now on, instead of attacking the problem directly as we did before, an indirect method will be adopted. We propose various transformations on the resolution maneuvers and study those properties which are invariant under such transformations. This strategy is a common practice in various branches of mathematics. Although it is debatable whether this new perspective is the single most important feature which distinguishes modern mathematics from it classical counterpart as some mathematicians have claimed, there is no doubt that, applied in an appropriate way, it can give us profound and sometime surprising insight about the object under inspection.

So much for the philosophy lesson and let us get back on track. Recall that in problem (7.2), $\mathbf{P}(R, a_1, a_2, b_1, b_2)$ denotes the set of all maneuvers in $\mathbf{P}$ with a MSE at least R when the starting positions are a_1, a_2 and destination positions b_1, b_2 respectively. Let $w \in \mathbf{R}^2$ be any vector. For any maneuver $\alpha = (\alpha_1, \alpha_2) \in \mathbf{P}(R, a_1, a_2, b_1, b_2)$, construct a new maneuver $\beta = (\beta_1, \beta_2)$ with the same starting positions but different destinations $b_1 + w, b_2 + w$ as:

$$\beta_i(t) = \alpha_i(t) + \frac{t - t_0}{t_f - t_0} w, \quad \forall t \in T_h,\ i = 1, 2$$

From the braid point of view, $\hat{\beta}$ is the linearly tilted version of $\hat{\alpha}$. Since $\|\beta_1(t) - \beta_2(t)\| = \|\alpha_1(t) - \alpha_2(t)\|$ for all t, we have $\beta \in \mathbf{P}(R, a_1, a_2, b_1 + w, b_2 + w)$. So if we denote $\beta = \mathcal{T}_w(\alpha)$, then $\mathcal{T}_w$ is a map from $\mathbf{P}(R, a_1, a_2, b_1, b_2)$ to $\mathbf{P}(R, a_1, a_2, b_1 + w, b_2 + w)$ for each R, and moreover, because of the easily checked fact that $\mathcal{T}_w \circ \mathcal{T}_{-w} = id$, is also a bijection between them. Less obviously

Proposition 12 *Suppose α^* is the optimal solution for problem (7.2) in $\mathbf{P}(R, a_1, a_2, b_1, b_2)$. Then $\beta = \mathcal{T}_w(\alpha^*)$ is the optimal solution for problem (7.2) in $\mathbf{P}(R, a_1, a_2, b_1 + w, b_2 + w)$.*

Proof: Take any $\alpha = (\alpha_1, \alpha_2) \in \mathbf{P}(R, a_1, a_2, b_1, b_2)$ and let $\beta = (\beta_1, \beta_2) = \mathcal{T}_w(\alpha)$, then

$$\begin{aligned} J(\beta_1) + J(\beta_2) &= \int_{t_0}^{t_f} [\|\dot\beta_1(t)\|^2 + \|\dot\beta_2(t)\|^2]\, dt \\ &= \int_{t_0}^{t_f} \left[\left\| \dot\alpha_1(t) + \frac{w}{t_f - t_0} \right\|^2 + \left\| \dot\alpha_2(t) + \frac{w}{t_f - t_0} \right\|^2 \right] dt \\ &= \int_{t_0}^{t_f} [\|\dot\alpha_1(t)\|^2 + \|\dot\alpha_2(t)\|^2]\, dt + \int_{t_0}^{t_f} \frac{2w^T}{t_f - t_0} [\dot\alpha_1(t) + \dot\alpha_2(t)]\, dt + \frac{2\|w\|^2}{t_f - t_0} \\ &= J(\alpha_1) + J(\alpha_2) + \frac{2w^T(b_1 + b_2 - a_1 - a_2 + w)}{t_f - t_0} \end{aligned}$$

Notice that the last term is a constant independent of α. Denote it by C, then

$$\begin{aligned} &\inf\{J(\beta_1) + J(\beta_2) : \beta \in \mathbf{P}(R, a_1, a_2, b_1 + w, b_2 + w)\} \\ &= \inf\{J(\alpha_1) + J(\alpha_2) + C : \alpha \in \mathbf{P}(R, a_1, a_2, b_1, b_2)\} \qquad (\text{let } \alpha = \mathcal{T}_{-w}(\beta)) \\ &= J(\alpha_1^*) + J(\alpha_2^*) + C \end{aligned}$$

where the equality holds if and only if $\mathcal{T}_{-w}(\beta) = \alpha^*$, *i.e.* if and only if $\beta = \mathcal{T}_w(\alpha^*)$. ∎

The reason we introduce this new operation is illustrated by the following proposition.

Proposition 13 *Suppose α^* is the optimal solution for problem (7.2) in $\mathbf{P}(R, a_1, a_2, b_1, b_2)$, and suppose in addition $a_1 + a_2 = b_1 + b_2$. Then*

$$\alpha_1^*(t) + \alpha_2^*(t) = a_1 + a_2 = b_1 + b_2, \quad \forall t \in T_h$$

Proof: To simplify notation, let $\alpha = \alpha^* = (\alpha_1, \alpha_2)$. Denote $e = (a_1 + a_2)/2 = (b_1 + b_2)/2$. Define a new maneuver $\beta = (\beta_1, \beta_2)$ by

$$\begin{cases} \beta_1(t) = \frac{\alpha_1(t) - \alpha_2(t)}{2} + e \\ \beta_2(t) = \frac{\alpha_2(t) - \alpha_1(t)}{2} + e \end{cases} \quad \forall t \in T_h$$

Then it can be checked that β has the same starting and destination position as α and moreover, $\|\beta_1(t) - \beta_2(t)\| = \|\alpha_1(t) - \alpha_2(t)\|$ for all $t \in T_h$. Therefore $\beta \in \mathbf{P}(R, a_1, a_2, b_1, b_2)$. Notice that $\dot\beta_1(t) = (\dot\alpha_1(t) - \dot\alpha_2(t))/2$, $\dot\beta_2(t) = (\dot\alpha_2(t) - \dot\alpha_1(t))/2$, we have

$$\begin{aligned} J(\beta_1) + J(\beta_2) &= \int_{t_0}^{t_f} \left[\left\| \frac{\dot\alpha_1(t) - \dot\alpha_2(t)}{2} \right\|^2 + \left\| \frac{\dot\alpha_2(t) - \dot\alpha_1(t)}{2} \right\|^2 \right] dt \\ &= \int_{t_0}^{t_f} \frac{\|\dot\alpha_1(t) - \dot\alpha_2(t)\|^2}{2}\, dt \\ &\le \int_{t_0}^{t_f} [\|\dot\alpha_1(t)\|^2 + \|\dot\alpha_2(t)\|^2]\, dt \\ &= J(\alpha_1) + J(\alpha_2) \end{aligned}$$

By hypothesis, $J(\alpha_1) + J(\alpha_2) \le J(\beta_1) + J(\beta_2)$, so the equality holds. But this is possible if and only if $\|\dot\alpha_1(t) - \dot\alpha_2(t)\|^2 = 2\|\dot\alpha_1(t)\|^2 + 2\|\dot\alpha_2(t)\|^2$, *i.e.* if and only $\dot\alpha_1(t) = -\dot\alpha_2(t)$ for almost all $t \in T_h$. Integrating from t_0 to t, we get

$$\alpha_1(t) + \alpha_2(t) = \alpha_1(t_0) + \alpha_2(t_0) + \int_{t_0}^{t} [\dot\alpha_1(t) + \dot\alpha_2(t)]\, dt = \alpha_1(t_0) + \alpha_2(t_0)$$

for all $t \in T_h$ which is the desired conclusion. ∎

Now we can extend condition (7.14) to the infinite-legged case.

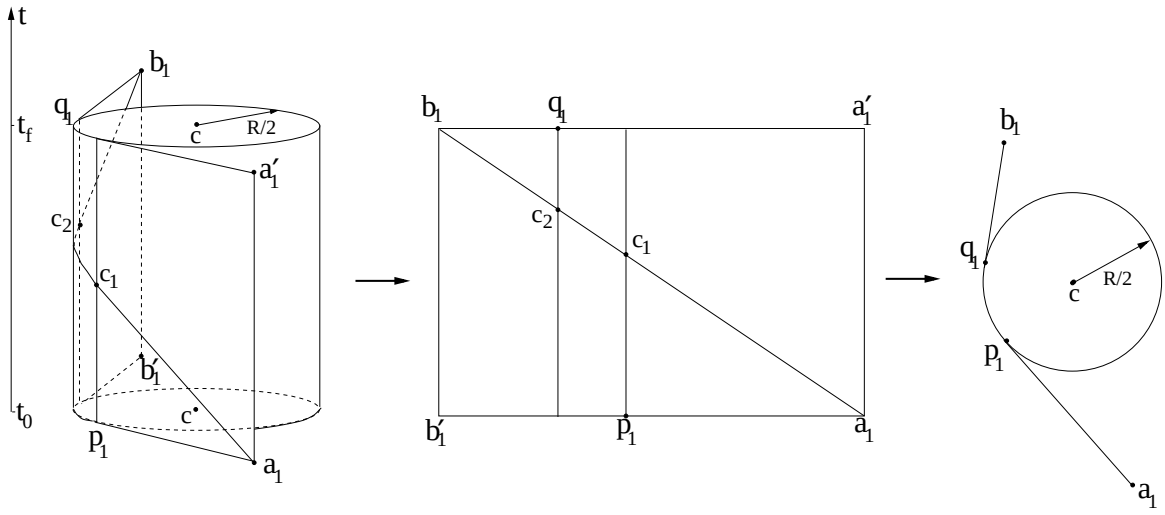

Figure 7.8: Braid for the optimal maneuver

Corollary 4 *Suppose α^* is the optimal solution for problem (7.2) in $\mathbf{P}(R, a_1, a_2, b_1, b_2)$. Then*

$$\frac{\alpha_1^*(t) + \alpha_2^*(t)}{2} = \frac{(t_f - t)(a_1 + a_2) + (t - t_0)(b_1 + b_2)}{2(t_f - t_0)}, \quad \forall t \in T_h$$

Proof: Let $w = (a_1 + a_2 - b_1 - b_2)/2$. Then $\mathcal{T}_w$ maps α^* to $\beta^* = \mathcal{T}_w(\alpha^*)$ which, by Proposition 12, is the optimal solution to problem (7.2) in $\mathbf{P}(R, a_1, a_2, b'_1, b'_2)$ with $b'_1 = b_1 + w$, $b'_2 = b_2 + w$ satisfying $b'_1 + b'_2 = a_1 + a_2$. Therefore by Proposition 13, $\beta_1^*(t) + \beta_2^*(t) = a_1 + a_2$ for all $t \in T_h$. The desired conclusion follows by noting $\alpha^* = \mathcal{T}_{-w}(\beta^*)$ and the definition of $\mathcal{T}_{-w}$. ■

Remark 8 It is easily seen that $\mathcal{T}_w$ maps n-legged maneuvers to n-legged maneuvers with the same epochs. Therefore the conclusions of Proposition 12, Proposition 13 and Corollary 4 remains true if we replace each occurrence of $\mathbf{P}$ by $\mathbf{P}^n$ for arbitrary n.

The trick in the above proof can always be carried out, so we will restrict our discussion to the case when $a_1 + a_2 = b_1 + b_2$ at the moment and derive the optimal resolution maneuver. In this case, if α^* is the optimal solution to problem (7.2) in $\mathbf{P}(R, a_1, a_2, b_1, b_2)$, then Proposition 13 says $[\alpha_1^*(t) + \alpha_2^*(t)]/2$ is the constant $c = (a_1 + a_2)/2 = (b_1 + b_2)/2$ throughout T_h, in other word, $\alpha_1^*(t)$ and $\alpha_2^*(t)$ are always symmetric with respect to c, specifying one of them, say, α_1^*, is enough to describe the maneuver. The MSE constraint becomes $\inf_{t \in T_h} \|\alpha_1^*(t) - c\| \geq R/2$, or equivalently, $\alpha_1^*(t) \notin B(c, R/2)$ where $B(c, R/2)$ is the open disk of radius $R/2$ around c. Moreover, $J(\alpha_1^*) = J(\alpha_2^*)$ since $\dot{\alpha}_1^*(t) = -\dot{\alpha}_2^*(t)$ for all $t \in T_h$.

Therefore, to find α^*, we need only to focus on those elements of $\mathbf{P}(R, a_1, a_2, b_1, b_2)$ satisfying the above properties and problem (7.2) translates into

$$\text{Minimize } J(\alpha_1) \quad \text{for all } \alpha_1 : T_h \to B(c, R/2)^c \text{ satisfying } \alpha_1(t_0) = a_1, \alpha_2(t_f) = b_1. \tag{7.15}$$

Instead of working on α_1, we work on its corresponding braid $\hat{\alpha_1}$ defined as $\hat{\alpha}_1(t) = (\alpha_1(t), t)$. This point of view has several advantages. First, the energy of α_1 and $\hat{\alpha}_1$ has a simple relation

$$J(\hat{\alpha}_1) \triangleq \int_{t_0}^{t_f} \left\| \frac{d\hat{\alpha}_1}{dt} \right\|^2 dt = \int_{t_0}^{t_f} [\|\dot{\alpha}_1(t)\|^2 + 1]\, dt = J(\alpha_1) + (t_f - t_0)$$

Hence the optimal α_1 corresponds to $\hat{\alpha}_1$ with the least J energy. Second and more important, each $\hat{\alpha}_1$ is completely characterized by its image in $\mathbf{R}^2 \times T_h$, therefore by the discussion at the beginning of this section, we do not need to consider the problem of different reparameterization and minimizing J energy is equivalent to minimizing the arc length of $\hat{\alpha}_1$. This observation will make the geometric interpretation of the optimal solution possible.

The constraint for $\hat{\alpha}_1$ inherited from α_1 becomes that $\hat{\alpha}_1$ can not intersect the cylinder of radius $R/2$ around the line (c, t), $t_0 \leq t \leq t_f$. So the problem is to find the shortest curve in $\mathbf{R}^2 \times T_h$ joining (a_1, t_0) to (b_1, t_f) without intersecting the cylinder. Obviously choosing one side of the cylinder is equivalent to choosing a particular fundamental type of resolution. Figure 7.8 shows the shortest curve for one such choice. From points (a_1, t_0) and (b_1, t_f), draw vertical planes tangent to the cylinder. The optimal $\hat{\alpha}_1^*$ should lie on a portion of these two planes and the surface of cylinder (otherwise we can always project it back to these surfaces and reduce its length). We can unwrap these surfaces to a flat one without changing the length of curves lying on it (see the first step in Figure 7.8). Now it is very clear that $\hat{\alpha}_1^*$ must correspond to the line segment joining a_1 and b_1 in the unwrapped flat surface. Since this line segment has constant slope, the corresponding α_1^* is of constant speed. Moreover, optimal waypoint c_1 corresponds to p_1 in $\mathbf{R}^2$ such that line joining a_1 and p_1 is tangent to the circle $\partial B(c, R/2)$. Similarly c_2 corresponds to q_1 such that line from b_1 to q_1 is tangent to $\partial B(c, R/2)$. p_1 and q_1 are properly chosen such that they are on the correct side (see the rightmost part of Figure 7.8).

Proposition 14 *The optimal solution α_1^* to problem (7.15) of a certain fundamental type is a constant speed motion consisting of three stages: first from a_1 to p_1 along the straight line, then from p_1 to q_1 along the circle $\partial B(c, R/2)$, and last from q_1 to b_1 along the straight line.*

Denote the optimal solution given in Proposition 14 as $\gamma^*(a_1, a_2, b_1, b_2)$ highlighting its dependence on a_1, a_2, b_1, b_2. Now we can state the theorem about the general case.

Theorem 4 *The optimal solution α^* to problem (7.2) in $\mathbf{P}(R, a_1, a_2, b_1, b_2)$ of a certain fundamental type is:*

$$\begin{cases} \alpha_1^*(t) = \gamma^*(a_1, a_2, b_1 + w, b_2 + w)(t) - \frac{t - t_0}{t_f - t_0} w, \\ \alpha_2^*(t) = a_1 + a_2 - \gamma^*(a_1, a_2, b_1 + w, b_2 + w)(t) - \frac{t - t_0}{t_f - t_0} w, \quad \forall t \in T_h \end{cases}$$

where $w \triangleq (a_1 + a_2 - b_1 - b_2)/2$.

In the above theorem, $\gamma^*(a_1, a_2, b_1 + w, b_2 + w)$ has to be properly chosen such that its type matches that of α^*. Figure 7.9 shows the plot of two such optimal resolution maneuvers. Compared with Figure 7.6, it can be seen that as the number of legs becomes large enough, the optimal resolution maneuver α^* can be approximated arbitrarily closely. Although $\gamma^*(a_1, a_2, b_1 + w, b_2 + w)$ is a constant speed motion, in general α_1^* and α_2^* are not since they have an additional drift term and the larger the difference w is between $a_1 + a_2$ and $b_1 + b_2$, the larger the variation in speed. This will explain why the first case has a optimal resolution maneuver closer to a constant speed motion.

One can say more about the relation between n-legged and infinite-legged solution. Denote with $J^{n,*}$ the cost corresponding to the optimal solution $\alpha^{n,*}$ to problem (7.11). Denote with J^* the optimal cost of problem (7.2). We will write $J^*(R)$ to indicate its dependence on R whenever necessary. It can be expected that $J^{n,*} \to J^*$ as $n \to \infty$. To show this we need the following lemma.

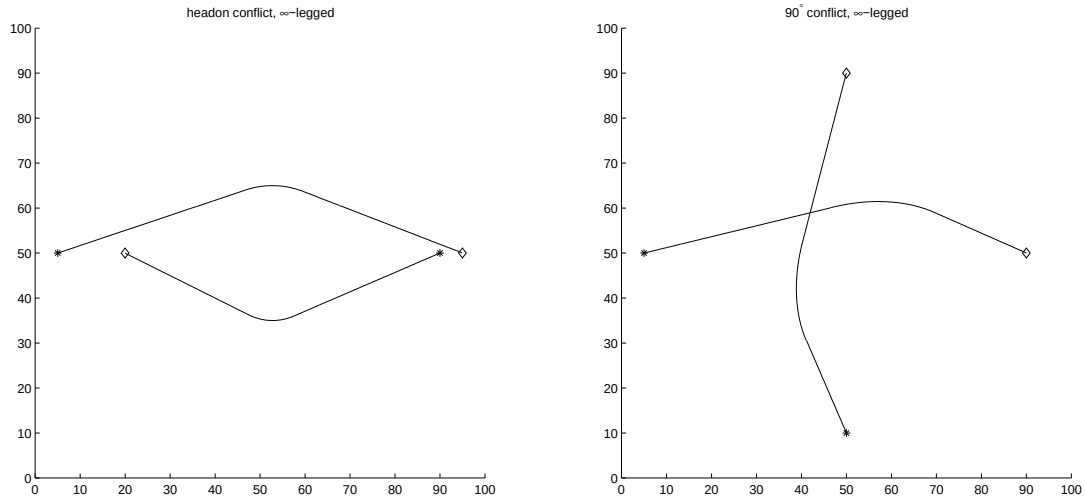

Figure 7.9: Infinite-legged optimal resolution maneuvers

Lemma 11 *$J^*(R)$ is continuous in R provided $0 < R < \min\{\|a_1 - a_2\|, \|b_1 - b_2\|\}$.*

Proof: First notice that $J^*(R)$ is nondecreasing for $0 < R < \min\{\|a_1 - a_2\|, \|b_1 - b_2\|\}$. Suppose the optimal maneuver for problem (7.2) corresponding to some R is $\alpha = (\alpha_1, \alpha_2) \in \mathbf{P}(R)$. Then $J^*(R) = J(\alpha_1) + J(\alpha_2)$ by hypothesis. Define a local deformation $\alpha^\lambda = (\alpha_1^\lambda, \alpha_2^\lambda)$ of α parameterized by λ as:

$$\begin{cases} \alpha_1^\lambda(t) = \alpha_1(t) \\ \alpha_2^\lambda(t) = \alpha_1(t) + (\max\{\|\alpha_2(t) - \alpha_1(t)\|, R + \lambda\}, [\alpha_2(t) - \alpha_1(t)])_{polar} \quad \forall t \in T_h \end{cases}$$

for $\lambda \geq 0$ sufficiently small. Here $(\cdot,\cdot)_{polar}$ is defined in Chapter 6. It is easily checked that $\alpha^\lambda \in \mathbf{P}(R + \lambda)$ and $\alpha^0 = \alpha$. Furthermore, $J(\lambda) \triangleq J(\alpha_1^\lambda) + J(\alpha_2^\lambda)$ is continuous for λ small enough. Therefore, for any $\varepsilon > 0$, we can always find a $\lambda > 0$ small enough such that $J(\lambda) < J(0) + \varepsilon = J^*(R) + \varepsilon$. This implies

$$J^*(R) \leq J^*(R + \lambda) \leq J(\lambda) < J^*(R) + \varepsilon$$

Therefore J^* is right continuous at R. A similar argument can establish the left continuity of J^* at R. Hence $J^*(R)$ is continuous at R for $0 < R < \min\{\|a_1 - a_2\|, \|b_1 - b_2\|\}$. ■

By using exactly the same argument, we can also show that $J_n^*(R)$ is continuous in R. Therefore

Proposition 15 *For any $0 < R < \min\{\|a_1 - a_2\|, \|b_1 - b_2\|\}$, $J_n^*(R) \to J^*(R)$ as $n \to \infty$*

Proof: Fixed R. It is obvious that $J_n^*(R)$ is nonincreasing in n. Suppose $\alpha = (\alpha_1, \alpha_2) \in \mathbf{P}(R)$ is the optimal solution for problem (7.2). Then since α_1, α_2 are piecewise smooth and T_h is compact, we can find piecewise linear approximation $\alpha^n = (\alpha_1^n, \alpha_2^n) \in \mathbf{P}^n$ for them respectively such that

$$\sup_{t \in T_h} \|\alpha_i(t) - \alpha_i^n(t)\| < \delta \qquad \sup_{t \in T_h} \|\dot{\alpha}_i(t) - \dot{\alpha}_i^n(t)\| < \eta \qquad i = 1, 2$$

for any $\delta > 0, \eta > 0$ provided n is large enough. The first inequality implies that $\alpha^n \in \mathbf{P}^n(R - 2\delta)$, while the second inequality implies that $J(\alpha_1^n) + J(\alpha_2^n)$ can be made arbitrarily close to $J(\alpha_1) + J(\alpha_2) = J^*(R)$, say, within ε. Therefore

$$J^*(R - 2\delta) \leq J_n^*(R - 2\delta) \leq J(\alpha_1^n) + J(\alpha_2^n) \leq J^*(R) + \varepsilon$$

The desired conclusion follows by using Lemma 11 and the arbitrariness of δ and ε. ■

7.5 Multiple Aircraft Case: Global Analysis

In this section, the n aircraft case will be considered. Suppose we have n aircraft with starting positions $\mathbf{a} = (a_1, a_2, \cdots, a_n)$ and destination positions $\mathbf{b} = (b_1, \cdots, b_n)$ respectively. For simplicity we will use $\mathbf{P}(R, \mathbf{a}, \mathbf{b})$ to denote the set of all n-joint maneuvers which have MSE of at least R between any pair of the n aircraft. The problem is to

$$\text{Minimize } \sum_{i=1}^{n} J(\alpha_i) \text{ for all } \alpha \in \mathbf{P}(R, \mathbf{a}, \mathbf{b}) \tag{7.16}$$

Many results in the previous section have their counterparts here. For example, for any $w \in \mathbf{R}^2$, define $\mathbf{b} + w = (b_1 + w, b_2 + 2, \cdots, b_n + w)$. The operation $\mathcal{T}_w$ is defined as before, *i.e.* for any $\alpha \in \mathbf{P}(R, \mathbf{a}, \mathbf{b})$, $\beta = \mathcal{T}_w(\alpha)$ is

$$\beta_i(t) = \alpha_i(t) + \frac{t - t_0}{t_f - t_0} w, \quad \forall t \in T_h, \quad i = 1, \cdots, n$$

Proposition 16 *$\mathcal{T}_w$ is a bijection from $\mathbf{P}(R, \mathbf{a}, \mathbf{b})$ to $\mathbf{P}(R, \mathbf{a}, \mathbf{b} + w)$ and it maps optimal solution of problem (7.16) in $\mathbf{P}(R, \mathbf{a}, \mathbf{b})$ to its optimal solution in $\mathbf{P}(R, \mathbf{a}, \mathbf{b} + w)$.*

Proposition 17 *Suppose α^* is the optimal solution of problem (7.16) in $\mathbf{P}(R, \mathbf{a}, \mathbf{b})$. Then*

$$\frac{1}{n} \sum_{i=1}^{n} \alpha_i(t) = \frac{(t_f - t) \sum_{i=1}^{n} a_i + (t - t_0) \sum_{i=1}^{n} b_i}{n(t_f - t_0)} \quad \forall t \in T_h$$

In particular, if $\sum_{i=1}^{n} a_i = \sum_{i=1}^{n} b_i = c$, then $\sum_{i=1}^{n} \alpha_i(t) = c, \quad \forall t \in T_h$.

The proofs of these two propositions resemble those of the two aircraft case and we will not repeat them again. There is, however, an alternative way of proving Proposition 17, which is the preferred one since it opens up the possibility of proving various other characteristics of the optimal solution of problem (7.16). This will constitute the main theme of the rest of this section.

Proof: Let $\gamma : T_h \to \mathbf{R}^2$ be a differentiable mapping such that $\gamma(t_0) = \gamma(t_f) = 0$. For each maneuver $\alpha \in \mathbf{P}(R, \mathbf{a}, \mathbf{b})$ and each $\lambda \in \mathbf{R}^1$, define a new maneuver $\beta = \mathcal{D}_{\lambda\gamma}(\alpha)$ by

$$\beta_i(t) = \alpha_i(t) + \lambda\gamma(t), \quad \forall t \in T_h, \; i = 1, \cdots, n$$

Then $\beta \in \mathbf{P}(R, \mathbf{a}, \mathbf{b})$. The energy of β is

$$\begin{aligned} J(\beta) &= \sum_{i=1}^{n} J(\beta_i) = \sum_{i=1}^{n} \int_{t_0}^{t_f} \|\dot{\beta}_i(t)\|^2 \, dt = \sum_{i=1}^{n} \int_{t_0}^{t_f} \|\dot{\alpha}_i(t) + \lambda\dot{\gamma}(t)\|^2 \, dt \\ &= J(\alpha) + n\lambda^2 \int_{t_0}^{t_f} \|\dot{\gamma}(t)\|^2 \, dt + 2\lambda \int_{t_0}^{t_f} \dot{\gamma}(t)^T \sum_{i=1}^{n} \dot{\alpha}_i(t) \, dt \end{aligned}$$

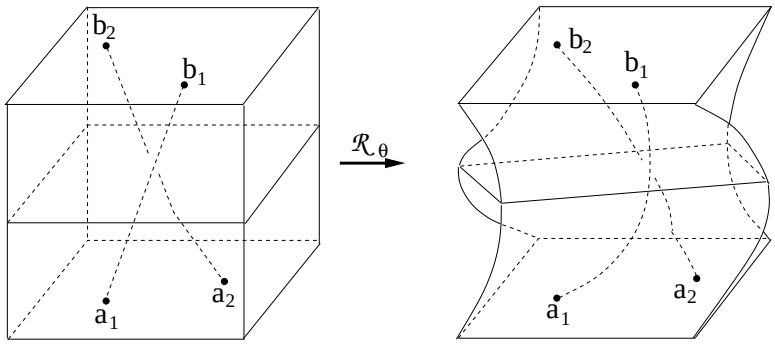

Figure 7.10: Twist operation $\mathcal{R}_\theta$ on braids.

So the energy difference $\Delta J \triangleq J(\beta) - J(\alpha)$ is a quadratic function of λ. Now suppose $\alpha = \alpha^*$ is the optimal solution of problem (7.16), then $\Delta J \geq 0$ for all λ. Hence $\int_{t_0}^{t_f} \dot{\gamma}(t)^T \sum_{i=1}^n \dot{\alpha}_i(t)\, dt = 0$. But this should hold for any choice of γ, say, $\sum_{i=1}^n \dot{\alpha}_i(t)$, therefore $\sum_{i=1}^n \dot{\alpha}_i(t) = 0$ for almost all $t \in T_h$ which is the desired conclusion. ■

To further study the property of the optimal solution to problem (7.16), we introduce the following operator. Because of Proposition 16, we can assume $\sum_{i=1}^n a_i = \sum_{i=1}^n b_i = 0$ at the moment. Suppose $\theta : T_h \to \mathbf{R}$ is a differentiable mapping satisfying $\theta(t_0) = 0$, $\theta(t_f) = 2k\pi$ for some integer k. For each maneuver $\alpha \in \mathbf{P}(R, \mathbf{a}, \mathbf{b})$, define a new maneuver β by twisting α by an angle $\theta(t)$ at time t. More precisely, $\beta = (\beta_1, \cdots, \beta_n)$ with

$$\beta_i(t) = T_{\theta(t)}\alpha_i(t), \quad \forall t \in T_h,\ i = 1, 2, \cdots, n$$

where $T_{\theta(t)}$ is the matrix corresponding to a rotation of angle $\theta(t)$ counterclockwise

$$T_{\theta(t)} = \begin{pmatrix} \cos[\theta(t)] & -\sin[\theta(t)] \\ \sin[\theta(t)] & \cos[\theta(t)] \end{pmatrix}$$

Denote $\beta = \mathcal{R}_\theta(\alpha)$. Then since $T_{\theta(t_0)}$ and $T_{\theta(t_f)}$ are both identity and $T_{\theta(t)}$ leaves the distance of any two points unchanged, $\beta \in \mathbf{P}(R, \mathbf{a}, \mathbf{b})$ hence $\mathcal{R}_\theta$ defines a map from $\mathbf{P}(R, a, b)$ to itself. It is actually a bijection since $\mathcal{R}_\theta \circ \mathcal{R}_{-\theta} = \mathcal{R}_{-\theta} \circ \mathcal{R}_\theta = id$ as can be easily verified. Figure 7.10 shows the effect of operation $\mathcal{R}_\theta$ on some maneuver.

It is interesting to see what is the energy of the new maneuver β. First notice that for each i,

$$\dot{\beta}_i(t) = T_{\theta(t)}\dot{\alpha}_i(t) + \frac{d}{dt}T_{\theta(t)}\alpha_i(t) = T_{\theta(t)}\dot{\alpha}_i(t) + \dot{\theta}(t)T_{\frac{\pi}{2}+\theta(t)}\alpha_i(t)$$

Therefore

$$\begin{aligned} \|\dot{\beta}_i(t)\|^2 &= \|T_{\theta(t)}\dot{\alpha}_i(t)\|2 + \|\dot{\theta}(t)T_{\frac{\pi}{2}+\theta(t)}\alpha_i(t)\|^2 + 2\dot{\theta}(t)\alpha_i^T(t)T_{\frac{\pi}{2}+\theta(t)}^T T_{\theta(t)}\dot{\alpha}_i(t) \\ &= \|\dot{\alpha}_i(t)\|^2 + \|\alpha_i(t)\|^2|\dot{\theta}(t)|^2 + 2\dot{\theta}(t)\alpha_i^T(t)T_{-\frac{\pi}{2}}\dot{\alpha}_i(t) \end{aligned}$$

where we used the fact that $T_{\frac{\pi}{2}+\theta(t)}^T = T_{-\frac{\pi}{2}-\theta(t)}$. Integrating and summing up

$$\begin{aligned} J(\beta) &= \sum_{i=1}^n \int_{t_0}^{t_f} \left[\|\dot{\alpha}_i(t)\|^2\, dt + \|\alpha_i(t)\|^2|\dot{\theta}(t)|^2 + 2\dot{\theta}(t)\alpha_i^T(t)T_{-\frac{\pi}{2}}\dot{\alpha}_i(t)\right] dt \\ &= J(\alpha) + \int_{t_0}^{t_f} [f(t)|\dot{\theta}(t)|^2 + 2g(t)\dot{\theta}(t)]\, dt \end{aligned} \tag{7.17}$$

where f and g are defined by

$$f(t) \triangleq \sum_{i=1}^{n} \|\alpha_i(t)\|^2, \quad g(t) \triangleq \sum_{i=1}^{n} \alpha_i^T(t) T_{-\frac{\pi}{2}} \dot{\alpha}_i(t) \tag{7.18}$$

The difference of energy between α and β is defined as $\Delta J(\theta)$ which is

$$\Delta J(\theta) = J(\beta) - J(\alpha) = \int_{t_0}^{t_f} [f(t)|\dot{\theta}(t)|^2 + 2g(t)\dot{\theta}(t)]\, dt \tag{7.19}$$

$\Delta J(\theta)$ is a function of θ and we wish to know what is the optimal twist angle θ such that $\Delta J(\theta)$ is minimized. θ is subject to the constraint that $\theta(t_0) = 0$, $\theta(t_f) = 2k\pi$ for some *fixed* integer k. For $\dot{\theta}$ this translates into $\int_{t_0}^{t_f} \dot{\theta}(t)\, dt = 2k\pi$. Write out the Lagrangian function for this problem:

$$\begin{aligned}
\Delta J(\theta, \lambda) &\triangleq \Delta J(\theta) + \lambda \left[\int_{t_0}^{t_f} \dot{\theta}(t)\, dt - 2k\pi \right] \\
&= \int_{t_0}^{t_f} [f(t)|\dot{\theta}(t)|^2 + 2(g(t) + \frac{\lambda}{2})\dot{\theta}(t)]\, dt - 2\lambda k\pi \\
&= \int_{t_0}^{t_f} \left\{ f(t)[\dot{\theta}(t) + \frac{g(t) + \frac{\lambda}{2}}{f(t)}]^2 - \frac{[g(t) + \frac{\lambda}{2}]^2}{f(t)} \right\} dt - 2\lambda k\pi
\end{aligned}$$

Therefore the optimal θ^* satisfies $\dot{\theta}^*(t) = -[g(t) + \lambda/2]/f(t)$ which together with the constraint $\int_{t_0}^{t_f} \dot{\theta}(t)\, dt = 2k\pi$ yields the optimal λ^*:

$$\lambda^* = -2 \left[\int_{t_0}^{t_f} \frac{g(t)}{f(t)}\, dt + 2k\pi \right] \Big/ \int_{t_0}^{t_f} \frac{1}{f(t)}\, dt$$

In other word, the optimal θ^* is

$$\dot{\theta}^*(t) = -\frac{g(t)}{f(t)} + \left[\int_{t_0}^{t_f} \frac{g(t)}{f(t)}\, dt + 2k\pi \right] \Big/ \left[f(t) \int_{t_0}^{t_f} \frac{1}{f(t)}\, dt \right]$$

Substituting this into equation (7.19), we get the minimal $\Delta J(\theta)$ as

$$\Delta J(\theta^*) = \left[\int_{t_0}^{t_f} \frac{g(t)}{f(t)}\, dt + 2k\pi \right]^2 \Big/ \int_{t_0}^{t_f} \frac{1}{f(t)}\, dt - \int_{t_0}^{t_f} \frac{g^2(t)}{f(t)}\, dt$$

If α is the optimal maneuver, then $\Delta J(\theta^*) \geq 0$, *i.e.* we can not gain by choosing different θ. Hence

$$\left[\int_{t_0}^{t_f} \frac{g(t)}{f(t)}\, dt + 2k\pi \right]^2 \geq \int_{t_0}^{t_f} \frac{1}{f(t)}\, dt \cdot \int_{t_0}^{t_f} \frac{g^2(t)}{f(t)}\, dt \tag{7.20}$$

The situation becomes more interesting when $k = 0$. In this case equality holds in equation (7.20) since the lower bound $\Delta J(\theta^*) \geq 0$ can be strictly achieved by choosing $\theta^*(t) \equiv 0$. Therefore

$$\left[\int_{t_0}^{t_f} \frac{g(t)}{f(t)}\, dt \right]^2 = \int_{t_0}^{t_f} \frac{1}{f(t)}\, dt \cdot \int_{t_0}^{t_f} \frac{g^2(t)}{f(t)}\, dt$$

But an application of Cauchy-Schwartz inequality to the function $1/\sqrt{f(t)}$ and $g(t)/\sqrt{f(t)}$ implies that the equality is possible if and only if $g(t)/\sqrt{f(t)} = C/\sqrt{f(t)}$ for some constant C, *i.e.* if and only if $g(t) \equiv C$. Then equation (7.20) can be simplified to

$$(Cz + 2k\pi)^2 \geq C^2 z^2, \quad \forall k \in \mathbf{Z}$$

where $z = \int_{t_0}^{t_f} 1/f(t)\, dt$, or equivalently, $k\pi Cz + k^2\pi^2 \geq 0$ for all $k \in \mathbf{Z}$. This is possible if and only if $-\pi \leq Cz \leq \pi$. Hence

Proposition 18 *Suppose* $\mathbf{a} = (a_1, \cdots, a_n)$, $\mathbf{b} = (b_1, \cdots, b_n)$ *satisfy* $\sum_{i=1}^n a_i = \sum_{i=1}^n b_i = 0$ *and* α *is the optimal solution to problem (7.16) in* $\mathbf{P}(R, \mathbf{a}, \mathbf{b})$. *Then*

$$\sum_{i=1}^{n} \alpha_i^T(t) T_{-\frac{\pi}{2}} \dot{\alpha}_i(t) \equiv C \in [-\frac{\pi}{z}, \frac{\pi}{z}], \quad \forall t \in T_h$$

where $z = \int_{t_0}^{t_f} \left[\sum_{i=1}^n \|\alpha_i(t)\|^2\right]^{-1} dt$.

In fact, what we have proved is stronger: the above equality holds for those and only those α whose energy can not be decreased under any twist $\mathcal{R}_\theta$. The optimal α is one of them. In the two aircraft case, since the optimal α satisfies $\alpha_1(t) = -\alpha_2(t)$ for all t, the above condition is actually that $\alpha_1^T(t) T_{-\frac{\pi}{2}} \dot{\alpha}_1(t)$ is constant for all $t \in T_h$. As a verification, the reader can check that the α plotted in Figure 7.8 indeed satisfies this condition. Similar result for general $\mathbf{a}, \mathbf{b}$ can be obtained by performing a T_w operation for some suitable w and then a translation of both $\mathbf{a}$ and $\mathbf{b}$.

Proposition 19 *For* $\mathbf{a} = (a_1, \cdots, a_n)$, $\mathbf{b} = (b_1, \cdots, b_n)$, *define* $e_a = \sum_{i=1}^n a_i/n$, $e_b = \sum_{i=1}^n b_i/n$. *Then the optimal solution to problem (7.16) in* $\mathbf{P}(R, \mathbf{a}, \mathbf{b})$ *satisfies*

$$\sum_{i=1}^{n} \left[\alpha_i(t) - \frac{t_f - t}{t_f - t_0} e_a - \frac{t - t_0}{t_f - t_0} e_b\right]^T T_{-\frac{\pi}{2}} \left[\dot{\alpha}_i(t) + \frac{e_a - e_b}{t_f - t_0}\right] \equiv C$$

for some constant C *such that* $|C| \leq \pi/z$ *with* z *defined by*

$$z = \int_{t_0}^{t_f} \left[\sum_{i=1}^{n} \left\| \alpha_i(t) - \frac{t_f - t}{t_f - t_0} e_a - \frac{t - t_0}{t_f - t_0} e_b \right\|^2\right]^{-1} dt$$

Since by Proposition 16, $\sum_{i=1}^n \dot{\alpha}_i(t)$ is a constant, we can discard the constant terms in the above condition, hence obtaining

Corollary 5 *For* $\mathbf{a} = (a_1, \cdots, a_n)$, $\mathbf{b} = (b_1, \cdots, b_n)$, *let* e_a, e_b *be defined as above. Then the optimal solution to problem (7.16) in* $\mathbf{P}(R, \mathbf{a}, \mathbf{b})$ *satisfies*

$$\sum_{i=1}^{n} \left[\alpha_i(t) - \frac{e_a - e_b}{t_f - t_0} \cdot t\right]^T T_{-\frac{\pi}{2}} \left[\dot{\alpha}_i(t) + \frac{e_a - e_b}{t_f - t_0}\right]$$

is a constant for all $t \in T_h$.

The next operation on maneuvers we will introduce is the reparameterization operator. For any general $\mathbf{a}$ and $\mathbf{b}$, suppose $\alpha \in \mathbf{P}(R, \mathbf{a}, \mathbf{b})$. Let $h : T_h \to T_h$ be a C^1 diffeomorphism such that $h(t_0) = t_0$ and $h(t_f) = t_f$. Then necessarily $\dot{h}(t) > 0$ for all $t \in T_h$. Define a new maneuver $\beta = \mathcal{G}_h$ by: $\beta = (\beta_1, \cdots, \beta_n)$ with

$$\beta_i(t) = \alpha_i[h(t)], \quad \forall t \in T_h, \quad i = 1, \cdots, n$$

Then $\beta \in \mathbf{P}(R, \mathbf{a}, \mathbf{b})$ and $\mathcal{G}_h$ defines a maps from $\mathbf{P}(R, \mathbf{a}, \mathbf{b})$ to itself which can be further shown to be a bijection since $\mathcal{G}_h \circ \mathcal{G}_{h^{-1}} = \mathcal{G}_{h^{-1}} \circ \mathcal{G}_h = id$. In the braid point of view, $\hat{\beta}$ is the vertically

deformed version of $\hat{\alpha}$. The energy of β is

$$\begin{aligned} J(\beta) &= \int_{t_0}^{t_f} \sum_{i=1}^{n} \|\dot{\alpha}_i[h(t)]\|^2 |\dot{h}(t)|^2 \, dt \\ &\geq \frac{1}{t_f - t_0} \left[\int_{t_0}^{t_f} \sqrt{\Sigma_{i=1}^{n} \|\dot{\alpha}_i[h(t)]\|^2} \, \dot{h}(t) \, dt \right]^2 \\ &= \frac{1}{t_f - t_0} \left[\int_{t_0}^{t_f} \sqrt{\Sigma_{i=1}^{n} \|\dot{\alpha}_i(s)\|^2} \, ds \right]^2. \qquad (s = h(t)) \end{aligned} \tag{7.21}$$

An application of Cauchy-Schwartz inequality to function $\sqrt{\sum_{i=1}^{n} \|\dot{\alpha}_i[h(t)]\|^2}\, \dot{h}(t)$ and 1 leads to the inequality and equality holds if and only if $\sqrt{\sum_{i=1}^{n} \|\dot{\alpha}_i[h(t)]\|^2}\, \dot{h}(t)$ is some constant C_0 for all $t \in T_h$, or equivalently, if and only if

$$\int_{t_0}^{t'} \sqrt{\Sigma_{i=1}^{n} \|\dot{\alpha}_i[h(t)]\|^2} \, \dot{h}(t) \, dt = \int_{t_0}^{h(t')} \sqrt{\Sigma_{i=1}^{n} \|\dot{\alpha}_i(s)\|^2} \, ds = C_0(t' - t_0), \quad \forall t' \in T_h$$

Define $g(t) \triangleq \int_{t_0}^{t} \sqrt{\sum_{i=1}^{n} \|\dot{\alpha}(s)\|^2} \, ds$. Then if α satisfies that $\sum_{i=1}^{n} \|\dot{\alpha}(s)\|^2 > 0$ for almost all s on any subinterval of T_h, then g is strictly increasing hence invertible. The above condition becomes $h(t') = g^{-1}[C_0(t' - t_0)]$ for all $t' \in T_h$. Use this as the definition of h, then the lower bound on $J(\beta)$ in equation (7.21) can be strictly achieved.

Now assume that α is the optimal solution of problem (7.16) in $\mathbf{P}(R, \mathbf{a}, \mathbf{b})$, and $a_i \neq b_i$ for at least one i in $\{1, \cdots, n\}$, then α clearly satisfies the condition $\sum_{i=1}^{n} \|\dot{\alpha}(s)\|^2 > 0$ for almost all s in any subinterval of T_h, hence equality in (7.21) is achieved. However since $\beta \in \mathbf{P}(R, \mathbf{a}, \mathbf{b})$ and by hypothesis, α is optimal in $\mathbf{P}(R, \mathbf{a}, \mathbf{b})$, this lower bound have to be the same as $J(\alpha)$. Therefore

$$\frac{1}{t_f - t_0} \left[\int_{t_0}^{t_f} \sqrt{\Sigma_{i=1}^{n} \|\dot{\alpha}_i(t)\|^2} \, dt \right]^2 = J(\alpha) = \int_{t_0}^{t_f} \sum_{i=1}^{n} \|\dot{\alpha}_i(t)\|^2 \, dt$$

Another application of Cauchy-Schwartz inequality to functions $\sqrt{\sum_{i=1}^{n} \|\dot{\alpha}_i(t)\|^2}$ and 1 reveals that this is possible if and only if $\sum_{i=1}^{n} \|\dot{\alpha}_i(t)\|^2 \equiv D$ for some constant D. This certainly holds for the trivial case when $a_i = b_i$, $i = 1, \cdots, n$. Hence

Proposition 20 *For any* $\mathbf{a} = (a_1, \cdots, a_n)$, $\mathbf{b} = (b_1, \cdots, b_n)$, *if* α *is the optimal solution to problem (7.16) in* $\mathbf{P}(R, a, b)$, *then* α *satisfies*

$$\sum_{i=1}^{n} \|\dot{\alpha}_i(t)\|^2 \equiv D, \quad \forall t \in T_h$$

7.6 Multiple Aircraft Case: Local Analysis

To get further characteristics of the optimal solution, we have to work harder and look deeper into its structure. Suppose α is the optimal solution of problem (7.16) in $\mathbf{P}(R, \mathbf{a}, \mathbf{b})$, then we can subdivide $[t_0, t_f]$ into $t_0 < t_1 < \cdots < t_{m-1} < t_m = t_f$ such that on each subinterval (t_k, t_{k+1}), $k = 0, 1, \cdots, m-1$, either of the following occurs:

1. The distance of any pair of aircraft is strictly greater than R;

2. The distances of some pairs of aircraft are equal to R for some $t \in (t_k, t_{k+1})$. For each time $t \in (t_k, t_{k+1})$, we can construct a graph whose vertices are numbered from 1 to n, and an edge between vertices i and j exists if and only if aircraft i and aircraft j have a distance equal to R at time t (we will say aircraft i and j *contact* at time t in this case and call the resulting graph *contact graph* at time t). We assume (t_k, t_{k+1}) are chosen such that this graph remains constant during this subinterval, and successive subintervals correspond to different contact graphs.

Although for the sake of rigor, one has to justify if such a partition exists for optimal α, we will not concern ourself with the technicality arising from wild α. We assume α is well behaved, say, piecewise C^1 and does not oscillate too much, as is the case for two aircraft. Therefore the above partition is possible.

It is clear that in subinterval of the first type, each α_i should be constant speed motion along straight line, for otherwise one can always decrease the energy by pulling the string it corresponds to in $\hat{\alpha}$ closer to the straight line connecting a_i to b_i. Actually the argument can lead to stronger assertion, *i.e.* for aircraft i, its optimal motion α_i is of constant speed along straight line in any interval such that $\alpha_i(t)$ has a distance strictly greater than R to any of the other aircraft.

The situation is more complicated for subinterval of the second type. Obvious we can break the n aircraft into several subgroups, each of which corresponds to a maximal connected subgraph of the contact graph in this subinterval, and study them separately using the fact that α is optimal in T_h if and only if its restriction to any subinterval $[t_k, t_{k+1}]$ is also the optimal solution to problem (7.16) with starting positions $\{\alpha_i(t_k)\}_{i=1}^n$ and destination positions $\{\alpha_i(t_{k=1})\}_{i=1}^n$.

We will study at this moment the necessary condition the motion of aircraft corresponding to the leafs in the contact graph must satisfy for optimality. To this end, let us start with a very special case. Assume that for some $\mathbf{a} = (a_1, \cdots, a_n)$, $\mathbf{b} = (b_1, \cdots, b_n)$, α is a maneuver in $\mathbf{P}(R, \mathbf{a}, \mathbf{b})$ such that during $T_h = [t_0, t_f]$, the distance of aircraft 1 with any of the other aircraft is strictly greater than R except possibly with aircraft 2. Therefore, the only aircraft that aircraft 1 can contact during T_h is aircraft 2. We will focus on these two aircraft and introduce an operator which will leave α_i unchanged for $i = 2, 3, \cdots, n$ and perturb α_1 slightly, while the perturbed α_1 has a distance of at least R with α_2 at any time in T_h. If such perturbation is small enough then there is no possibility that the perturbed α_1 will cause conflict with any of the rest aircraft $i \geq 3$. Therefore a necessary condition for α to be optimal is that that the energy of α_1 will not decrease under such small perturbation.

One such perturbation is described by the following: Let $h : T_h \to T_h$ be a diffeomorphism such that $h(t_0) = t_0$ and $h(t_f) = t_f$. Define a new maneuver β by

$$\beta_i(t) = \begin{cases} \alpha_1[h(t)] - \alpha_2[h(t)] + \alpha_2(t) & i = 1 \\ \alpha_i(t) & i = 2, \cdots, n, \quad \forall t \in T_h \end{cases}$$

Then β has the same starting and destination positions as α. Furthermore, $\inf\{\|\beta_1(t) - \beta_2(t)\| : t \in T_h\} = \inf\{\|\alpha_1(t) - \alpha_2(t)\| : t \in T_h\}$, and for h sufficiently close to identity map, the minimal distance between β_1 and β_i is greater than R for $i \geq 3$, *i.e.* $\beta \in \mathbf{P}(R, \mathbf{a}, \mathbf{b})$. To get the geometric intuition of how β is constructed, see Figure 7.11. β is obtained in several steps:

1. First perform the operator $\mathcal{D}_{\alpha_2 - \bar{\alpha}_2}$ on α to "straighten" the string α_2 corresponding to, here $\bar{\alpha}_2$ denotes the constant speed motion along straight line between a_2 and b_2. Then operator

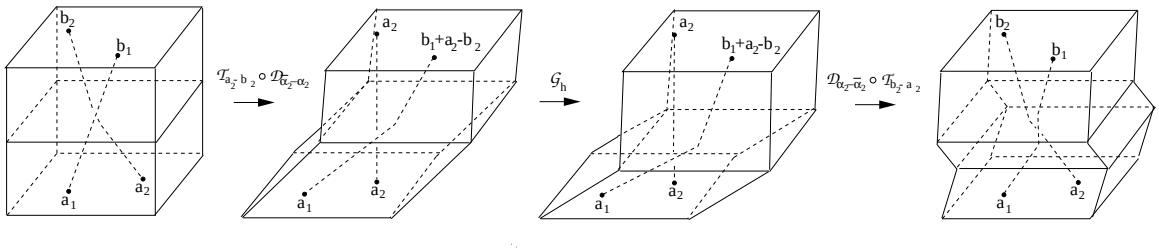

Figure 7.11: Slip operation

$\mathcal{T}_{a_2-b_2}$ is performed on the resulting maneuver to get γ. In the braid representation $\hat{\gamma}$, $\hat{\gamma}_2$ corresponds to a vertical line. Explicitly, $\gamma_1 = \alpha_1 - \alpha_2 + a_2$ and $\gamma_2 = a_2$;

2. $\mathcal{G}_h$ is perform on γ to obtain η with $\eta_1 = \alpha_1 \circ h - \alpha_2 \circ h + a_2$ and $\eta_2 = a_2$;

3. Finally β is obtain by applying the reversed procedure of step 1 on γ, *i.e.* $\beta = \mathcal{D}_{\bar{\alpha}_2-\alpha_2} \circ \mathcal{T}_{b_2-a_2}(\gamma)$.

It is remarked here that all the operations mentioned above are actually local in the sense that they operate only on the first two strings of the maneuver while leaving the rest of them unchanged. It is clear from the above construction that β is obtained by "sliding" α_1 along α_2. Therefore we will denote it by $\beta = \mathcal{L}_h^{12}(\alpha)$, where the superscript indicates which two strings we are working on and h indicates the scaling diffeomorphism. Instead of working on general h, we consider h of a very special form. Suppose $t_1 \in (t_0, t_f)$, define h by:

$$h(t) = \begin{cases} h_1(t) = \frac{t-t_0}{t_1-t_0}(t_1 + \epsilon - t_0) + t_0 & \text{if } t_0 \le t \le t_1 \\ h_2(t) = \frac{t-t_f}{t_1-t_f}(t_1 + \epsilon - t_f) + t_f & \text{if } t_1 \le t \le t_f \end{cases}$$

Parameter ϵ control the deviation of h from the identity map. Under our hypotheses, $\beta \in \mathbf{P}(R, \mathbf{a}, \mathbf{b})$ for ϵ small enough. The energy of β_1 is a function of ϵ and can be calculated as:

$$\begin{aligned} J(\epsilon) &= \int_{t_0}^{t_f} \|[\dot{\alpha}_1(h(t)) - \dot{\alpha}_2(h(t))]\dot{h}(t) + \dot{\alpha}_2(t)\|^2 \, dt \\ &= \int_{t_0}^{t_1} \left\| \frac{t_1 + \epsilon - t_0}{t_1 - t_0}[\dot{\alpha}_1(h_1(t)) - \dot{\alpha}_2(h_1(t))] + \dot{\alpha}_2(t) \right\|^2 dt \\ &+ \int_{t_1}^{t_f} \left\| \frac{t_1 + \epsilon - t_f}{t_1 - t_f}[\dot{\alpha}_1(h_2(t)) - \dot{\alpha}_2(h_2(t))] + \dot{\alpha}_2(t) \right\|^2 dt \end{aligned}$$

The differentiate of $J(\epsilon)$ at $\epsilon = 0$ is:

$$\begin{aligned} J'(0) = &\int_{t_0}^{t_1} 2\dot{\alpha}_1(t)^T \left[\frac{t - t_0}{t_1 - t_0}(\ddot{\alpha}_1(t) - \ddot{\alpha}_2(t)) + \frac{1}{t_1 - t_0}(\dot{\alpha}_1(t) - \dot{\alpha}_2(t)) \right] dt \\ + &\int_{t_1}^{t_f} 2\dot{\alpha}_1(t)^T \left[\frac{t - t_f}{t_1 - t_f}(\ddot{\alpha}_1(t) - \ddot{\alpha}_2(t)) + \frac{1}{t_1 - t_f}(\dot{\alpha}_1(t) - \dot{\alpha}_2(t)) \right] dt \end{aligned}$$

Notice that $(\ddot{\alpha}_1(t) - \ddot{\alpha}_2(t))(t - t_0) + (\dot{\alpha}_1(t) - \dot{\alpha}_2(t)) = d[(\dot{\alpha}_1(t) - \dot{\alpha}_2(t))(t - t_0)]$, we have

$$\begin{aligned}
&\int_{t_0}^{t_1} 2\dot{\alpha}_1(t)^T \left[\frac{t - t_0}{t_1 - t_0}(\ddot{\alpha}_1(t) - \ddot{\alpha}_2(t)) + \frac{1}{t_1 - t_0}(\dot{\alpha}_1(t) - \dot{\alpha}_2(t)) \right] dt \\
&= \int_{t_0}^{t_1} \frac{2\dot{\alpha}_1(t)^T}{t_1 - t_0}\, d[(\dot{\alpha}_1(t) - \dot{\alpha}_2(t))(t - t_0)] \\
&= 2\dot{\alpha}_1(t)^T(\dot{\alpha}_1(t_1) - \dot{\alpha}_2(t_1)) - 2\int_{t_0}^{t_1} \frac{t - t_0}{t_1 - t_0}\ddot{\alpha}_1(t)^T(\dot{\alpha}_1(t) - \dot{\alpha}_2(t))\, dt
\end{aligned}$$

by integration by part. Similarly

$$\begin{aligned}
&\int_{t_1}^{t_f} 2\dot{\alpha}_1(t)^T \left[\frac{t - t_f}{t_1 - t_f}(\ddot{\alpha}_1(t) - \ddot{\alpha}_2(t)) + \frac{1}{t_1 - t_f}(\dot{\alpha}_1(t) - \dot{\alpha}_2(t)) \right] dt \\
&= -2\dot{\alpha}_1(t)^T(\dot{\alpha}_1(t_1) - \dot{\alpha}_2(t_1)) - 2\int_{t_1}^{t_f} \frac{t - t_f}{t_1 - t_f}\ddot{\alpha}_1(t)^T(\dot{\alpha}_1(t) - \dot{\alpha}_2(t))\, dt
\end{aligned}$$

Hence

$$J'(0) = -2\int_{t_0}^{t_1} \frac{t - t_0}{t_1 - t_0}\ddot{\alpha}_1(t)^T(\dot{\alpha}_1(t) - \dot{\alpha}_2(t))\, dt - 2\int_{t_1}^{t_f} \frac{t - t_f}{t_1 - t_f}\ddot{\alpha}_1(t)^T(\dot{\alpha}_1(t) - \dot{\alpha}_2(t))\, dt$$

If α is optimal, then $J(\epsilon)$ assumes minimum at $\epsilon = 0$ hence $J'(0) = 0$. An important observation at this point is that since α is optimal at any subinterval of T_h, say, any subinterval $[t_0', t_f']$ containing t_1, we can carry out the above analysis for the piece of α in this subinterval and the resulting $J'(0)$ should also be zero. Therefore

$$\int_{t_0'}^{t_1} \frac{t - t_0'}{t_1 - t_0'}\ddot{\alpha}_1(t)^T(\dot{\alpha}_1(t) - \dot{\alpha}_2(t))\, dt + \int_{t_1}^{t_f'} \frac{t - t_f'}{t_1 - t_f'}\ddot{\alpha}_1(t)^T(\dot{\alpha}_1(t) - \dot{\alpha}_2(t))\, dt \equiv 0$$

for all $t_0 \le t_0' < t_1 < t_f' \le t_f$. Notice that for fixed t_1, the first term is independent of t_f' and the second term is independent of t_0', so there exists a constant C such that the first term is equal to C for all t_0' and second term is equal to $-C$ for all t_f' when t_1 is fixed. However for any fixed t_1,

$$\begin{aligned}
&\lim_{t_0' \to t_1} \int_{t_0'}^{t_1} \frac{t - t_0'}{t_1 - t_0'}\ddot{\alpha}_1(t)^T(\dot{\alpha}_1(t) - \dot{\alpha}_2(t))\, dt \\
&= -\left.\frac{d}{dt_0'}\right|_{t_0' = t_1} \int_{t_0'}^{t_1} (t - t_0')\ddot{\alpha}_1(t)^T(\dot{\alpha}_1(t) - \dot{\alpha}_2(t))\, dt \\
&= 0
\end{aligned}$$

Therefore $C = 0$, *i.e.* $\int_{t_0'}^{t_1}(t - t_0')\ddot{\alpha}_1(t)^T(\dot{\alpha}_1(t) - \dot{\alpha}_2(t))\, dt \equiv 0$ for all t_0' and t_1 such that $t_0' \le t_1$. Differentiate w.r.t. t_1, we have $(t_1 - t_0')\ddot{\alpha}_1(t_1)^T(\dot{\alpha}_1(t_1) - \dot{\alpha}_2(t_1)) \equiv 0$ for all $t_0' \le t_1$. Hence

Proposition 21 *For any* $\mathbf{a} = (a_1, \cdots, a_n)$, $\mathbf{b} = (b_1, \cdots, b_n)$, *if* α *is the optimal solution to problem (7.16) in* $\mathbf{P}(R, \mathbf{a}, \mathbf{b})$, *and suppose that* $\|\alpha_1(t) - \alpha_i(t)\| > R$, $i = 3, \cdots, n$ *holds for* t *belonging to some subinterval* $\in [t_1, t_2] \subset [t_0, t_f]$, *Then* α *satisfies*

$$\ddot{\alpha}_1(t)^T(\dot{\alpha}_1(t) - \dot{\alpha}_2(t)) \equiv 0, \qquad \forall t \in [t_1, t_2] \tag{7.22}$$

Instead of slipping the trajectory of one aircraft with respect to another, we can use rotation alternatively. Let $\alpha \in \mathbf{P}(R, \mathbf{a}, \mathbf{b})$ satisfy the condition in Proposition 21, define maneuver β by:

$$\beta_i(t) = \begin{cases} T_\theta(t)[\alpha_1(t) - \alpha_2(t)] + \alpha_2(t) & i = 1 \\ \alpha_i(t) & i = 2, \cdots, n, \quad \forall t \in T_h \end{cases}$$

where $\theta : T_h \to \mathbf{R}$ is piecewise differentiable satisfying $\theta(t_0) = \theta(t_f) = 0$. One can employ similar steps as we did for the previous case in Figure 7.11 to convince himself that this is indeed the local rotation of the trajectory of aircraft 1 with respect to that of aircraft 2. Suppose θ is of the form:

$$\theta(t) = \begin{cases} \frac{t-t_0}{t_1-t_0}\epsilon & \text{if } t_0 \le t \le t_1 \\ \frac{t-t_f}{t_1-t_f}\epsilon & \text{if } t_1 \le t \le t_f \end{cases}$$

for some ϵ, then $\beta \in \mathbf{P}(R, \mathbf{a}, \mathbf{b})$ for ϵ small enough by hypotheses on α. The energy of β_1 is a function of ϵ and the optimality of α implies that its derivative at 0 should vanish. Therefore we can carry out exactly the same analysis as before. We will not repeat it here and instead list the conclusion as follow:

Proposition 22 *Under the same hypotheses of Proposition 21, α satisfies*

$$\ddot{\alpha}_1(t)^T T_{\frac{\pi}{2}}(\alpha_1(t) - \alpha_2(t)) \equiv 0, \qquad \forall t \in [t_1, t_2] \tag{7.23}$$

In the two aircraft case, the assumptions in Proposition 21 and Proposition 22 are always satisfied and it is checked that the optimal solution obtained there does satisfy condition (7.22) and (7.23).

Conditions in Proposition 21 and Proposition 22 are the strongest ones we have obtained so far. It is worth pointing out that under the additional assumption that the distance of aircraft 1 and aircraft 2 is indeed R for $t \in T_h$, then the two conditions are equivalent. For in this case, $\|\alpha_1 - \alpha_2\|^2 \equiv R$ implies that $(\dot{\alpha}_1 - \dot{\alpha}_2)^T(\alpha_1 - \alpha_2) \equiv 0$, *i.e.* $\dot{\alpha}_1 - \dot{\alpha}_2$ and $T_{\frac{\pi}{2}}(\alpha_1 - \alpha_2)$ are of the same direction (including the case when one or both of them are zero vectors). Therefore, $\dot{\alpha}_1 - \dot{\alpha}_2$ is orthogonal to $\ddot{\alpha}_1$ if and only if $T_{\frac{\pi}{2}}(\alpha_1 - \alpha_2)$ is, establishing the equivalence between condition (7.22) and (7.23). The intuitive understanding of this equivalence is that the slip and rotation operation of a curve on the surface of a cylinder lead to the same perturbation.

As an immediate extension, the above analysis can be applied to a group of aircraft instead of a single one. In this case the corresponding operator will slip (rotate) the trajectories of a group of aircraft with respect to the trajectory of another one and we have the new necessary condition on optimality as:

Proposition 23 *For any $\mathbf{a} = (a_1, \cdots, a_n)$, $\mathbf{b} = (b_1, \cdots, b_n)$, if α is the optimal solution to problem (7.16) in $\mathbf{P}(R, \mathbf{a}, \mathbf{b})$, and suppose that the contact graph remains constant on some subinterval $[t_1, t_2] \subset [t_0, t_f]$. Then pick any aircraft, say, aircraft 1, let $\mathcal{I} \subset \{2, 3, \cdots, n\}$ be a group of aircraft which corresponds to a maximal connected component of the graph obtained by removing node 1 and all the edges connecting to it from the contact graph. Then*

$$\begin{aligned} &\sum_{j \in \mathcal{I}} \ddot{\alpha}_j(t)^T(\dot{\alpha}_j(t) - \dot{\alpha}_1(t)) \equiv 0, \\ &\sum_{j \in \mathcal{I}} \ddot{\alpha}_j(t)^T T_{\frac{\pi}{2}}(\alpha_j(t) - \alpha_1(t)) \equiv 0, \qquad \forall t \in [t_1, t_2] \end{aligned} \tag{7.24}$$

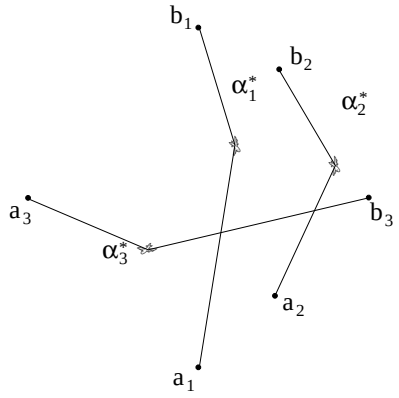

Figure 7.12: Special case of 3 aircraft resolution

In some simple cases, the optimal 2-legged resolution involving n aircraft can be obtained by using the results from two aircraft case and Proposition 17. For example, one such situation is shown in Figure 7.12. Suppose (β_1, β_3) is the optimal 2-legged resolution maneuver between aircraft 1 and 3 if we ignore aircraft 2, and suppose (γ_1, γ_2) is the optimal 2-legged resolution maneuver for aircraft 1 and 2 ignoring aircraft 3. Then since there is no need to worry about the collision between aircraft 2 and 3, the optimal 2-legged resolution maneuver α^* is the normalized version of both (β_1, β_3) and (γ_1, γ_2) satisfying

$$\begin{cases} \alpha_3^*(t) - \alpha_1^*(t) = \beta_3(t) - \beta_1(t), \\ \alpha_2^*(t) - \alpha_1^*(t) = \gamma_2(t) - \gamma_1(t), \\ \sum_{i=1}^3 \alpha_i^*(t) = \frac{t_f - t}{t_f - t_0} \sum_{i=1}^3 a_i + \frac{t - t_0}{t_f - t_0} \sum_{i=1}^3 b_i \quad \forall t \in T_h \end{cases}$$

Then α^* can be obtained by solving the above equations. From the braid point of view, this is nothing but a twist-and-fit operation on two shortest braids. Obvious this decoupled condition has its generalization when $n > 3$ in which we can isolate the aircraft into several subgroup, the intersection of them are the pivotal aircrafts. In this way, the problem can be solved by a divide-and-conquer way. We will not pursue any further in this direction here since this technique fails notable in the infinite-legged case. Even for the simplest 3 aircraft case and we know the contact graph, say, there are edges between aircraft 1 and 2, between aircraft 2 and 3 but no edge between aircraft 1 and 3, the optimal infinite-legged motion still resists analytical expression. We are still working on this respect.

7.7 Convex Optimization in Finding Optimal 2-legged Resolution Maneuver

General speaking, the nature of n aircraft resolution problem is mainly combinatorial in that the major task is to choose a particular type of resolution maneuver and then find the optimal representative from it. There are various heuristic ways of choosing resolution type. In the next subsection, we will give one based on the probability of collision calculated before. The focus of this section, however, will be the less difficult task of finding the optimal maneuver with a given type. Furthermore, we will only discuss the two-legged maneuvers since optimal multi-legged or infinite-legged maneuver can be obtained subsequently by using Algorithm 1.

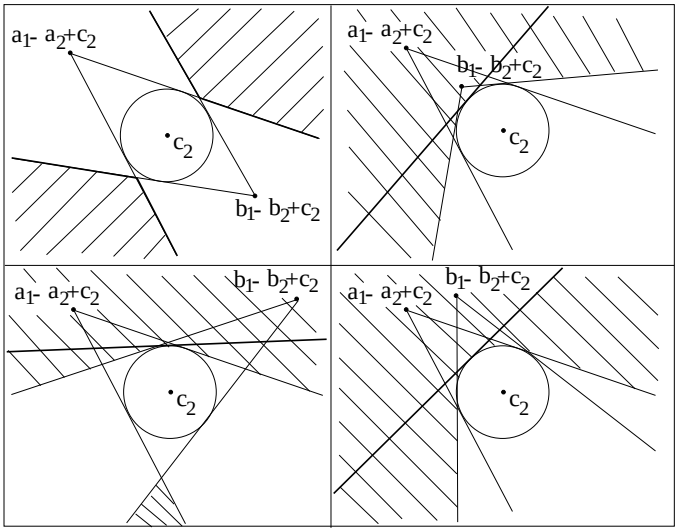

Figure 7.13: Convex approximation of feasible set of c_1 given c_2

Suppose we choose epoch $t_m \in T_h$. Then the problem is to find the waypoints $c_1, \cdots, c_n$ to

$$\text{Minimze } J = \sum_{i=1}^{n} \|c_i - c_i^u\|^2 \quad \text{subject to } c_i \in A_{ij}^{\pm}(c_j), \quad 1 \le i < j \le n. \tag{7.25}$$

where $A_{ij}(c_j)$ is the feasible set of c_i for fixed c_j calculated in section 7.2 with a_i, b_i, a_j, b_j in the place of a_1, b_1, a_2, b_2 there respectively. Symbol $\pm$ means the properly chosen connected component of $A_{ij}(c_j)$ which matches our desired resolution type. Figure 7.13 redraws the four possible configurations of $A_{ij}(c_j)$ depending on the relative position of a_i, b_i, a_j, b_j. Notice that in all but the first configuration, one of the connected component of $A_{ij}(c_j)$ is nonconvex. In general, solving nonconvex problem is a great challenge, even if the objective function is quadratic. Therefore if this is the case, we "linearize" the constraint by using a half plane inner approximation $A'_{ij}(c_j)$ shown in Figure 7.13. Although it leaves out some originally feasible c_1, it contains the unconstrained optimal c_i^u if c_j is chosen to be c_j^u. Therefore it is expected that the approximation will not be too loose. In the special case when any pair of aircraft is of the first configuration, *i.e.* there is a conflict for the unresolved maneuver of any aircraft pair, the approximation is tight. Symmetric encounter is such a case. And such encounters are among the most dangerous ones of all possible encounters.

So then we have a linearly constrained quadratic optimization which can be solved by all kinds of software package, say, MATLAB. As an example, let us consider the three aircraft cases. Since the number of aircraft is small, we have the luxury of running the optimization for each fundamental type of resolution and pick the one with the optimal cost. Simulation results for two encounters are shown in Figure 7.14. In the first case, we have a nearly symmetric encounter, and in the second one there is a headon conflict between two aircraft and a third aircraft has path angle 90° with both of them. In either case, each pair of the three aircraft is of configuration 1, hence our linearization remain tight and the maneuvers we found are actually the optimal maneuvers for the original problems.

However, as n get larger, the number of resolution type gets inhibitively large and such an exhaust search becomes impossible. If we only consider the fundamental type of resolution, then there are

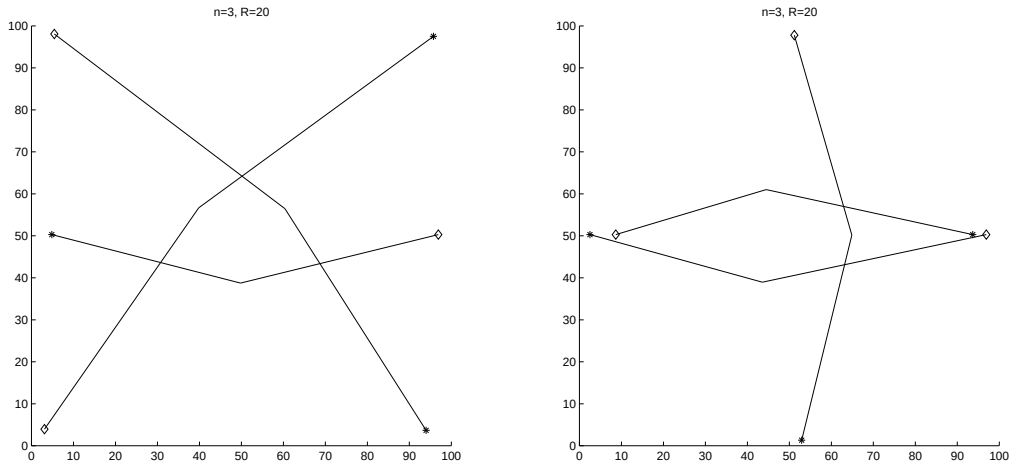

Figure 7.14: Globally optimal resolution maneuver for three aircraft encounters

$2^{n(n-1)/2}$ of them and this number grows even faster than exponentially! Therefore, some scheme must be propose to choose a relatively "good" type of resolution in the first hand. This will be the theme of next section.

Chapter 8

Probabilistic Resolution Algorithm

In this chapter, we introduce a decentralized conflict resolution algorithm which exploits the probability of conflict calculated in chapter 4 to guide each aircraft to their desired destinations, while avoiding possible situations of conflict with other aircraft flying in the same region of the airspace. Although we are specifically dealing with ATMS, the following discussion regards the general issue of path planning for multiple agents moving in a dynamic environment. In [6], an algorithm for aircraft conflict resolution is proposed based on the potential and vortex field method, which has its origin in the robotics field. However, since the potential field defined there depends only on the distance between aircraft, the two cases when two aircraft are flying one towards each other and away from each other lead to the same repulsive force whenever the distances between them are the same. As a consequence, the resolution algorithm may generate abrupt avoidance maneuvers and hence non-flyable paths. The idea of the algorithm proposed here is to use the information not only on the current positions but also on the current headings and speeds of the surrounding aircraft in order to generate less abrupt resolution maneuvers and flyable resolution paths.

Consider first the case when two aircraft (labeled 1 and 2) start from positions a_1 and a_2 and have destinations b_1 and b_2 respectively. Assume their initial headings are toward their own destinations and they fly at a constant speed, say v_1 and v_2 respectively. At each time instant t, the probability of conflict $P_c(t)$ can be calculated by equation (4.10) or equation (4.11) for some fixed horizon t_f using the positions $z_1(t), z_2(t)$ and velocities $u_1(t), u_2(t)$ of the two aircraft at this moment.

We define for each aircraft three particular headings of interest:

- *Current heading θ_c:* Direction along which the aircraft is currently flying. Due to physical limits on aircraft capability, the new heading proposed by the resolution algorithm should not deviate too much from θ_c.
- *Destination heading θ_d:* Direction defined by the current aircraft position and its desired destination.
- *Gradient heading θ_g:* Direction corresponding to the highest decrease of PC. Since both aircraft maintain their velocities within a short time, θ_g can be chosen as the direction of the negative gradient of P_c as a function only of the current position of the aircraft.

Our resolution strategy aims at making each aircraft reach the desired destination while avoiding situations of conflict by appropriately changing the heading, while taking into account the constraints due to the nonholonomic nature in aircraft motion.

Algorithm 2 1. Set the initial positions $z_1[0] = a_1$, $z_2[0] = a_2$ and initial velocities $u_1[0]$ and $u_2[0]$ at time 0.

2. At time n, compute the PC of two aircraft as $P_c[n]$ using $z_1[n], z_2[n], u_1[n], u_2[n]$. For each aircraft $i = 1, 2$, compute its current heading $\theta_{c,i}[n]$, destination heading $\theta_{d,i}[n]$ and gradient heading $\theta_{g,i}[n]$ at this time respectively.

3. Choose the new heading for aircraft $i = 1, 2$ at step n by

$$\theta_i[n+1] = \begin{cases} \bar{\theta}_i[n+1] & \text{if } |\bar{\theta}_i[n+1] - \theta_{c,i}[n]| < \beta \\ \theta_{c,i}[n] + \beta \cdot \text{sgn}(\bar{\theta}_i[n+1] - \theta_{c,i}[n]) & \text{otherwise,} \end{cases} \tag{8.1}$$

where β is the maximal turn angle allowed per time step Δt and

$$\bar{\theta}_i[n+1] = P_c[n]\theta_{g,i}[n] + (1 - P_c[n])\theta_{d,i}[n].$$

is the weighted sum of destination direction and gradient direction. Intuitively, if $P_c[n]$ is high, then decreasing PC becomes a priority and therefore the aircraft should pursue the gradient direction more. If instead, $P_c[n]$ is negligible, then the aircraft should pursue the destination direction. In any case, due to the nonholonomic nature in aircraft, the deviation from current heading is restricted by β and this is the reason why the new heading is chosen to be the one nearest to $\bar{\theta}_i[n]$ within the allowed range.

4. Set the aircraft velocities $u_i[n+1] = (v_i \cos(\theta_i[n+1]), v_i \sin(\theta_i[n+1]))^T$, $i = 1, 2$ and update the positions of two aircraft at step $n+1$ by

$$\begin{cases} z_1[n+1] = z_1[n] + u_1[n+1]\Delta t + T_{\theta_1[n+1]} \cdot \text{diag}(\sigma_1, \sigma_2) \cdot n_1[n+1], \\ z_2[n+1] = z_2[n] + u_2[n+1]\Delta t + T_{\theta_2[n+1]} \cdot \text{diag}(\sigma_1, \sigma_2) \cdot n_2[n+1] \end{cases}$$

where $T_{\theta_1[n+1]}$ and $T_{\theta_2[n+1])}$ are the rotation matrices of angles $\theta_1[n+1]$ and $\theta_2[n+1]$ respectively. $n_1[1], n_1[2], \cdots$ and $n_2[1], n_2[2], \cdots$ are independent two dimensional white Gaussian noises with unit covariance matrices.

5. If both of the aircraft have reach their destinations, then stop, otherwise $n = n + 1$ and go back to procedure 2.

Simulation results for the above algorithm are shown in Figure 8.1 for two typical encounters of two aircraft: Headon encounter and orthogonal encounter. The speeds of the two aircraft are chosen such that it takes 30 minutes for them to fly from their starting positions (marked with stars) to their destination positions (marked with diamonds) along the unresoluted straight line motion. The left column plot the analytic optimal resolution maneuvers calculated in Chapter 7 with $R = 20$ nmi. The middle column shows the simulation result for Algorithm 2 with $R = 10$ nmi. $\sigma_a = 0.25, \sigma_c = 0.2$, $\beta = \pi/25$. σ_a and σ_c are used both in the calculation of PC and in the generation of noises for the simulated trajectories. In general we could use different values for the two purposes, leading to different variations of the original algorithm. Circles marks the point where the minimal separation occurs. The rightmost column shows the histogram of MSE when we run Algorithm 2 for each encounter 100 times respectively. It can be seen that most MSE's center around $2R$. The factor 2 arises since each aircraft tries to maintain a distance of R from the other and there is no coordination between them. In addition, most of the simulated resolution maneuvers resemble the optimal maneuvers in each case, indicating a good efficiency of the algorithm.

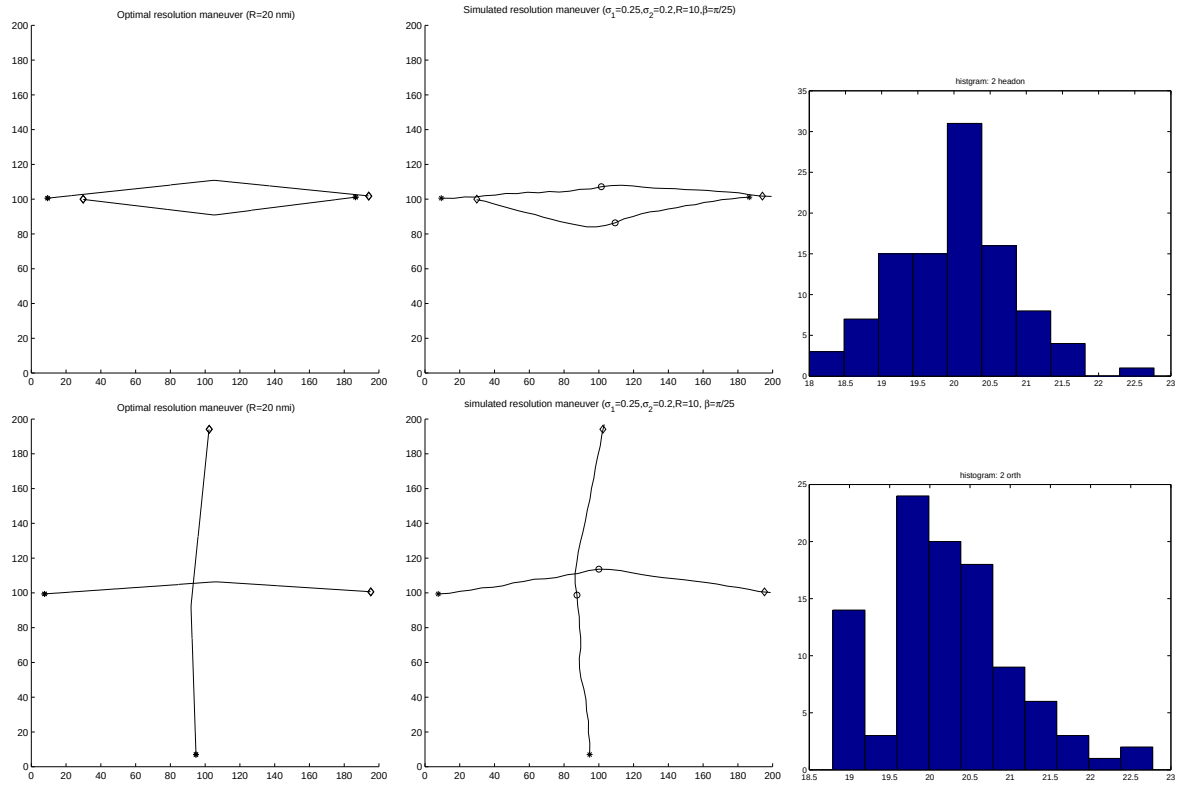

Figure 8.1: Optimal and simulated resolution maneuver for two aircraft encounter situations

In the simulations, the two aircraft update their heading every 1 minute, so a zoom in of the resolution trajectory will reveal lots of chattering between positions corresponding to higher P_c and lower P_c. This behaviors is expected, since the function P_c is very sensitive to the heading of the two aircraft. In order to get flyable paths, we can either update the heading at a larger time step or predict a certain period of time further into the future and take the average of the resolution headings during that period (which acts as a low pass filter).

Following a procedure similar to the one explained above, it is possible to extend our algorithm to the case of more than two aircraft, say n aircraft. The algorithm remains intact for all the steps except that in step 3, extra care must be taken to determine the new heading of each aircraft. For aircraft $i \in \{1, 2, \cdots, n\}$, we can calculate the probability of conflict between it and any of the other aircraft, say aircraft $j \neq i$, at time n as $P_c^{ij}[n]$, and therefore have a gradient heading $\theta_g^{ij}[n]$ corresponding to this aircraft pair. Denote the current heading and the destination heading of aircraft i at this time as $\theta_{c,i}[n]$ and $\theta_{d,i}[n]$ respectively. The the ideal new heading for aircraft i in the next time interval can be chosen as:

$$\bar{\theta}_i[n+1] = P_{cm}[n]\frac{\sum_{j\neq i} P_c^{ij}[n]\theta_g^{ij}[n]}{\sum_{j\neq i} P_c^{ij}[n]} + (1 - P_{cm}[n])\theta_{d,i}[n]$$

where $P_{cm}[n] = \max_{j\neq i} P_c^{ij}[n]$ is the maximal PC of all aircraft pairs involving aircraft i and is used as an indicator of the degree of danger for aircraft i in multiple aircraft setting. There are certainly other alternative ways of choosing $\bar{\theta}_i[n+1]$ and it is not clear which one is the best. All of them are based on the intuitive understanding that new heading should be a weighted sum of all the gradient directions and the current heading, and increasing PC of one particular aircraft

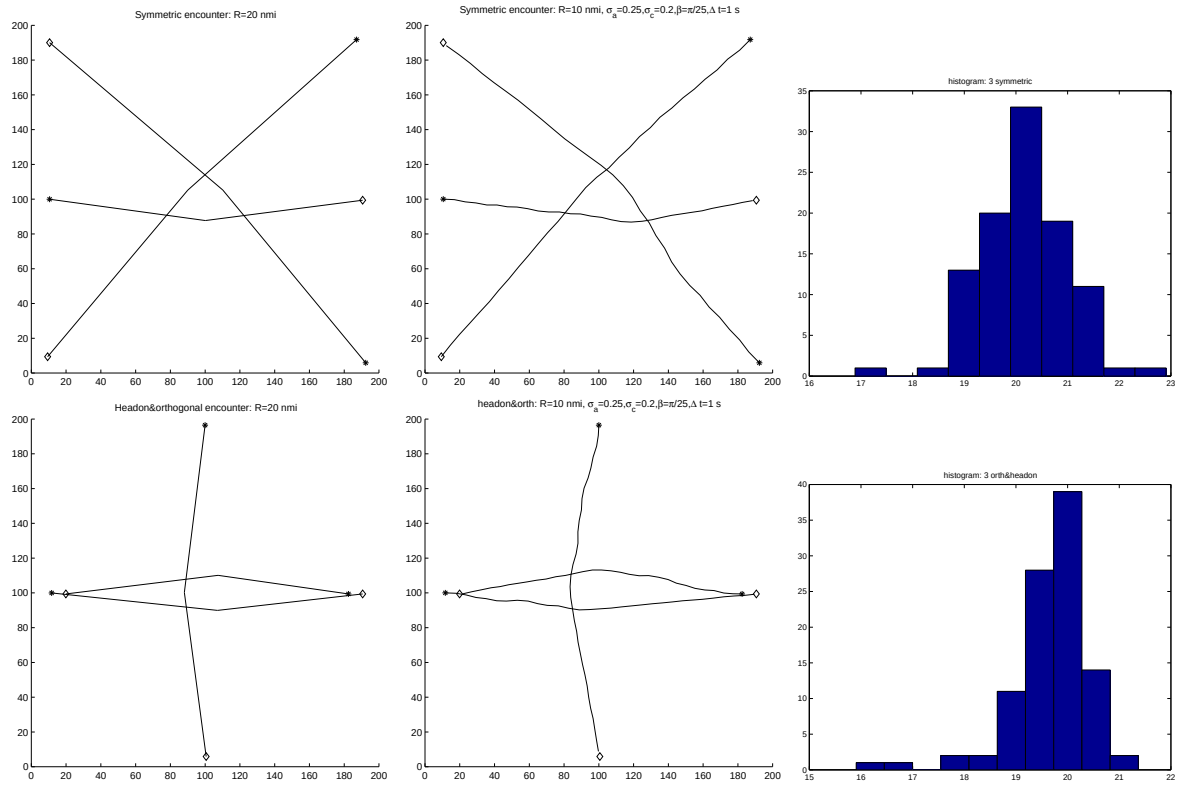

Figure 8.2: Resolution for three aircraft encounter situations

pair should leads to larger weight of the gradient direction associated with this pair. We choose the current one because of simplicity and the fact that unless the PC between aircraft i and one of the other aircraft is higher than a threshold, the resolution endeavor will barely interfere with each aircraft's motion. To accommodate the nohomolonomic limit, the final new heading is chosen by equation (8.1) as before.

Simulation results for several three aircraft encounter situations are shown in Figure 8.2. All parameters remain the same as in the two aircraft cases. The left column show the optimal two-legged resolutions calculated by the exhaust search mentioned in Chapter 7 with $R = 20$ nmi. The middle column is one realization of the simulated resolution maneuvers using the above algorithm with $R = 10$ nmi. The right column is the histogram of MSE's over 100 runs. Since the air space is not considerably more congested than the more aircraft case, nearly all the MSE centered around $2R$ as before.

The situation becomes more complicated when the number of aircraft increases to, say, 8. In this case it is no longer plausible to perform the exhaust search to find the global optimal two-legged resolution. However, Algorithm 2 can be used as a random "type chooser" for the optimization process. We show this by two 8-aircraft encounter in Figure 8.3. The first one is the symmetric encounter in which eight aircraft pass through a common point at angles evenly distributed in $[0, 2\pi]$. In the second example, eight aircraft are divided into two groups. Aircraft in each group follow each other in a streamline and the trajectories of two group are orthogonal to each other. As before, the middle column shows the simulation results of Algorithm 2. The left column shows the results of the convex optimization process for the particular type of maneuvers specified by the

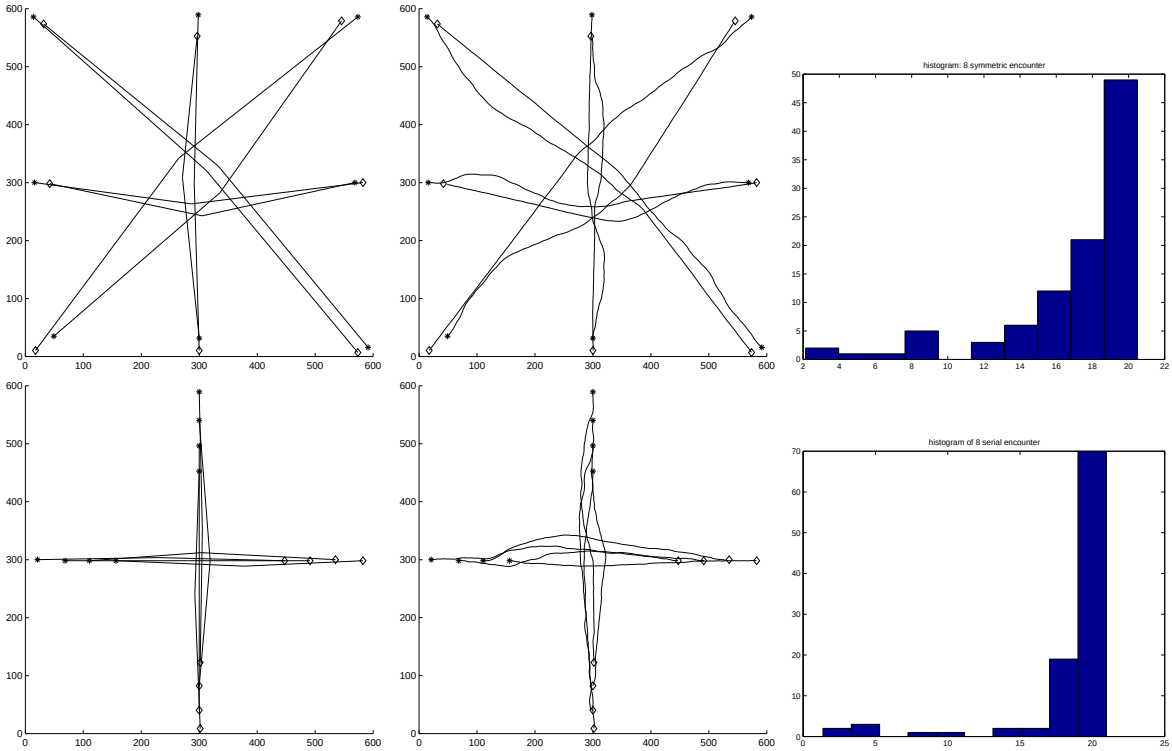

Figure 8.3: Resolution for eight aircraft encounter situations

middel column and the right column shows the historgram of MSE over 100 run of Algorithm 2. Note that in this case, Algorithm 2 can not guarantee absolutely safety. The minimal seperation of $R = 10$ nmi is satisfied for 92% of the 100 runs for the first example and 94% for the second one.

See Figure 8.4 for a wilder example in which two realizations of Algorithm 2 for symmetric 16-aircraft encounter are shown to give the readers some idea on how complicated the resolution maneuvers can be and how different they are under different runs.

Remark 9 (Centralized vs. Decentralized Resolution) It should be noted that in some cases, Algorithm 2 fails to achieve the ultimate goal – bring every aircraft to its destination. As a simple example let us consider two aircraft which are flying at the same speed with orthogonal (90°) unresoluted paths. If the starting and destination positions of them are placed symmetrically with respect to a certain line and assume there is no noise in their motions, then under Algorithm 2, they will fail to reach their destinations since both of them are equipped with the same resolution algorithm and hence they make symmetric resolution decisions. Therefore, coordination among aircraft turns out to be crucial to ensure that the ultimate goal of reaching the destination will not fail due to an excessive 'mutual politeness' of the aircraft involved. Furthermore, there is little doubt that the existence of inter-aircraft coordination will improve the overall system efficiency.

On the other hand, although centralized resolution algorithms such as the one based on convex optimization generate provable safe resolution maneuvers, Algorithm 2 has some distinctive features due to its decentralized philosophy. For example, in this paper we assume that we can isolate a group of aircraft from the rest in a certain region of the airspace as the ones with "high potential" of conflict. In practice, this is no easy job. Adding aircraft to or deleting aircraft from this group will generally be more computationally expensive for centralized than for decentralized algorithms

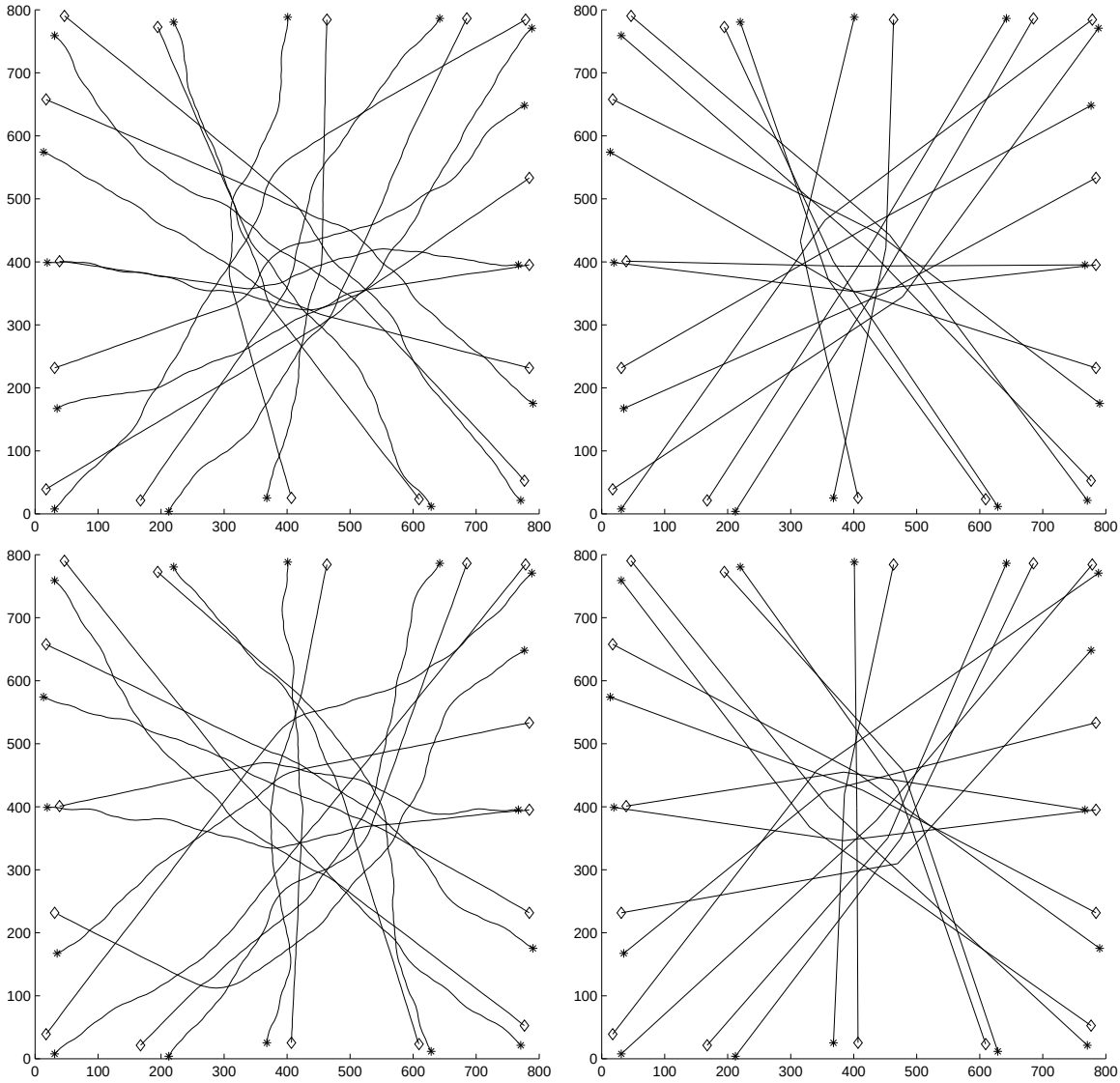

Figure 8.4: Resolution for 16 aircraft encounter situations

such as Algorithm 2. Furthermore and maybe the most important, using decentralizing algorithm, (at least in the strategic level), there is no risk of a major disastor due to the collapse of the central decision making agency, which has been becoming more than ever a distinctive possiblility considering the increasingly complex equipments and the explosively increasing air traffic. It is not the aim of this paper to discuss the general issue of which philosophy suits better in the free flight situation, though the authors do believe that the one finally adopted should be one combining both of them, *i.e.* at least part of the conflicted detection and resolution responsibilities are distributed to individual aircraft and there is some information hierarchy imposing on it.

Chapter 9

Conclusion and Future Directions

It might be worthwhile to sum up what we have accomplished so far. On the one hand, approximated probabilities of conflict for aircraft pair are obtained together with bounds on the error of the approximations. Along this line, a decentralized multi-aircraft resolution algorithm is proposed by using PC as the potential function. On the other hand, to fully understand the nature of the problem, we need to classify different types of resolution maneuvers and find the optimal representative within each class. These are made precise at the beginning of the second part and for two aircraft case, analytical solution is possible, both for two-legged and infinite-legged motion. For the general multiple aircraft case, some properties of the optimal maneuver are known and convex optimization can be used to get the two-legged approximation to it. These two lines merged in the end by noting that the stochastic algorithm can serve as the random "type chooser" for the convex optimization process, leading to an overall randomized combinatorial optimization algorithm.

We focus on planar case in this paper. One immediate extension is to consider the practical situation of three dimensional conflict detection and resolution. In a way similar to the 2-D case, the approximated PC for 3-D case can be calculated, and this extended PC can be used to derived a decentralized 3-D resolution algorithm. However, it is considerably harder to get meaningful bounds for the error of such approximations. It should also be pointed out here that due to the shape of 3-D protection zone, it is expected that most resolution will be vertical maneuvers under this algorithm. Currently there is still debate on the extent that vertical maneuvers should be employed in conflict resolution.

In some sense (or as it is always the case when one try to solve problems beyond his reach), the problems answered in this paper are far less than the problems it comes up with. We will not pretend that these directions are mere trivial extensions of the current one. Instead, radically different treatment might be needed. We choose to stop here because of the bounds on time, energy and capability.

Appendix A

Formulae

Formula 1 $F(\alpha) \triangleq \int_0^\infty e^{-(t-\alpha/t)^2} dt = \frac{\sqrt{\pi}}{2}, \quad \forall \alpha > 0$

Proof: On the one hand, let $s = 1/t$, we have $F(\alpha) = \int_0^\infty \frac{1}{s^2} e^{-(\alpha s - 1/s)^2}\, ds$. On the other hand, let $s = t/\alpha$, we have $F(\alpha) = \int_0^\infty \alpha\, e^{-(\alpha s - 1/s)^2}\, ds$. Combining:

$$2F(\alpha) = \int_0^\infty (\alpha + 1/s^2) e^{-(\alpha s - 1/s)^2} ds = \int_0^\infty e^{-(\alpha s - 1/s)^2} d(\alpha s - 1/s) = \int_{-\infty}^\infty e^{-v^2} dv = \sqrt{\pi}$$

Notice that $\alpha > 0$ is used in determining the integral bound after the change of variable. ■

Formula 2 $g(x) \triangleq \int_0^\infty \lambda\, e^{-\lambda t} \frac{1}{\sqrt{2\pi t}} \exp[-\frac{(x-\mu t)^2}{2t}] dt = \frac{\lambda}{\sqrt{2\lambda+\mu^2}} \exp(\mu x - |x|\sqrt{2\lambda+\mu^2}), \quad \forall \lambda > 0, \forall \mu$

Proof: Let $t = s^2$ and then $v = s\sqrt{\lambda + \mu^2/2}$, we have

$$\begin{aligned} g(x) &= \int_0^\infty \frac{2\lambda}{\sqrt{2\pi}} \exp[-\lambda s^2 - \frac{(x - \mu s^2)^2}{2s^2}]\, ds \\ &= \frac{2\lambda}{\sqrt{2\pi}} \exp(\mu x - |x|\sqrt{2\lambda+\mu^2}) \int_0^\infty \exp[-(s\sqrt{\lambda + \mu^2/2} - \frac{|x|}{s\sqrt{2}})^2]\, ds \\ &= \frac{2\lambda}{\sqrt{\pi(2\lambda+\mu^2)}} \exp(\mu x - |x|\sqrt{2\lambda+\mu^2}) \int_0^\infty \exp[-(v - \frac{|x|}{2v}\sqrt{2\lambda+\mu^2})^2]\, dv \\ &= \frac{\lambda}{\sqrt{2\lambda+\mu^2}} \exp(\mu x - |x|\sqrt{2\lambda+\mu^2}) \end{aligned}$$

where the last step follows from Formula 1 by letting $\alpha = \frac{1}{2}|x|\sqrt{2\lambda+\mu^2}$. ■

Formula 2 simplifies to $g(x) = \frac{\lambda}{\sqrt{2\lambda+\mu^2}} \exp[(\mu - \sqrt{2\lambda+\mu^2})x]$ in the case $x > 0$. Differentiate it with respect to x, we can easily get (The technicality of exchanging the order of differentiation and integration can be overcome by using dominated convergence theorem for a proper bound.)

Formula 3 $\int_0^\infty e^{-\lambda t} \frac{x}{\sqrt{2\pi t^3}} \exp[-\frac{(x-\mu t)^2}{2t}] dt = \exp[(\mu - \sqrt{2\lambda+\mu^2})x], \quad \forall x > 0, \lambda > 0$

Formula 4 *Denote* $Q(x) = \int_x^\infty \frac{1}{\sqrt{2\pi}} \exp(-t^2/2)\, dt$. *Then for* $a > 0, b \neq 0, s > 0$

$$\int_0^s \frac{a}{\sqrt{2\pi t^3}} \exp[-\frac{(a+bt)^2}{2t}]\, dt = Q(\frac{a+bs}{\sqrt{s}}) + e^{-2ab} Q(\frac{a-bs}{\sqrt{s}})$$

$$\int_0^s \frac{a}{\sqrt{2\pi t}} \exp[-\frac{(a+bt)^2}{2t}]\, dt = -\frac{a}{b}\left[Q(\frac{a+bs}{\sqrt{s}}) - e^{-2ab} Q(\frac{a-bs}{\sqrt{s}})\right]$$

$$\int_0^s \frac{a\sqrt{t}}{\sqrt{2\pi}} \exp[-\frac{(a+bt)^2}{2t}]\, dt = (\frac{a^2}{b^2} - \frac{a}{b^3}) Q(\frac{a+bs}{\sqrt{s}}) + (\frac{a^2}{b^2} + \frac{a}{b^3}) e^{-2ab} Q(\frac{a-bs}{\sqrt{s}}) - \frac{2a}{b^2}\sqrt{\frac{s}{2\pi}} \exp[-\frac{(a+bs)^2}{2s}]$$

Proof: Define $I_1 \triangleq \int_0^s \frac{a}{\sqrt{2\pi t^3}} \exp[-\frac{(a+bt)^2}{2t}]\, dt$, $I_2 \triangleq \int_0^s \frac{-b}{\sqrt{2\pi t}} \exp[-\frac{(a+bt)^2}{2t}]\, dt$. Then

$$\begin{aligned} I_1 - I_2 &= \int_0^s \frac{a+bt}{\sqrt{2\pi t^3}} \exp[-\frac{(a+bt)^2}{2t}]\, dt \\ &= -2e^{-2ab} \int_0^s \frac{1}{\sqrt{2\pi}} \exp[-(\frac{(a-bt)}{\sqrt{t}})^2/2]\, d(\frac{a-bt}{\sqrt{t}}) \\ &= 2e^{-2ab} \int_{\frac{a-bs}{\sqrt{s}}}^\infty \frac{1}{\sqrt{2\pi}} \exp(-\frac{v^2}{2})\, dv \qquad (v = \frac{a-bt}{\sqrt{t}}) \\ &= 2e^{-2ab} Q(\frac{a-bs}{\sqrt{s}}) \end{aligned}$$

Similarly $I_1 + I_2 = 2Q[(a+bs)/\sqrt{s}]$. Hence the first and second equations. The third one follows by differentiation of I_2 w.r.t. b. ■

Let $s \to \infty$ in Formula 4 and assume $a = x > 0, b = -v < 0$, we have

Formula 5 *For* $x > 0, v > 0$

$$\int_0^\infty \frac{x}{\sqrt{2\pi t^3}} \exp[-\frac{(x-vt)^2}{2t}]\, dt = 1$$

$$\int_0^\infty \frac{x}{\sqrt{2\pi t}} \exp[-\frac{(x-vt)^2}{2t}]\, dt = \frac{x}{v}$$

$$\int_0^\infty \frac{x\sqrt{t}}{\sqrt{2\pi}} \exp[-\frac{(x-vt)^2}{2t}]\, dt = \frac{x^2}{v^2} + \frac{x}{v^3}$$

$$\int_0^\infty \frac{x\sqrt{t^3}}{\sqrt{2\pi}} \exp[-\frac{(x-vt)^2}{2t}]\, dt = \frac{x^3}{v^3} + \frac{3x^2}{v^4} + \frac{3x}{v^5}$$

Note the last equation follows by differentiating the third one with respect to v.

Alternatively assume $a = x > 0, b = v > 0$ in Formula 4 and let $s \to \infty$, we have

Formula 6 *For* $x > 0, v > 0$

$$\int_0^\infty \frac{x}{\sqrt{2\pi t^3}} \exp[-\frac{(x+vt)^2}{2t}]\, dt = e^{-2xv}$$

$$\int_0^\infty \frac{x}{\sqrt{2\pi t}} \exp[-\frac{(x+vt)^2}{2t}]\, dt = \frac{x}{v} e^{-2xv}$$

$$\int_0^\infty \frac{x\sqrt{t}}{\sqrt{2\pi}} \exp[-\frac{(x+vt)^2}{2t}]\, dt = (\frac{x^2}{v^2} + \frac{x}{v^3}) e^{-2xv}$$

Bibliography

[1] R. Durrett. *Brownian motion and martingale in analysis.* Wadsworth Advanced Books and Software, 1984.

[2] R. Durrett. *Probability: theory and examples, Second edition.* Duxbury Press, 1996.

[3] Radio Technical Commission for Aeronautics. Minimum aviation system performance standards for automatic dependent surveillance-broadcast (ads-b). *Technical report*, RTCA-186, 1997. DRAFT 4.0.

[4] E. Frazzoli, Z.-H. Mao, J.-H. Oh, and E. Feron. Resolution of conflicts involving many aircraft via semidefinite programming. *Preprint*, 1999.

[5] J. Hu, J. Lygeros, M. Prandini, and S. Sastry. A probabilistic framework for highway safety analysis. In *IEEE Conference on Decision and Control*, Pheonix, AZ, 1999. To appear.

[6] J. Kosecka, C. Tomlin, G. Pappas, and S. Sastry. Generation of Conflict Resolution Maneuvers For Air Traffic Management. In *IEEE Conference on Intelligent Robotics and System '97*, volume 3, pages 1598–1603, 1997.

[7] J. Krozel and M. Peters. Strategic conflict detection and resolution for free flight. In *IEEE Conference on Decision and Control*, San Diego, 1996.

[8] J. Kuchar and L.C. Yang. Survey of conflict detection and resolution modeling methods. In *AIAA Guidance, Navigation, and Control Conference*, New Orleans, LA, 1997.

[9] J.W. Milnor. *Morse theory.* Annals of mathematics studies ; 51. Princeton University Press, 1963. Based on lecture notes by M. Spivak and R. Wells.

[10] S. Morgan. *The mathematical theory of knots and braids: an introduction.* North-Holland, 1991.

[11] K. Murasugi and B. Kurpita. *A study of braids.* Boston: Kluwer Academic, 1999.

[12] B. Oksendal. *Stochastic Differential Equations, an introduction with application. Fifth edition.* Springer-Verlag, 1998.

[13] R.A. Paielli and H.Erzberger. Conflict probability estimation for free flight. *Journal of Guidance, Control and Dynamics*, 20(3):588–596, 1997.

[14] S. Port and C. Stone. *Brownian motion and classical potential theory.* Academic Press, New York, 1978.

[15] M. Prandini, J. Lygeros, A. Nilim, and S. Sastry. A probabilistic framework for aircraft conflict detection. In *AIAA Guidance, Navigation and Control*, 1999. Accepted.

[16] S. Sastry, G. Meyer, C. Tomlin, J. Lygeros, D. Godbole, and G. Pappas. Hybrid systems in air traffic control. In *IEEE Conference on Decision and Control*, pages 1478–1483, New Orleans, LA, 1995.

[17] C. Tomlin. Conflict resolution for air traffic management: a study in multi-agent hybrid systems. *ERL Memorandum, UC Berkeley*, UCB/ERL M97/33, 1997.

[18] C. Tomlin. Hybrid control of air traffic management system. *Ph.D. thesis*, EECS Department, UC Berkeley, 1997.

[19] P. Varaiya. Smart cars on smart roads: problems of control. *IEEE Transaction on Automatic Control*, AC-38(2), 1993.

[20] L.C. Yang and J. Kuchar. Prototype conflict alerting logic for free flight. In *Proc. 35th AIAA Airspace Science Meeting & Exhibit, AIAA 97-0220*, January 1997.